Modelling a PV powered Methanol Synthesis Microplant

Kushal Gorti

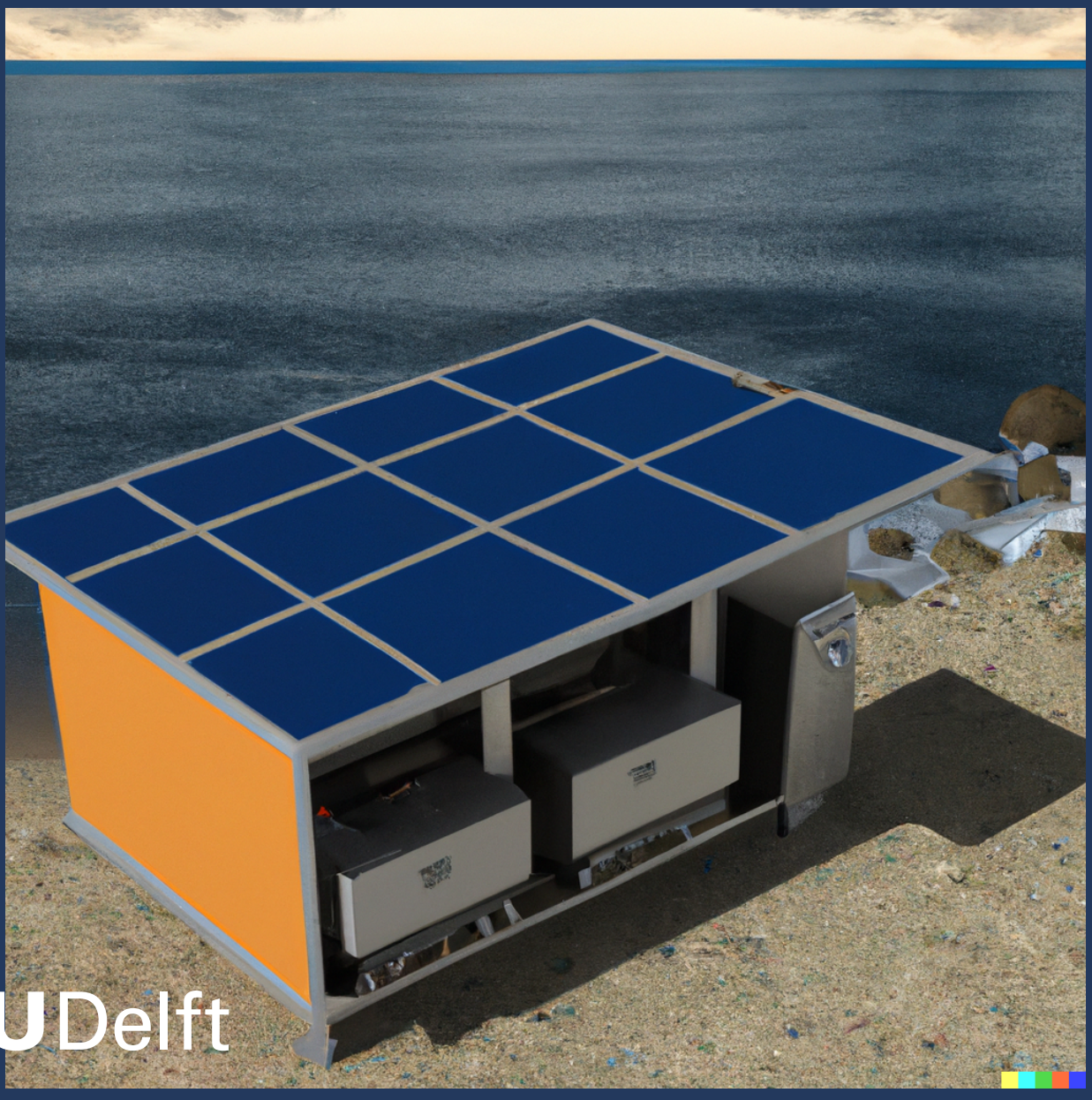

TU Delft

Modelling a PV powered Methanol Synthesis Microplant

Thesis report

by

Kushal Gorti

to obtain the degree of Master of Science
at the Delft University of Technology
to be defended publicly on September 27, 2023 at 09:30

Thesis committee:

Chair:	Dr. ir. Olindo Isabella, TU Delft
Committee Members:	Dr. ir. Rudi Santbergen, TU Delft
	Dr. ir. Gijsbert Korevaar, TU Delft
	Ir. Jan van Kranendonk, ZEF B.V.
Place:	Van Katwijkzaal, EEMCS, Delft
Project Duration:	January, 2023 - September, 2023
Student number:	5296595

An electronic version of this thesis is available at `http://repository.tudelft.nl/`.

Faculty of Electrical Engineering, Mathematics and Computer Science · Delft University of Technology

Abstract

Climate change is real. Energy transition plays a crucial role in addressing climate change where solar fuels have emerged as a critical player in reducing the dependence on fossil fuels in industries that cannot transition into renewable electricity as an energy source such as aviation, industrial feedstocks etc. Green methanol is a promising solar fuel if it is sourced via carbon capture technologies. This thesis aims to build and use a model of an integrated methanol synthesis microplant as a tool to predict methanol production and the performance of the microplant under multiple system architectures at Zero Emission Fuels B.V (ZEF) who are developing a solar powered green methanol synthesis plant. The research commenced with data preprocessing which utilised historical weather data from the C3S database. Subsequently, individual subsystem models were developed such as solar photovoltaic (PV) modules, direct air capture (DAC), fluid machinery (FM), alkaline electrolysis cell (AEC), methanol synthesis (MS), distillation (DS), buffer tanks, and battery system. To ensure the microplant's functionality, a sophisticated control algorithm was devised, operating on two distinct levels: battery management and power distribution. Moreover, diverse microplant architectures were designed, to address unique operational scenarios and environmental conditions. The investigation further explored the influence of temporal granularity, and component sizing on microplant behavior. Ultimately, this thesis establishes the feasibility of the ZEF microplant, offering valuable insights for practical implementation across multiple locations. Consequently, it underscores the potential of the ZEF microplant as a promising solution in the transition towards sustainable energy alternatives.

Acknowledgements

As I reflect on the culmination of this thesis, I realise this would not have been possible without some legendary humans whom I am fortunate enough to have known.

I cannot thank my daily supervisor Jan, as much as you deserve. Your constant support during my thesis and your amazing insights have been a source of inspiration. You are an engineering wizard!

To Dr. Rudi Santbergen, my thesis supervisor, I thank you for guiding me through this thesis. Your feedback has been especially valuable and your belief in me and my thesis has been monumental in making this possible. You are one of the kindest people I have ever had the opportunity to know.

The amazing team at ZEF needs a huge shout-out, especially Ulrich and Mrigank! I thank Ulrich who was my first contact at ZEF for making this journey as smooth as possible! Mrigank, your experience and guidance during my project at ZEF has been nothing short of amazing. Your work ethic and attention to detail is something I would strive to gain.

I would also extend my gratitude to my thesis committee, Dr. Olindo Isabella to chair my thesis committee and Dr. Gijsbert Korevaar for accepting and agreeing to be my external supervisor. I am extremely honoured to have you on my committee.

Amma and Nana, you both have been the best parents in the world and there's no contesting it. You have always been there with me, for me without a break. For everything I have troubled you over these years, everything you had to go through for me and everything you had to give up, this thesis is the beginning of the journey where I can take the opportunity to give back what I have received - a goal I believe can never be achieved for the sheer amount of love you have showered on me.

I can't thank my grandparents enough for being the earliest sources of inspiration and learning! I thank you for letting me dream, and shower unconditional love towards me since the first time I cried! Thank you Tatagaru for being the math genius I needed, and thank you amamma for always having faith in me. Thank you mama for always being that one person who would always be ready to do all you can for me even when you couldn't! And I know Tatagaru would be proud to see me become an engineer. Gopi babayya, Purna atta and Vidu pinni you have been the best family I could ever ask for! Love you all!

And now, to all my friends, who have in fact been more family than friends, you are all amazing human beings! Swetha, Priya and Sultan, what you have done for me has been unparalleled. I cannot ask for anyone else who has gone through so much trouble, pain and trauma for my sake. You three have been my lifeline in the Netherlands and I cannot even imagine a time without you in my life. You have taught me to never give up on someone you love - I love you 3,000 and more! (hope you get what I mean!!!!) And of course, the constant fun, support and amazing trips we've had together all the Homies, you live up to your name! You folks are the best bunch of people!

I have been super lucky to have some human gems back home who have always rooted for me and have been an important part of my life. Without you all, I wouldn't be here, you all drove me out of India! Ram battebaaz ga, nuvvu thope ra! You have been an anchor and a compass for me! Anvita, if I am considered a smart human, you have been the reason I always challenged myself, and mostly, thank you for always being a phone call away and my morning alarm! Vijay and Vijay, you are the two people who have known me since forever. This time biryani is on me. Vaidehi, kutti, I shall not forgive you for stealing my roti! You have been a pillar I never knew I needed. Which city do we meet in next? Samridhi, you've just been a tiny package of fun during my journey of my thesis, thank you for letting me redeem those brownie points! Abdus, thank you for being the bakchod I always keep missing. Kharul, I am going to pronounce your name right one day, thank you for being that daily dose of awesomeness!

Also, I can't express my gratitude to Michelle who has helped me through some quite tough times this year.

And, finally, I bow down to everyone else whom I have had the privilege to know and haven't been able to name, you have all been silent guardians, let's grab a coffee sometime soon!

Contents

List of Figures

List of Tables

1

Introduction

The global challenge of human-induced climate change poses a profound threat to our planet's ecosystems, biodiversity, food security, and overall well-being. With approximately 3.3 billion people residing in regions highly vulnerable to climate change, we stand at a pivotal moment where our actions will determine the trajectory of this crisis. The heavy reliance on fossil fuels, responsible for the majority of greenhouse gas emissions, underscores the urgency for transitioning to cleaner energy sources and exploring innovative technologies. This chapter shall give an insight into the problem and a solution proposed by Zero Emission Fuels B.V. Next, an introduction into the thesis shall be provided.

1.1. Climate Change

The sustenance of all human life, the ecology and biodiversity, food systems, health and wellbeing of all life forms is at the mercy of human-induced climate change. About 3.3 billion people in the world currently live in regions with a high vulnerability to climate change [1]. It is imperative that the global average temperature must not increase above 1.5°C when compared to the global average of pre-industrial revolution levels [2].

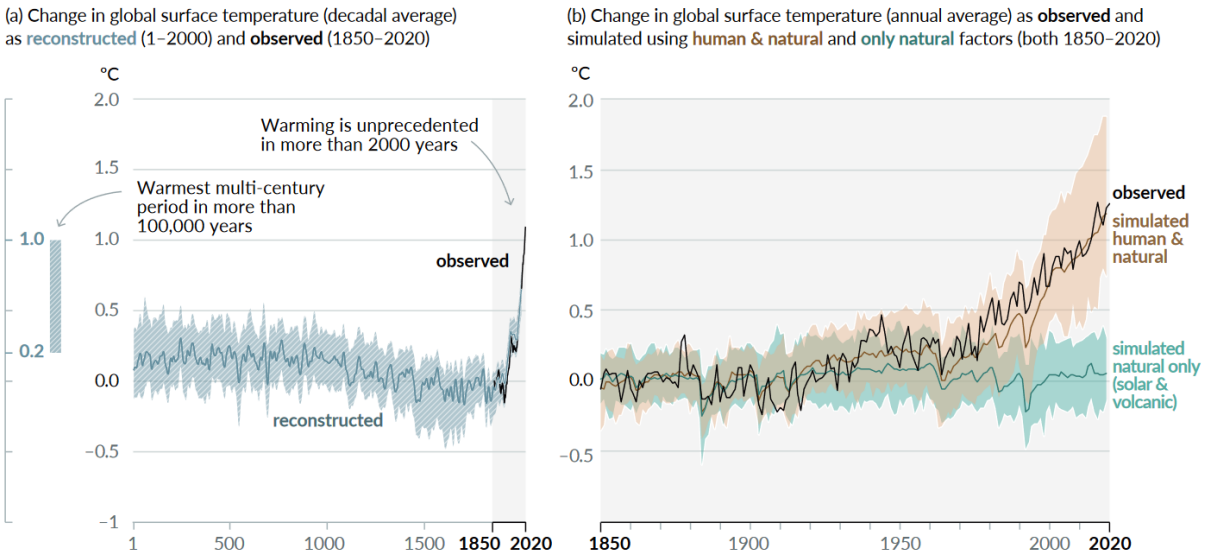

Figure 1.1: Change in global surface temperature reconstructed, observed and simulated. Directly adapted from [3]

It has been established that human-induced climate change is correlated with the increase of greenhouse gases, especially Carbon Dioxide, whose current atmospheric concentration is higher than at any point

of time in the last 800,00 years reaching 409.9 parts per million (ppm) in 2019 [4]. This poses a risk of global average temperatures increasing over 1.5°C and worse, a catastrophic increase to 2°C.

The post-industrial era has been characterized by the increased use of fossil fuels, particularly coal and oil, which release large amounts of CO_2 when burned. The burning of these fuels has caused a steady increase in atmospheric CO_2 concentrations, reaching above 400 ppm for the first time in recorded history in 2013. This increase is alarming because it is well beyond the pre-industrial level of 280 ppm, and it is expected to cause significant global warming and climate change.

The heavy reliance on fossil fuels is the primary driver of CO_2 emissions, which have contributed to the ongoing climate crisis. Burning fossil fuels releases CO_2 into the atmosphere, which traps heat and causes global warming. As the planet warms, it leads to various negative impacts, including sea-level rise, more frequent and intense heatwaves and wildfires, and more severe storms and flooding.

Currently, three fourths of the greenhouse gas emissions are caused by the energy sector [5]. This calls for an immediate requirement for transition to cleaner energy sources. Renewable energy sources, thus, play crucial roles in efforts to de-carbonize energy supplies and mitigate climate change-related negative impacts. Diverse sources are utilized and energy generation is localized in renewable energy systems, thereby reducing transport expenses and long-term price volatility. Now, 19.3% of the world's total energy consumption in 2018 has been supplied by renewables [6].

To combat climate change, urgent action is needed to transition to a low-carbon energy system. This will require a significant shift away from fossil fuels towards renewable energy sources [7]. There are many benefits to transitioning to renewable energy, including reducing greenhouse gas emissions, improving air quality, and reducing dependence on finite resources. Renewable energy sources such as wind and solar can also play a critical role in carbon capture.

1.2. Rectifying Solutions

In the quest for a sustainable and environmentally friendly energy transition, solar fuels have emerged as a critical player. A major challenge in transitioning into a circular and renewable energy economy is storage and transportation [8]. One of the big solutions is to electrify industries using renewable energy. 20% of industrial energy needs are supplied through electricity. 35% is used in the form of feedstock to produce other materials and the remaining 45% is essentially used for industrial processes like heating, drying melting etc [9]. But most of these requirements are not entirely possible to electrify, such as aviation fuel requirements, high temperature heating above 1000°C in industries also cannot be electrified according to the report by Roelofsen et al.

This can be solved by storing the generated energy from renewable energy sources such as solar energy by converting it into chemical energy. Solar fuels are energy-rich fuels generated from an abundant cheap substance such as water or CO_2 using sunlight as the only primary energy input [10]. These fuels are pivotal in addressing the challenges of reducing greenhouse gas emissions, decreasing our dependence on fossil fuels, and achieving a cleaner energy future.

Methanol as an Ideal Solar Fuel

Methanol, in particular, stands out as a promising solar fuel due to several key characteristics. First and foremost, methanol possesses a high energy density of approximately 20.1 megajoules per kilogram (MJ/kg), making it an efficient energy carrier [11]. This characteristic makes methanol an ideal candidate for both energy storage and transportation applications, as it can be easily transported and stored.

Furthermore, methanol holds versatility as a chemical feedstock [12], opening the door to a wide range of synthetic processes and applications beyond its use as a fuel. It can serve as a precursor for various chemicals and materials, contributing to the diversification of sustainable industries. Most prominently Methanol is used as a feedstock to produce kerosene to produce synthetic aviation fuels and Dimethyl ether is used as a cleaner alternative to diesel in buses and trucks. Methanol is also used in multiple industries such as in the production of Acetic acid used from the synthesis of fabrics like polyester to it being a flavouring agent and preservative in food. Methanol is also used in the production of rubber and resins [13].

Carbon Capture-Based Methanol Production via Solar PV
To fully harness the potential of methanol as a solar fuel and contribute to the energy transition [12], it is crucial to consider sustainable production methods. Carbon capture-based methanol production, coupled with solar photovoltaic (PV) technology, presents an essential avenue in this endeavour.

This innovative approach involves utilizing solar PV systems to power the conversion of carbon dioxide (CO_2) into methanol. Carbon capture technologies capture CO_2 emissions from industrial processes or directly from the atmosphere. When this captured CO_2 is combined with hydrogen generated from water electrolysis, using electricity from solar PV panels, it undergoes a transformation into methanol. This process offers a twofold benefit: it reduces atmospheric CO_2 levels, thus mitigating climate change, while simultaneously producing a valuable and versatile energy carrier.

In the larger context of the energy transition, carbon capture-based methanol production via solar PV not only contributes to a sustainable and circular carbon economy but also aligns with the overarching goal of achieving a cleaner, renewable, and economically viable energy landscape. It embodies the spirit of converting a greenhouse gas into a valuable resource while simultaneously powering it with renewable energy sources, thus exemplifying the potential of solar fuels in reshaping our energy future.

1.3. State of the art technologies: Renewable Methanol Synthesis

Methanol has traditionally been produced on an industrial scale using synthesis gas, or ”syngas” [14]. This syngas is primarily derived from non-renewable, unsustainable greenhouse gas-emitting fuels like coal or natural gas. These processes also brought out multiple other by-products apart from methanol. The separation of these coproducts from the desired methanol requires significant energy and cost. However, with an ever-increasing focus on environmental performance, new technologies are emerging to redefine the way we synthesize methanol, reducing its environmental footprint while increasing efficiency.

One groundbreaking approach is the direct hydrogenation of CO_2, which has the potential to revolutionize methanol synthesis [15]. By sidestepping the traditional syngas route, this method holds the promise of not only producing methanol more efficiently but also significantly reducing coproducts and emissions.

One standout example of this innovative approach is Carbon Recycling International’s (CRI) George Olah Plant in Iceland. Fully commissioned in 2012, this facility represents a new frontier in methanol production. It operates using electricity sourced from Iceland’s fully renewable grid, utilizing electrolysis to generate hydrogen. This hydrogen is then combined with locally sourced carbon dioxide from a geothermal power station by consuming 1.4 CO_2 tons per ton of Methanol when compared to the traditional method that emits 4 CO_2 tons per ton Methanol [16]. By tapping into renewable energy sources and minimizing emissions, CRI’s plant sets new standards for environmental responsibility in methanol production. Other emerging plants are also considering the benefits of bypassing traditional steam reformers and adopting similar green hydrogen-based technologies. Northwest Innovation Works (NWIW) in the USA, for instance, is planning to implement this technology in one of the largest methanol plants globally. By adopting these advanced methods, they aim to achieve not only efficiency but also reduce emissions substantially [14].

These projects are still large-scale endeavours which depend on industrial emissions or the grid for their energy supply. To achieve location independence, Direct Air Capture sites have been introduced. Some pioneering companies are Climeworks, Skytree Technologies and Soletair power. Climeworks has developed a delocalised Direct air capture plant, Orca which is powered by Geothermal energy that can capture up to 4000 tons of CO_2 per year[17]. This project is the forerunner of DAC technology in the world. But, it nevertheless lacks flexibility. Flexibility can be achieved through modular DAC systems as developed by Skytree Technologies which builds modular DAC systems for greenhouses and agricultural process [18] while Soletair power delivers HVAC integrated DAC systems for buildings and industries [19]. Both of these technologies are energy agnostic and have not been implemented with a direct connection with renewable energy.

Zero Emission Fuels B.V. (ZEF) is strategically positioned to develop micro-scale renewable methanol synthesis plants through direct air capture and electrolysis of water. ZEF’s approach stands out due to its unique micro-scale production capacity, providing a solution that is both location-independent and off-grid. This innovation harnesses the full potential of renewable energy sources, offering a sustainable and decentralized method for methanol production. As we move toward a greener future, ZEF’s micro-scale

methanol synthesis plants promise to be a game-changer, providing a truly renewable and off-grid solution to minimizing our environmental impact in producing methanol.

1.4. Zero Emission Fuels

Zero Emission Fuels B.V. (ZEF) is a Dutch startup with a mission to develop a standalone micro-plant that produces methanol using solar radiation as its primary energy source. Founded by Jan van Kranendonk, Ulrich Starke, and Hessel Jongebreur in 2017, ZEF is based in TU Delft, leveraging access to lab facilities and expertise. The company's workforce includes a core team of engineers, with each member leading specific subsystems of the micro-plant. A significant portion of ZEF's workforce comprises students at various educational levels who contribute through internships and thesis projects. ZEF follows an iterative approach to product development, starting a new iteration cycle every six months. Each cycle focuses on developing prototypes and subsystem components, incorporating insights from previous iterations and emerging theories.ZEF aims to address the need for renewable and sustainable methanol production, ultimately contributing to a cleaner and more efficient energy future.

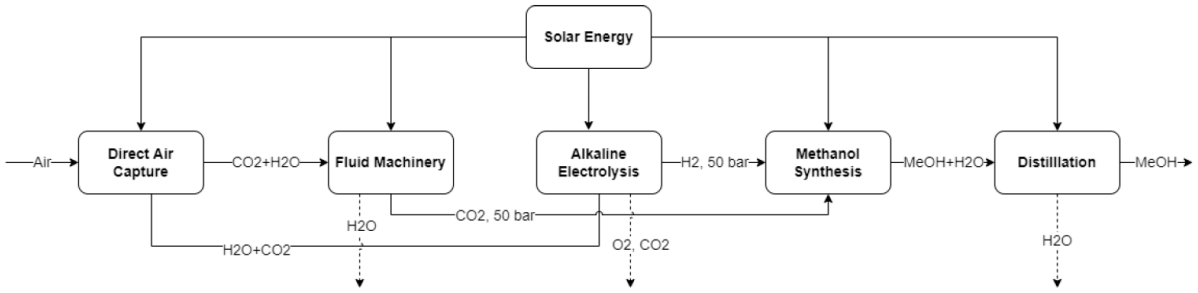

Figure 1.2: The ZEF microplant [20]

Process Methodology (Subsystems): ZEF's methanol production process involves several subsystems as shown in Figure 1.2, each contributing to the overall objective:

- **Photovoltaic Energy (SOL):** Provides the necessary power to operate all subsystems, with solar panels serving as the primary energy source.
- **Direct Air Capture (DAC):** Captures CO_2 and H_2O directly from ambient air using absorption and desorption processes.
- **Fluid Machinery (FM):** Dries and compresses the captured CO_2 to 50 bar for use in the methanol reactor subsystem.
- **Alkaline Electrolysis Cell (AEC):** Splits captured water into its constituents (hydrogen and oxygen) using an alkaline electrolysis process.
- **Methanol Synthesis (MS):** Facilitates the synthesis of methanol from CO_2 and hydrogen.
- **Distillation (DS):** Separates methanol and water, yielding a final product stream of high-purity methanol.

As of now the status of research and development at Zero Emission Fuels provides interesting research gaps. At ZEF, all the subsystems have been developed to various degrees of commissioning readiness. The DAC system has a working prototype while there is research going on to improve the efficiency of the process and sorbent selection. The AEC subsystem has been developed and is currently tackling issues of Hydrogen crossover. The MS subsystem is developed and research is ongoing to improve the process outputs. The DS column is built and is able to deliver Methanol with a purity higher than 98%. The FM system currently requires research into improving the drying system. The system has not been integrated with each other as a single unit until now.

1.5. This Thesis

ZEF aims to build a microplant which would have dimensions about 2m x 1m x 3m (length x breadth x height) which can be productized and scaled up. Additionally, powering the microplant with solar energy

gives an added advantage of the production of Methanol off-grid and in remote locations. This gives the company the freedom to install the microplant anywhere. As mentioned in Section 1.4, a research gap is identified to be the understanding of the behaviour of a fully integrated micro plant. This requires identification and analysis of various system architectures and also to predict the output of the system when connected to a solar PV array.

This thesis is aimed to aid in predicting the methanol production, provide sizing options before productizing a fully functional integrated microplant and gauge the geographic feasibilities of the microplant.

The main research objective of this thesis is:

To build and use a model of an integrated microplant as a tool to predict methanol production and the performance of the microplant under multiple system architectures.

In order to achieve this there are sub-objectives which would be

- **Research sub-objective 1:** Build a roadmap outlining the research procedure.
- **Research sub-objective 2:** Model each subsystem.
- **Research sub-objective 3:** Design the control algorithms and integrate the model.
- **Research sub-objective 4:** Analyse the microplant behaviour and predict the Methanol yield by implementing a cost-effective microplant system architecture at various geographic locations.

2

Theoretical Background

This chapter gives the theoretical background to understanding the working principles and theory behind the operations of all the subsystems.

2.1. Subsystems

2.1.1. Solar PV

The objective of modelling a solar PV module is to accurately predict its electrical output, primarily consisting of the key parameters V_{mpp} (Voltage at Maximum Power Point), I_{MPP} (Current at Maximum Power Point), and P_{mpp} (Power at Maximum Power Point) based on the weather data provided. These parameters are crucial to estimate the power input to the microplant and to charge the battery. Achieving this involves a series of steps, including determining the optimal module tilt, calculating the plane of array (PoA) irradiance, finding the module temperature, and finally, evaluating the electrical properties.

Optimum Module Tilt

The optimal module tilt plays a pivotal role in optimizing the energy capture of a solar PV module. To find the optimal tilt, especially for a single-axis PV tracker, it is essential to determine the position of the sun throughout the day. This involves calculating two key angles: altitude and azimuth of the sun and involves complex astronomical calculations that account for the module's geographic location and the time of day based on the methods in the Solar Energy textbook [21]. A fixed ground-mounted system is also being modelled where the optimal module tilt is given in Equation 2.1 where θ_m is the optimal module tilt angle and lat is the latitude in degrees [22].

$$\theta_m = 0.76lat + 3.1° \tag{2.1}$$

Plane of Array Irradiance

The plane of array (PoA) irradiance is a critical factor in determining the energy output of a solar PV module. It represents the total solar radiation incident on the module's surface. The PoA irradiance is composed of three main components: G_{direct} (direct normal irradiance), $G_{diffuse}$ (diffuse irradiance), and $G_{reflected}$ (reflected irradiance) given by Equation 2.2.

$$\begin{aligned} G_{dir} &= DNI \times \cos(\theta_M) \\ G_{diff} &= \text{DHI}\left(\frac{1+\cos(\theta_M)}{2}\right) + GHI\left(0.012\,(90-\theta_M)\,\frac{(1-\cos\theta_M}{2}\right) \\ G_{ref} &= GHI \times albedo + \left(\frac{1+\cos(\theta_M)}{2}\right) \end{aligned} \tag{2.2}$$

The G_{dir} component represents the direct sunlight that reaches the module without scattering. Diffuse irradiance (G_{difF}) is the sunlight scattered by the atmosphere which is calculated by using the simple Sandia sky diffuse model [23]. Reflected irradiance (G_{ref}) is the sunlight that strikes the module after being reflected from nearby surfaces. It is influenced by the albedo of the surrounding environment, which is the ratio of reflected solar radiation to total incoming solar radiation. Various surfaces have different albedo values, and this component can significantly affect module performance.

Module Temperature
The temperature of the solar PV module has a substantial impact on its electrical performance. Higher temperatures generally lead to reduced efficiency. There are three widely used models for calculating module temperature. First, the Simple Steady State Model calculates module temperature based on a simplified energy balance equation. It assumes steady-state conditions and provides a quick estimation of module temperature. Second, the Duffie-Beckman Model is more comprehensive and considers the impact of wind, including conduction, convection, and radiation. It is more accurate than the simple steady-state model and is often used for detailed simulations. Third, the Fluid Dynamic Model using methods outlined in the textbook [21], accounts for the conduction, convection and radiation effects to calculate the model temperature.

$$T_M = T_{amb} + \frac{T_{NOCT} - 20^\circ}{800} G_{aoi}$$
$$T_M = T_{2mb} + \frac{T_{NOCT} - 20^\circ}{800} G_{20i} \left(\frac{9.5}{5 \cdot 7 + 3 \cdot 8\omega} \right) \left(1 - \frac{\eta_{cell}}{T\alpha} \right) \tag{2.3}$$

Electrical Properties
Finally, to predict the electrical output of a solar PV module, the effects of irradiance and temperature must be considered. The following parameters are crucial. Open-circuit voltage (V_{oc}) decreases as temperature increases, and it increases with irradiance. Short-Circuit Current (Isc): Isc is directly proportional to irradiance and decreases with rising temperature. It can also be estimated using empirical equations. Maximum Power Point (MPP): The power at the maximum power point (Pmpp) depends on both irradiance and temperature effects. It is crucial for assessing the overall performance of the solar PV module. The V_{mpp} and I_{mpp} are finally calculated by using the methods described in the research by Boke [24].

Accurate predictions of Vmpp, Impp, and Pmpp require a thorough understanding of the module's parameters based on the module specification sheets and the local environmental conditions, and the interplay between irradiance and temperature effects on electrical properties.

2.1.2. Direct Air Carbon Capture

Direct air carbon capture can be defined as capturing CO_2 directly from the ambient atmosphere [25]. Direct Air carbon capture has several advantages. DAC can potentially reduce emissions that are difficult to avoid or legacy emissions. DAC has the advantage of flexible siting constraints as it does not cater towards point sources of CO_2, hence catering towards location independence. This is because the concentration of CO_2 is infinite and mostly uniform at 400 ppm. DAC gives an opportunity for a focus on process efficiency instead of volume captured [26].

The DAC process occurs in two stages, namely absorption and desorption (or stripping).

In the ZEF DAC subsystem, once the sorbent absorbs CO_2 and H_2O, the rich sorbent is pumped into the stripper at a higher temperature where it undergoes a regeneration process.

Sorbents
CO_2 is captured by processes based on the exothermic reaction of absorption by allowing atmospheric air to pass over sorbents, either solid or liquid. The sorbents are usually amines such as Tetraethylenepolyamide (TEPA), Diethanolamine(DEA) or other sorbents such as Potassium Hydroxide (KOH) [27]. In the absorber column, ambient air at atmospheric pressure encounters a CO_2 lean sorbent. It is at this moment that Carbon dioxide and water are absorbed by the sorbent. This sorbent which now has a higher concentration of CO_2 is now called the rich sorbent is further sent into the stripper column where the endothermic regeneration process occurs. In addition, a sorbent requires high CO_2 capacity, fast reaction kinetics, low volatility and low viscosity, and high thermal stability among others [28].

In addition to the sorbent, a diluent is used which plays an important role in reducing the viscosity of the the rich sorbent.

Absorption Column
In this column, lean sorbent is mixed with an incoming stream of ambient air. The absorption occurs when the Hydrogen atoms are replaced by CO_2. The absorption process occurs in four steps [28]:

- Diffusion of carbon dioxide from the ambient gas at the gas-liquid interface through Fick's first law of diffusion [28].
- Dissolution of Carbon dioxide in the thin film through Henry's law.
- The chemical absorption of the amine groups present in the sorbent where primary and secondary amines react with CO_2 to form Carbamates and tertiary amines react with CO_2 to form bicarbonates.
- Diffusion of the reacted compounds into the bulk of the liquid sorbent again through Fick's law.

Stripping Column
In the stripping column, the desorption or the regeneration of the sorbent takes place through an endothermic process. Heat hence is provided to convert the Carbamates and Bicarbonates present in the rich sorbent to release CO_2 and H_2O. Fick's law governs the diffusion of water and carbon dioxide into the gas-liquid interface. In the ZEf stripper column, the rich sorbent is loaded from the top and flows downwards through a series of packing materials. The energy required for the desorption is provided at the bottom of the column at the reboiler.

It is hence in the stripper column that consumes most of the energy supplied DAC. This demand occurs due to the following processes.

- **Sensible heat:** The thermal energy that is required to heat the incoming feed up to the desorption temperature is the Sensible heat demanded [29].

$$Q_{sensible} = \dot{m} C_p (T_{desorption} - T_{feed,in}) \tag{2.4}$$

- **Heat of Absorption:** This is the energy required for the desorption of CO_2 from the carbamates and bicarbonates. This heat depends on the CO_2 loading [30].
- **heat of vaporization:** It is the energy required for the phase change from liquid water to vapour which is higher than the heat of vaporization of pure water. This data is available from previous experiments performed at ZEF [31].

External parameters
The DAC subsystem is the only subsystem that is dependent on meteorological data or external weather parameters, which introduces the most dynamics into the process. This is because the absorption of CO_2 and H_2O depends on the ambient temperature and absolute humidity.

Absolute humidity plays a pivotal role in the performance and efficiency of the Direct Air Capture (DAC) process. The presence of moisture within the ambient air significantly enhances the DAC performance by increasing its loading capacity [32] because of the reduction in viscosity and the promotion of hydronium carbamate and carbamic acid formation, thereby enhancing amine efficiency.

Temperature, another critical external parameter, exerts substantial influence over DAC. While thermodynamics favour CO_2 absorption at lower temperatures due to the exothermic nature of the absorption reactions, the practicality of DAC is hindered by reduced diffusion rates associated with higher viscosity at lower temperatures [33].

These factors go on to say that the higher the CO_2 absorption, due to higher humidity or a lower temperature, the energy demand during desorption is increased due to an increase in the heat of vaporisation and the heat of absorption.

2.1.3. Fluid Machinery

The fluid machinery (FM) subsystem at ZEF has a two-fold functionality. The first, being the dehumidification of the CO_2 stream and the second is the compression of the dried CO_2 from ambient pressure up to approximately 50 - 55 bar.

The compression process in general is considered to be adiabatic or isentropic. This implies that there is no heat exchange between the compressor and the environment. But this generally not the case as there is not enough time for adiabatic heat exchange to take place[34]. Hence, the polytropic index γ_c is used which is equal to 1 for an isothermal process and 1.28 for an adiabatic process to compress CO_2 at 70°C. Hence, the work done by the compressor is calculated by the polytropic compression equation Equation 2.5 [20].

$$W_{\text{comp}} = \frac{\dot{m}_{cmpr}}{\eta_{cmpr}} \left[\frac{\gamma_c}{\gamma_c - 1}\right] \frac{P_1}{\rho_1} \left[\left(\frac{P_2}{P_1}\right)^{\gamma_c - 1/\gamma_c} - 1\right] \tag{2.5}$$

Where T_1 and T_2 are the compressor inlet and outlet temperatures respectively. P_1 and P_2 are the compressor inlet and outlet pressures respectively. $\dot{m}_{cmpr}$ and η_{cmpr} are the mass flow rate and compressor efficiency while ρ_1 is the density at the compressor inlet.

The outlet temperature can be calculated by using Equation 2.6

$$T_2 = T_1(\frac{P_2}{P_1})^{\frac{\gamma_c - 1}{\gamma_c}} \tag{2.6}$$

The ZEF fluid machinery system
The CO_2 stream, when initially captured from the DAC subsystem, can contain often up to approximately 5% of water vapour depending on operating conditions. The presence of water vapour in the CO_2 stream can have detrimental effects on the entire CCS system, including pipelines, compressors, and lubricants. At ZEF, silica gel-based adsorption separation method is used for dehumidification.

Once the CO2 stream is effectively dehumidified, it proceeds to the compression system within the FM subsystem. This high-pressure CO2 is subsequently stored in a buffer tank before being supplied to the Methanol Synthesis (MS) subsystem.

2.1.4. Alkaline Electrolysis

Electrolysis is a fundamental electrochemical process that plays a crucial role in ZEF's process flow to produce Hydrogen as a feedstock for the methanol synthesis subsystem by using the water supplied from the DAC subsystem. Alkaline electrolysis uses Hydroxide ions (OH^-) ions as charge carriers in the process and with Potassium hydroxide (KOH) as the electrolyte. The fundamental equation for electrolysis is shown in Equation 2.7. This reaction represents the decomposition of water into its constituents: hydrogen gas (H_2) at the cathode and oxygen gas (O_2) at the anode within the electrolytic cell.

$$2H_2O_{(aq)} \rightarrow 2H_{2(g)} + O_{2(g)} \tag{2.7}$$

$$2H_2O_{(aq)} + 2e^- \rightarrow H_{2(g)} + 2OH^-_{(aq)}[Cathodic, (H_2)] \tag{2.8}$$

$$4OH^-_{(aq)} \rightarrow 2H_2O_{(aq)} + O_{2(g)} + 4e^-[Anodic, (O_2)] \tag{2.9}$$

First, at the negative cathode (Equation 2.8), the Hydrogen evolution reaction (HER) occurs where water is reduced to form hydrogen gas and hydroxide ions. Next, these negatively charged OH^- ions (charge carriers) move through the electrolyte through the separating diaphragm towards the positive anode. These OH^- ions are oxidised at the anode to form Oxygen and water in what is called the Oxygen evolution reaction (OER) [35].

To calculate the amount of substance produced at an electrode ($n_{produced}$) can be calculated using Faraday's law of electrolysis, as expressed by the equation:

$$n_{produced} = \frac{It}{zF} \tag{2.10}$$

Where, I is the current passed through the cell, t is the time duration that the current was passed, z is the number of moles of electrons exchanged during the reaction and F is Faraday's constant which is equal to 96500 [Coulombs/mol].

The performance of the electrolysis cell can be determined by calculating the efficiency of the stack by the Equation 2.11. The efficiency can be defined as the energy required under reversible conditions over the energy used by the system in reality [36].

$$\eta_{aec} = \frac{V_{reversible}}{V_{reversible} + Losses} = \frac{1.23}{V_{AEC}} \tag{2.11}$$

Where V_{AEC} is the voltage supplied to the stack while $V_{reversible}$ is the equilibrium cell voltage. This is also called Faradic efficiency. This includes all the losses in the system such as the overpotentials at the cathode, and anode and also the ohmic losses present in the stack [37]. The effect of the potential drawn by the stack is shown in Figure 2.1.

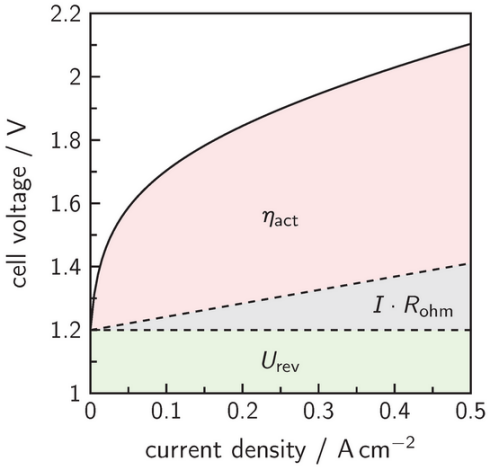

Figure 2.1: The voltage of an alkaline electrolyzer at 60°C vs. the current density. η_{act} is the total activation overvoltage of the cathode and the electrode, $I.R_{ohm}$ constitutes the ohmic losses and U_{rev} is the reversible cell voltage[37].

The ZEF Electrolyzer
The ZEF AEC subsystem performs the following processes.

- The electrolyzer stack is the most important aspect of the subsystem. The stack consists of a series of cells with separating membranes in between. On one side of the stack, Hydrogen is produced and on another, oxygen.
- The pressure booster increases the pressure of water from the buffer tank to the operating pressure of the AEC stack to minimize the complexity of pressurizing gases for further downstream requirements.

2.1.5. Methanol Synthesis

Methanol is mainly produced via CO_2 hydrogenation at ZEF [38]. Production of Methanol from CO_2 and H_2 is highly exothermic and can be formed due to the reactions as mentioned below.

$$CO_2 + 3H_2 \rightleftharpoons CH_3OH + H_2O \Delta H_{298K} = [-49.2kJ/mol] \tag{2.12}$$

$$CO_2 + H_2 \rightleftharpoons CO + H_2O \Delta H_{298K} = +40.6[kJ/mol] \tag{2.13}$$

$$CO + 2H_2 \rightleftharpoons CH_3OH \Delta H_{298K} = -90.8[kJ/mol] \tag{2.14}$$

CO_2 hydrogenation (Equation 2.12), being an exothermic reaction is favourable at low temperatures and at high pressures. But, this process is thermodynamically limited due to the inertness of CO_2 [39]. At higher temperatures, there is a possibility of the Water Gas Shift (WGS) reaction as shown in Equation 2.13 to occur where CO, an undesirable by-product is formed which is endothermic in nature. This is then followed by the exothermic hydrogenation of CO as seen in Equation 2.14.

Since all the above equations are equilibrium reactions, they follow Le Chatelier's principle [40]. In Equation 2.12 and Equation 2.14 if the reaction temperature declines, the reaction deviates from equilibrium leading to more methanol production. With an increase in pressure, the equilibrium would respond by trying to reduce the pressure and hence favour methanol synthesis. At around 240°C, CO_2 activation and methanol formation are promoted. Thus, methanol synthesis is performed at higher pressures and moderate temperatures.

2.1.6. Distillation System

Distillation is a process of separating two liquids based on the boiling points of the liquids to create two phases. This occurs when one of the liquids is comparatively more volatile and vaporises into the vapour phase. This concept is explained in the Vapour-Liquid equilibrium (VLE) curve as shown in Figure 2.2.

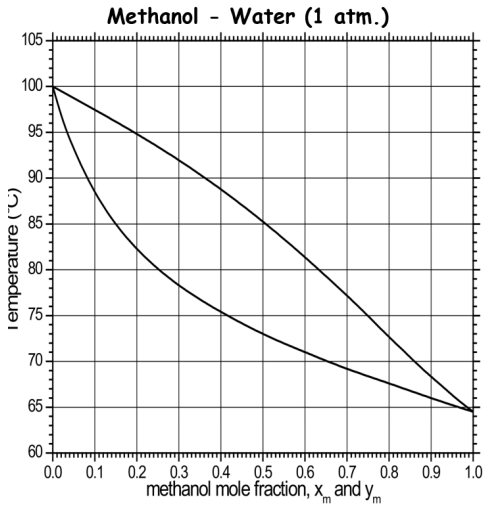

Figure 2.2: Methanol water VLE curve at 1 atm [41]

The VLE curve shows the relationship between the composition of a liquid mixture of Methanol and water and the composition of the vapor in equilibrium with it at a given temperature. The above curve depicts the dew point curve which shows the temperature at which the vapour mixture needs to be cooled to form the first drop of liquid and the one below is the bubble point curve shows the temperature at which the first bubble is formed [42]. The vapour liquid phase occurs between these two lines. At any given temperature a mole fraction of Methanol will be in the vapour phase and the rest will be in the liquid phase

The ZEF distillation column a continuous distillation column with packing material is used while the reboiler is located at the bottom of the column and the condenser in the top with a manually controlled reflux setup.

2.1.7. Battery

Currently, the ZEF microplant does not use batteries as an energy storage mechanism. It is hence, needed to understand the aspects of a battery system that shall be used.

The battery capacity can be calculated by the Equation 2.15.

$$Q_{bat} = I_{bat} \times T = \int_0^T I(t)dt \tag{2.15}$$

Where, Q_{bat} is the capacity of the battery in Ampere-hours, I_{bat} is the rated current during charge and discharge in hours [43]. The capacity can be calculated in Watt-hours once the operating voltage of the battery is known. The voltage of a battery varies based on the remaining capacity or the depth of discharge. The typical discharge pattern can be seen in Figure 2.3.

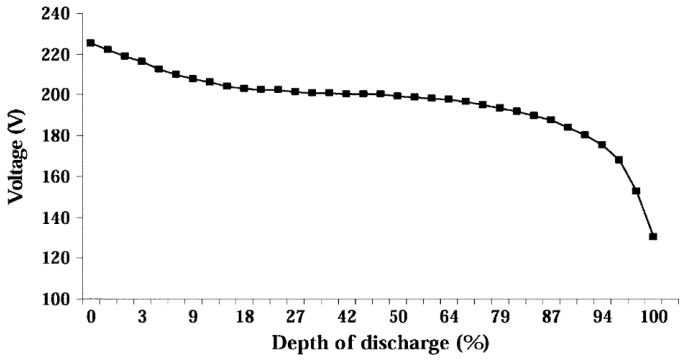

Figure 2.3: A typical battery discharge pattern [44]

It is evident that the Voltage drops steeply when the battery is almost completely charged or almost completely discharged. This implies that the overall capacity of the battery depends on the voltage.

Batteries also have several key features which are important in building a model. The state of charge (SoC) reflects the current relative capacity of a battery [45]. The battery is fully charged when the SoC is 100% and when it matches the rated charging capacity. The depth of discharge (DoD) is complementary to the state of charge which indicates the amount of capacity that has been utilized by the battery. The SoC and the DoD can be calculated based on the equations below:

$$\begin{aligned} SoC_t &= \frac{Q_{remaining}(t)}{Q_{max}(t)} \times 100\% \\ DoD_t &= \left[1 - \frac{Q_{remaining}(t)}{Q_{max}(t)}\right] \times 100\% \end{aligned} \tag{2.16}$$

The performance of batteries can be found based on their efficiencies. There are two efficiencies which are integral to understanding battery performance. Coulombic efficiency ($\eta_{coulombic}$) quantifies the ratio of the discharge capacity ($Q_{discharge}$) after the full charge and the charging capacity (Q_{charge}) of the same cycle. Voltaic efficiency ($\eta_{voltaicic}$) depicts the electrical energy delivered ($Q_{delivered}$) to the energy supplied ($Q_{supplied}$) to the battery [43]. The overall efficiency of a battery can hence be calculated by Equation 2.17.

$$\begin{aligned} \eta_{coulombic} &= \frac{Q_{discharge}}{Q_{charge}} \times 100\% \\ \eta_{voltaic} &= \frac{Q_{delivered}}{Q_{supplied}} \times 100\% \\ \eta_{battery} &= \eta_{coulombic} \times \eta_{voltaic} \end{aligned} \tag{2.17}$$

2.2. Data Sourcing

The thesis requires weather data for the duration of an entire year. This data can be accessed from multiple sources out of which three prominent sources are mentioned here, Meteonorm, SolarGIS and Copernicus Climate Change Service (C3S).

Meteonorm:
Meteonorm is a free/paid service which can provide weather data explained in Section 3.1 with a temporal resolution of sub 1-hour steps for one year. The service compiles data from a vast network of weather stations an satellite-based data sets. The service is limited in the free version with access to only a few locations.

SolarGIS:
SolarGIS specialises in solar radiation data with higher accuracy than the other models explained. This is a proprietary source which is expensive if access is required for multiple locations. This service can also provide sub 1-hour data for a few parameters depending on the location and data availability.

C3S:
The C3S data set is an open-access climate and weather data repository which is especially useful for the European region which is also the main area of interest in this thesis [46]. The dataset uses ERA5 hourly reanalysis data for solar irradiance and other weather parameters.

For this thesis, the Copernicus ERA5 hourly data has been chosen for its versatility with unlimited access to location data across the globe and high accuracy in European regions.

3

Modelling Roadmap

This chapter explores the modelling approach used for the time series model of solar PV and its integration with the ZEF microplant and its subsystems for methanol production. The tool developed is able to simulate Methanol production in different locations in Europe without having to change the system architecture. This chapter reflects on the research sub-objective 1: Build a roadmap outlining the research procedure.

The modelling approach requires three steps to be performed. Firstly, the preprocessing step deals with data collection and data preparation. Secondly, the building the model step entails building subsystem models, integrating the subsystems and developing a control algorithm. Finally, in the Simulation step, multiple simulations of the model are performed and insights are gleaned.

The model functions on two distinct levels, namely power balance and mass balance, each of which plays a crucial role in achieving the desired result.

Each time step requires the application of constant power and weather values, thus simulating actual conditions.

3.1. Pre processing

By assuring the readiness and quality of input data (weather data and physical parameters for subsystems), the pre-processing phase plays a crucial step in the development of an accurate and dependable model. This phase includes two essential tasks: importing data and data preparation. This section examines these tasks and emphasizes their importance in modelling.

3.1.1. Importing Data

The first task in the pre-processing phase involves importing relevant data that serves as the foundation for the model's analysis and simulation since data plays a crucial role in capturing the temporal dynamics of various parameters. In this thesis, data was obtained from the "Copernicus ERA5 hourly data on single levels from 1940 to the present" database [46], a trustworthy repository of environmental reanalysis data. The retrieved data from the Copernicus database consists of the following variables:

- Latitude (lat)
- Longitude (lon)
- Time (t) [hours]
- Dew point temperature (T_{dew}) [K]
- Ambient temperature (T_{amb}) [K]
- Ground surface temperature (T_{gr}) [K]
- Windspeed at 10m (v_{10m}) [m/s]
- Albedo (A)
- Ambient surface Pressure (P) [Pa]
- Global Horizontal Irradiance (GHI) [W/m^2]

- Direct Normal Irradiance (DNI) [W/m^2]

This data, collected at one-hour intervals, provides a comprehensive depiction of the altering environmental conditions influencing the system under investigation.

3.1.2. Data Preparation

Once the data is imported, it needs to be processed before using it in the simulation phase. There are two aspects of data preparation.

Firstly, the one-hour time steps may not be an accurate representation of real-world weather conditions which are constantly varying. This can be processed by interpolating data for the estimation of values at specific time intervals (< 60 minutes) that might not have direct measurements, ensuring continuity and uniformity in the time series. The data has been linearly interpolated between each time step. This does not account for a few weather events such as cloud cover and rainfall.

Secondly, the data imported must be useful parameters that are used by the model. The model requires wind speed at 2 meters (input for Solar PV subsystems) and absolute humidity (input for DAC) which is not available directly in the Copernicus database.

The wind speed at 2 meters is calculated using the logarithmic wind profile from v_{10m} at a reference height of 10 meters.

$$v(h) = v\left(h_{\text{ref}}\right) \frac{\ln\left(\frac{h}{z_0}\right)}{\ln\left(\frac{h_{\text{ref}}}{z_0}\right)} \tag{3.1}$$

Where,
$v(h)$ = wind velocity at height h [m/s]
$v(h_{\text{ref}})$ = Wind velocity at reference height [m/s]
h_{ref} = 10 [m]
h = 2 [m]
z_0 = surface roughness length = 0.2 [m]

To calculate the absolute humidity, the saturation and partial pressure of water vapour need to be calculated using the Tetens equation.

$$\begin{aligned} P_{sat} &= (0.61078 \times e^{\frac{17.27\times(T_{amb}-273.15)}{T_{amb}}}) \times 10 \\ P_{real} &= (0.61078 \times e^{\frac{17.27\times(T_{dew}-273.15)}{T_{dew}}}) \times 10 \end{aligned} \tag{3.2}$$

$$RH = \frac{P_{real}}{P_{sat}} \tag{3.3}$$

Where,
P_{sat} = Saturation pressure [mbar]
P_{real} = Partial pressure of water vapour[mbar]
RH = Relative humidity

The absolute humidity (AH) is calculated using the following formula in gram/m^3.

$$AH = \frac{P_{real}}{461.5 \times T_{amb}} \times 1000 \tag{3.4}$$

Now, the data is ready to be used as inputs to the model.

3.2. Building the Model

The simulation phase represents the heart of a model's functionality through the execution of two interconnected tasks: subsystem modelling and control algorithm design. The entire model would be programmed using MATLAB and COCO simulator.

3.2.1. Subsystem modelling

The subsystem modelling task entails utilizing energy captured from the converter to power the model's various subsystems. This task encompasses the fundamental functionalities of the various subsystems, including Direct Air Capture (DAC), Alkaline Electrolysis Cell (AEC), Methanol Synthesis (MS), and Methanol Dehydration (DS). Importantly, the process simulation must adhere to mass balance principles, ensuring that each subsystem's consumption and production of materials are in equilibrium.

$$\begin{aligned} m_{CO2,DAC} + m_{H2O,DAC} &= m_{stored} + m_{vented} + m_{waste} + m_{Methanol,DS} \\ m_{waste} &= m_{O2,AEC} + m_{H2O,DS} \end{aligned} \tag{3.5}$$

The above equation expresses the fundamental mass conservation in the model. The mass of Carbon dioxide($m_{CO2,DAC}$) and water ($m_{H2O,DAC}$) produced by the DAC subsystem is conserved by the mass stored in all the subsystems (m_{stored}), the mass vented from the buffer tanks (m_{vented}), the waste products ($m_{Methanol,DS}$) and finally, the mass of methanol ($m_{Methanol,DS}$)produced by the DS subsystem.

3.2.2. Integrating the model

The integrating the model sub-step is a bridge between all the subsystems over which the controller can perform. This step focuses on building multiple system architectures to work under different weather and geographical constraints. These microplant architectures are important to understand the behaviour of the microplant and its response to predict methanol outputs.

3.2.3. Control algorithm design

The control simulation task regulates the allocation of power input from the solar PV or battery to each subsystem concurrently with the process simulation. This decision-making process distributes energy to the subsystems to ensure optimal performance. The control mechanism adjusts the power supplied to each subsystem in response to environmental conditions and system states, among other variables. This adaptability enables the model to dynamically respond to changes in external conditions and internal requirements.

3.3. Simulation

The "Delivering Insights" phase of the system involves extracting valuable data from the simulation model, providing a comprehensive comprehension of the microplant's behaviour and dynamics, and facilitating well-informed decision-making. This phase includes two important aspects that significantly contribute to the model's behaviour and feasibility evaluation.

3.3.1. Model behaviour

The initial portion of this phase is devoted to dissecting the microplant's performance and evaluating various system architectures. This phase sheds light on how the system responds to different inputs and scenarios by simulating the microplant under various conditions. It permits a thorough analysis of the microplant's behaviour, performance trends, and the efficacy of various control mechanisms in optimizing its operations.

In addition, this phase investigates the effect of time step intervals on the accuracy and real-time applicability of the model. To evaluate the model's validity at different temporal resolutions, the simulation is conducted with variable time step lengths. This evaluation helps determine the optimal time step duration that strikes a balance between computational efficiency and precision, ensuring the model's dependability in real-time scenarios.

In addition, the "Model performance" step addresses the difficulties associated with system component sizing. This entails determining the appropriate capacities for subsystems, converters, and storage units to meet operational requirements in the actual world. This phase guides the implementation of functional real-time microplants capable of handling dynamic energy inputs and consumption by simulating the microplant's performance with varying component sizes.

In parallel, this phase includes experiments to determine the system's seasonal and daily responses. The simulation model is subjected to various meteorological conditions in order to capture variations in

solar irradiance, temperature, and other parameters. This analysis provides insight into the adaptability, resiliency, and potential vulnerabilities of the microplant under various environmental conditions.

3.3.2. Microplant Location-based analysis

This phase's second aspect focuses on financial viability and practicability. The simulation model is used to simulate a variety of scenarios by employing multiple system architectures in diverse geographical locations. This enables a comprehensive evaluation of the economic viability of the microplant, taking into consideration capital costs, operational expenses, and potential methanol production revenue.

The financial analysis conducted during this phase contributes to the recommendation of the Zero-Emission Fuel (ZEF) microplant's capital cost evaluation. It helps decision-makers comprehend the investment cost per Kg of Methanol. This analysis aids in making well-informed decisions regarding the deployment of microplants by investigating various scenarios and geographical locations.

3.4. Summary

- The model and simulation shall entail the preprocessing, building the model and simulation steps.
- The modelling roadmap has been laid down in this chapter and has achieved the research sub-objective 1: Build a roadmap outlining the research procedure.
- Further, it is necessary to build the subsystems for the microplant.

4

Modelling Subsystems

This chapter discusses the microplant ZEF modeling work. By the end of the chapter, the Research sub-objective 2: ”Model each subsystem”, shall be achieved. The following sections delve into the model characteristics, and performances.

4.1. Solar PV

The solar PV subsystem has been modelled to use weather and irradiance data and provide the output power supplied.

Model Assumptions

- The solar PV system assumes there are no shading effects.
- The irradiance is assumed to be equal on all modules.
- Cloud conditions and other weather effects have not been included

Model Inputs and Outputs

The Solar PV requires the following inputs

- **Ambitent temperature:** The ambient temperature is required to calculate the module temperatures.
- **Ground surface temperature:** This impacts the module temperatures and the overall performance of the PV module.
- **Wind speed:** The wind speed is an important factor while considering the module temperature based on the chosen module temperature model explained in Chapter 2.
- **Albedo:** Albedo impacts the amount of reflected irradiance onto the solar panel.
- **GHI:** The total solar irradiation on the surface including both the direct and diffuse irradiation components
- **DNI:** The Direct Normal Irradiance is the directly received solar irradiation received on the surface.

The Solar PV requires the following outputs:

- **Maximum power point Voltage:** The voltage of the PV system at the maximum power point.
- **Maximum power point Current:** The current of the PV system at the maximum power point.
- **Maximum power:** The power output of the PV system at the maximum power point.

Table 4.1: Input/output parameters for the Solar PV subsystem

Symbol	Input Parameters	Unit	Symbol	Output Parameters	Unit
T_{amb}	Ambient temperature	[K]	V_{MPP}	Voltage at MPP	[Volts]
T_{gr}	Ground surface temperature	[K]	I_{MPP}	Current at MPP	[Amp]
v_{wind}	Wind speed	[m/s]	P_{MPP}	Power at MPP	[Watts]
A	Albedo	[-]			
GHI	Global Horizontal Irradiance	[W/m^2]			
DNI	Direct Normal Irradiance	[W/m^2]			

Model Description

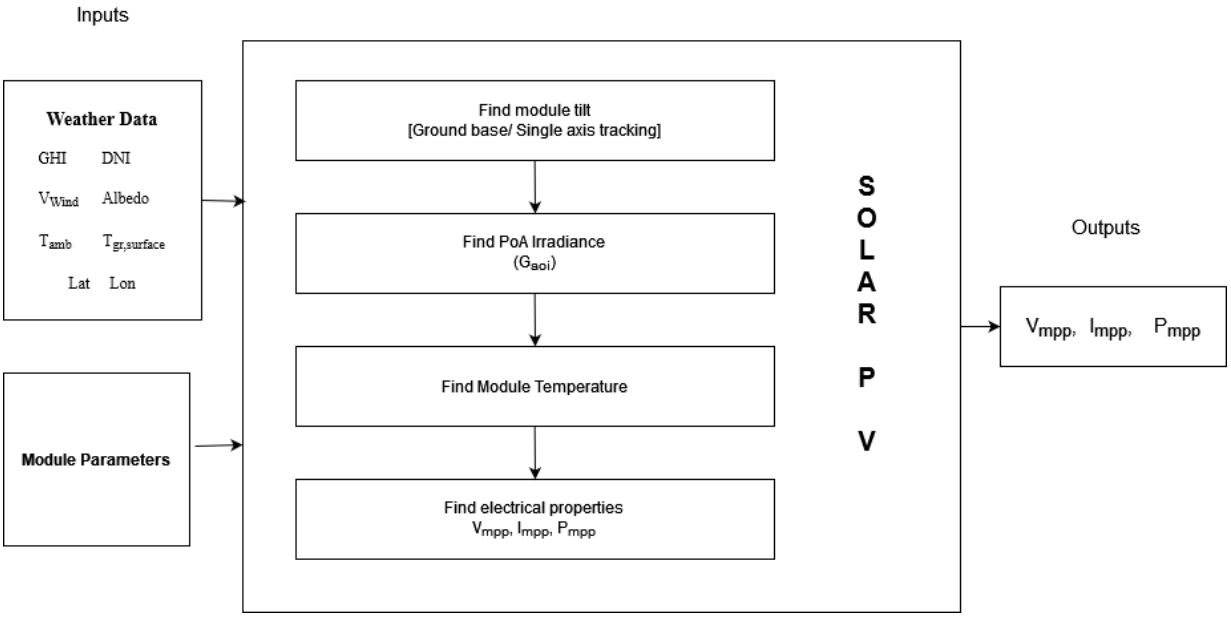

Figure 4.1: Solar PV model schematic

The purpose of the Solar PV model is to predict the Power output and V-I characteristics based on irradiance, temperature, location data and other module parameters from the specifications sheet. These calculations have been possible by performing the following steps.

Find module tilt: The solar PV module tilt is calculated in two steps. First, the altitude and azimuth angles of the sun are calculated over the duration of the data set based on geographic coordinates.Next, the module orientation is found for each time step based on a ground-mounted system and a single-axis PV tracker.

The solar PV subsystem generates the DC power that is distributed to the microplant. The electrical DC yield depends on two components, being irradiance and module temperature.

Plane of Array Irradiance: This is calculated at the angle of incidence by calculating the direct(G_{dir}), diffuse (G_{diff}) and reflected (G_{ref}) irradiance which uses the albedo values from the Copernicus database. This is performed by the following equation.

$$G_{aoi} = G_{dir} + G_{diff} + G_{ref} \tag{4.1}$$

The solar irradiance at the angle of plane of array incidence at the location intended as can be seen in Figure 4.5.

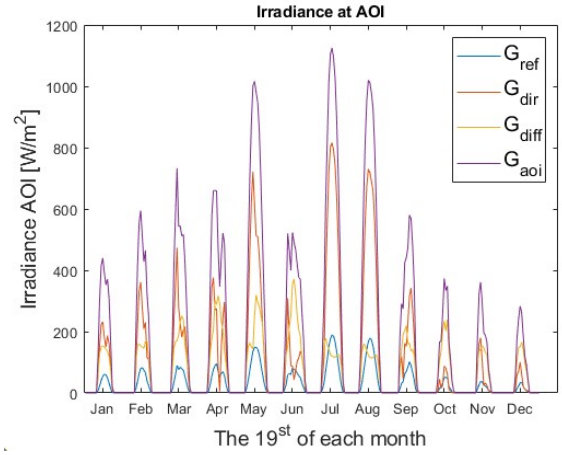

Figure 4.2: Solar PV irradiance

Module Temperature: It is then important to calculate the module temperature. Three models were used, the linear model, the Duffie-Beckman temperature model and the fluid-dynamic model. Figure 4.3 shows the difference between the module temperature and the ambient surroundings.

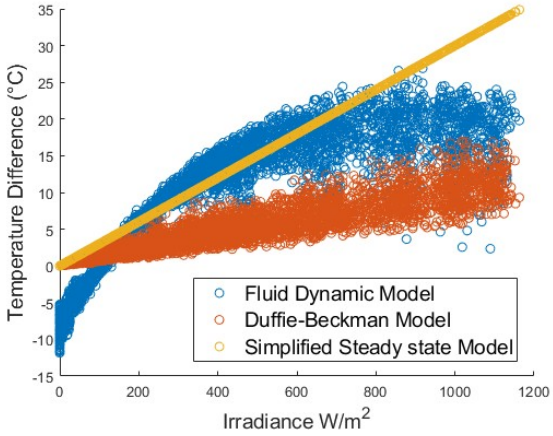

Figure 4.3: Difference between module temperature T_{module} and ambient temperature T_{amb}

The fluid dynamic model has been chosen for further calculations as it also considers other variables like wind speed, ground surface temperature and air temperature. Further fluid mechanic model is predicted to give improved temperature results, especially in early mornings and late evenings over steady state model [47].

Find electrical properties: The open circuit voltage and short circuit current are calculated based on irradiance and module temperature effects. The Maximum power point tracking was implemented by using the parameters given in on the solar PV specification sheet [24]. The calculation of both T_{module} and G_{aoi} gives us the maximum power point. The relation between the three parameters is shown in Figure 4.4.

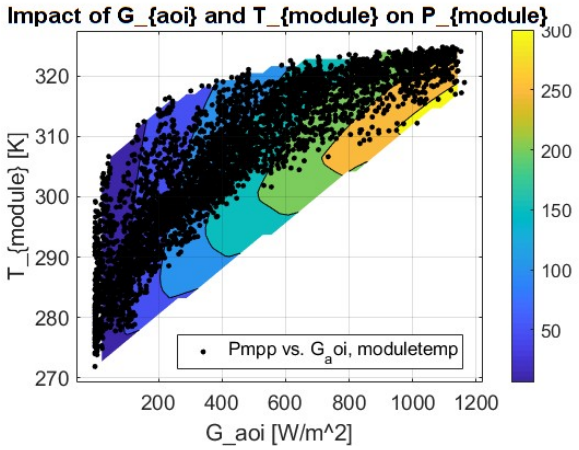

Figure 4.4: The relation between T_{module} and G_{aoi} are plotted. The gradient scale shows the correlation with P_{MPP} in Watts

Validation: The DC yield of the solar panels have been validated by comparing the model built with data from the Chint solar farm in Pias, Portugal [48] from February 2022 until July 2022 . The Figure 4.5 shows the match between the yield on site and the model built on a random chosen day of each month.

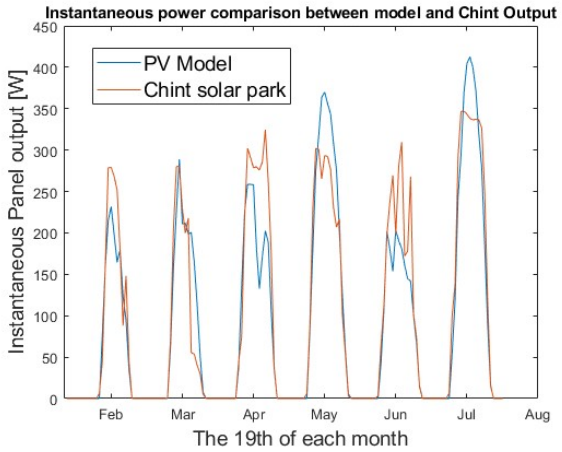

Figure 4.5: DC yield validation of the model with solar farm data

Recommendations: The solar PV model can be made much more accurate by incorporating a single diode PV model by deriving required parameters from the specification sheets.

4.2. Direct Air Carbon Capture (DAC)

The DAC subsystem model is based on the model previously developed at ZEF [49].

Model Assumptions

The DAC subsystem is modelled based on the assumptions

- The viscosity of the sorbent is constant throughout the entire process.
- There is no degradation of the sorbent over multiple absorption-stripping cycles. This assumes a constant performance.
- There are no losses assumed in this subsystem.

Model Inputs and Outputs
The DAC subsystem requires the following inputs:

- **Power input from the controller:** The power input dictates the production of Carbon dioxide and water in the DAC subsystem.
- **Absolute humidity:** This is required to estimate the absorption of water and Carbon dioxide in the absorber side.
- **Ambient Temperature:** The ambient temperature also plays a crucial role in estimating the absorbed contents.

The DAC subsystem requires the following outputs:

- **Moles of Carbon dioxide produced:** The amount of moles of Carbon dioxide produced by the DAC subsystem which would further downstream be utilized by the MS subsystem (Section 4.5) after being pressurized and dried in the FM subsystem (Section 4.4).
- **Moles of water produced:** The amount of water produced in moles that would be used by the AEC subsystem (Section 4.3).

Table 4.2: Input/output parameters for the DAC subsystem

Symbol	Input Parameters	Unit	Symbol	Output Parameters	Unit
Pow_{DAC}	Power to DAC	[Watts]	$n_{CO2,produced}$	Carbon dioxide produced	[mols]
T_{amb}	Ambient temperature	[K]	$n_{H2O,produced}$	Water produced	[mols]
AH	Absolute Humidity	[g/m^3]			

Model Description

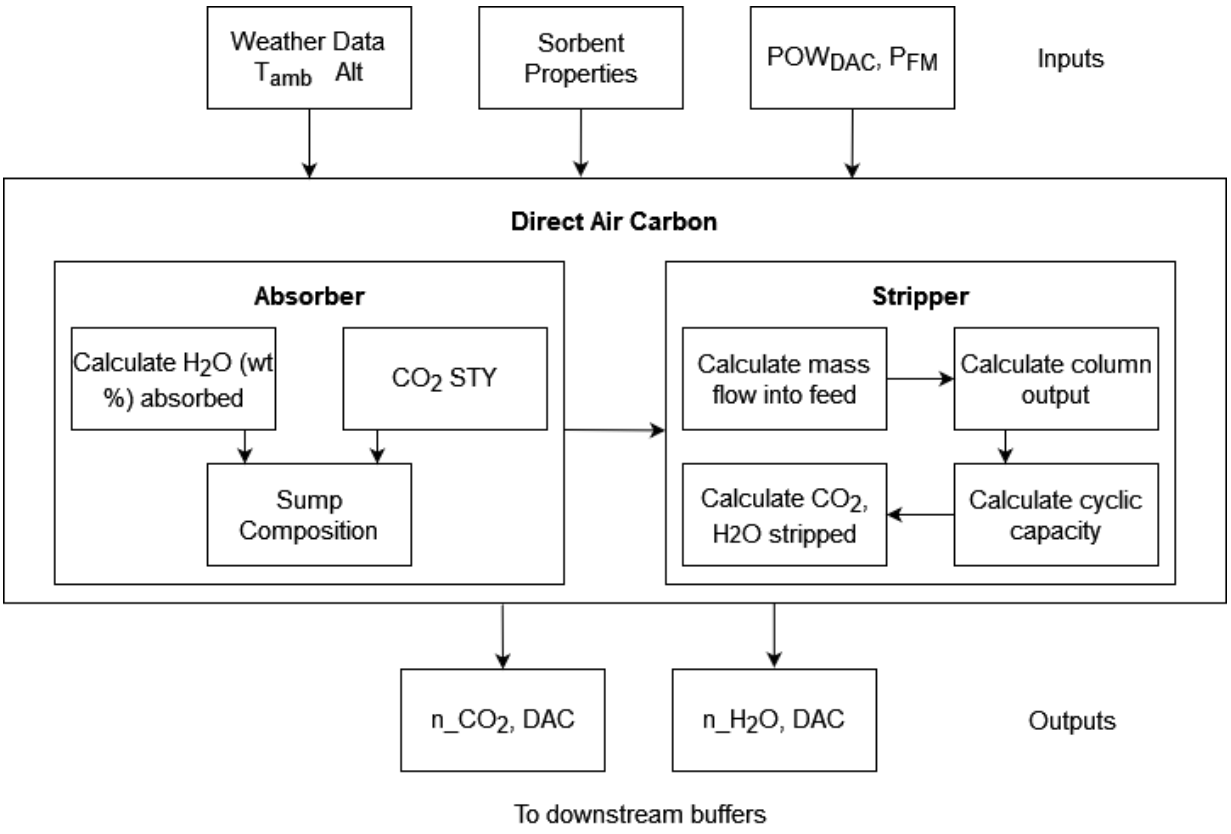

Figure 4.6: DAC subsystem model schematic

The DAC system's model performs various processes to ensure CO_2 capture from ambient air. The model operates in the following key phases:

Initialization: At the beginning of the simulation, various parameters, such as ambient temperature (T_{amb}), and sorbent composition in the sump based on the mass fractions of the sorbent, Carbon dioxide absorbed, water and diluent, are initialized. These parameters form the foundation for subsequent calculations.

VLE Calculation: Vapour-liquid equilibrium (VLE) calculations are employed to determine the composition of water vapour and CO_2 in the ambient air. This equilibrium behaviour guides the absorption process of CO_2 and water.

CO2 Production and Stripping: With the input power Pow_{DAC} being supplied to the reboiler which operates at the temperature $T_{reboiler}$, the stripping of Carbon dioxide and water from the sorbent is initiated. This gives out the cyclic capacity and the moles of Carbon dioxide and water produced by the DAC subsystem.

4.3. Alkaline Electrolysis (AEC)

The Alkaline Electrolysis (AEC) model focuses on simulating the behaviour of the AEC subsystem, which involves the electrolysis of water to produce hydrogen and oxygen gases. By simulating this process, the model aims to provide insights into the system's operational dynamics, efficiency, and yield in response to different input parameters determined by performing experiments and building the model based on them at ZEF [50].

Model Assumptions

The major assumptions made while modelling the AEC subsystem are:

- The electrolyser runs at ambient temperature. This means that the heat generated by the stack is effectively dissipated.
- The electrolyser stack operates at a constant pressure.

Model Inputs and Outputs

The AEC subsystem required the following inputs

- **Moles of water in the buffer tank:** The moles of water present in the upstream buffer tank is used to calculate the output of the AEC subsystem.
- **Ambient Temperature:** The ambient temperature is required since the AEC operates at the ambient temperature.
- **Voltage of the stack:** This determines the efficiency of the electrolyser stack.
- **Current density:** This determines the number of moles of Hydrogen and Oxygen produced.

The AEC subsystem required the following outputs

- **Moles of Hydrogen produced:** The moles of Hydrogen produced is later required to calculate the moles added to the buffer tank downstream.
- **Moles of Oxygen produced:** The total moles of Oxygen produced is released into the atmosphere.

Table 4.3: Input/output parameters for the AEC subsystem

Symbol	Input Parameters	Unit	Symbol	Output Parameter	Unit
$n_{H2Obuffer}$	Water Buffer tank moles	[mols]	$n_{H2,produced}$	Hydrogen produced	[mols]
T_{amb}	Ambient temperature	[K]	$n_{O2,produced}$	Oxygen produced	[mols]
V_{AEC}	Stack voltage	[Volts]			
cd_{AEC}	Stack current density	[mA/m^2]			

Model Description

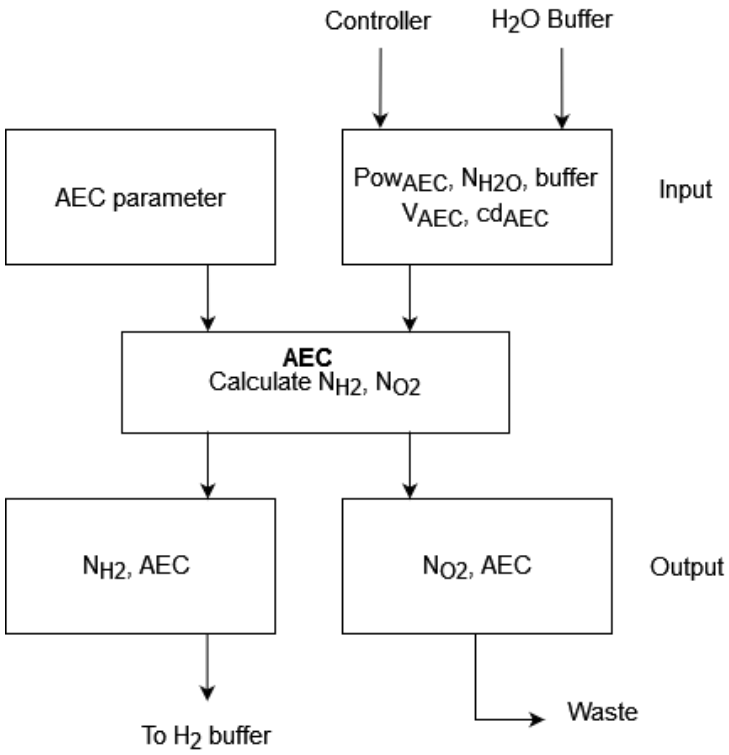

Figure 4.7: AEC subsystem model schematic

This model's primary objective is to simulate the operation of an alkaline electrolysis system, with an emphasis on the production of hydrogen and oxygen gases from water electrolysis. This is done by using the inputs to the system with the system parameters that influence the overall yield of the subsystem.

The yield of Hydrogen and Oxygen are estimated based on the total number of cells in the stack (Num_{cells}) and the area of each cell ($Area_{cell}$). The following equation is used to determine the yield.

$$\begin{aligned} n_{H2,produced} &= cd_{AEC} \times Area_{cell} \times Num_{cells})/(2 \times F) \\ n_{O2,produced} &= cd_{AEC} \times Area_{cell} \times Num_{cells})/(4 \times F) \end{aligned} \tag{4.2}$$

where, $F = 96500 Coulombs/mol$ is the Faraday's constant.

The production of Hydrogen is directly proportional to the current density when the area of the cell is constant as described in Equation 4.2. This can be seen in Figure 4.8.

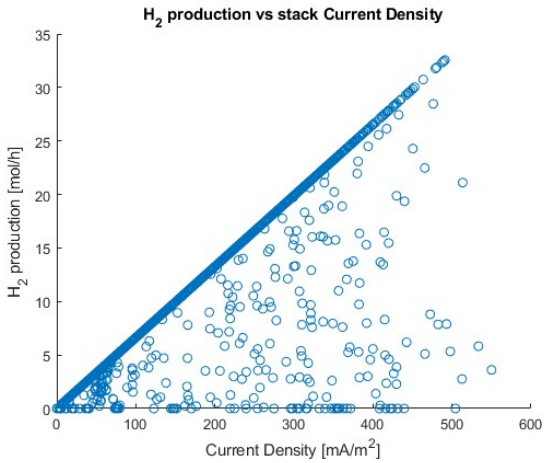

Figure 4.8: Hydrogen produced Vs current density

In the above figure, the direct proportionality can be seen. But, there are other instances as well which show a reduced production at a given current density. This is due to a shortage in the water buffer tank feed. This requires a better estimation and power distribution where the power can be distributed proportionally to the AEC subsystem.

Verification: The current density and the voltage are related based on the power input from the system. The potential is found based on the current density at which the stack operates by bisection. By this, the voltage of the electrolyser stack is calculated. The voltage at which the AEC stack operates defines the efficiency of the stack. It is necessary to verify the working model.

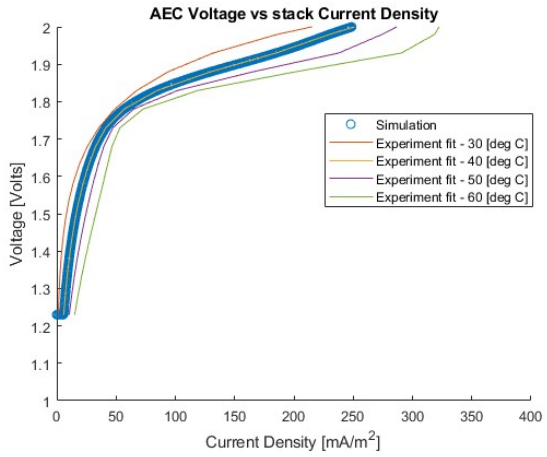

Figure 4.9: I-V curve comparison of electrolyser cell model and experiment fit

Figure 4.9 shows the current density- Voltage curve of the electrolyzer stack. The plot shows the operation of the electrolyser currently at 50 bar pressure are 40 °C. The cd-V curve conforms to the experimental curve fit from the ZEF experiments [50]. This curve can hence, prove the subsystem model's real-world effectiveness.

4.4. Fluid Machinery (FM)

The Fluid Machinery model is modelled to compress the products of the DAC subsystem to a pressure of 50 bars.

Model Assumptions

The FM model assumes the following:

- The Carbon dioxide feed into the fluid mechanic system is dry. This implies that there is no water vapour present in the input feed from the CO_2 buffer tank.
- Adiabatic single-stage compression is assumed.
- Liquid water at ambient temperature is fed into the system parallelly.

Model Inputs and Outputs
The input values for the FM subsystem are:

- **Moles of CO_2:** Input feed per time step of CO_2 from the CO_2 buffer tank.
- **Moles of H_2O:** Input feed per time step of H_2O from the H_2O buffer tank.

The output values for the FM subsystem are:

- **Power Recommended for CO_2 compression:** Power in Watts to be supplied to compress CO_2 produced in the current time step.
- **Power Recommended for H_2O compression:** Power in Watts to be supplied to compress H_2O produced in the current time step.

Model Description
The FM model's main output is the power required to compress the fluid (both gaseous CO_2 and liquid water) to 55 bars. This is done to ensure the AEC subsystem can run at a pressure of 50 bars. The recommended power is used in the time step $i+1$ to compress CO_2 and water are produced in the time step i.

4.5. Methanol Synthesis (MS)

The Methanol synthesis computes the moles of methanol and water produced based on the moles of CO2 and H2 input from buffer containers, as well as the input power and output power from the preceding time step. This model intends to shed light on the methanol synthesis process by taking into account various thermodynamic and operational variables. The model used in the current work uses data derived from experiments performed in previous work at ZEF by A.C. de Jong [38].

Model Assumptions
The main assumptions in this model are as follows:

- The reactor is perfectly insulated. This implies that the heat generated by the system is not lost to the environment until the next time step takes place.
- The molar ratio of the output is considered to be 1:1 based on the stoichiometric molar values. This assumption does not consider chemical kinetics as a function of the temperature of the system.

Model Inputs and Outputs
The inputs used in modelling the MS subsystem are described below:

- **Moles CO_2:** The number of moles of carbon dioxide consumed from the CO_2 buffer tank is used to calculate the stoichiometric equivalent moles of Methanol.
- **Moles H_2:** The amount of H_2 added into the MS reactor determines the amount of water produced.
- **Power Input:** This is the power supplied to the MS subsystem which is supplied to the heating elements to maintain optimum reaction temperatures inside the reactor.
- **Heat Stored:** The heat generated by the subsystem allows for the methanol reactor to maintain the set point temperature by drawing minimum power from the solar PV input.

The outputs of the model are:

- **Moles of Methanol and Water produced:** The final output of the methanol reactor is the mixture of methanol and water that are produced from the reactor.
- **Power generated as heat:** The heat generated due to the exothermicity of the reaction.
- **Recommended Power:** The recommended power needed to be supplied to the MS subsystem

in the next time step after accounting for the heat generated. This is the power recommended to ensure the temperature of the reactor stays at the set point temperature.

- **Minimum recommended Power:** The minimum required power that needs to be supplied to the reactor to run the reactor at the minimum temperature below which there is no significant production of methanol and water.

Table 4.4: Input/output parameters for MS subsystem

Symbol	Input Parameters	Unit	Symbol	Output Parameters	Unit
$n_{CO2,buffer}$	Carbon dioxide buffer tank moles	[mols]	$n_{Methanol+Water}$	Methanol water mixture produced	[mols]
$n_{H2,buffer}$	Hydrogen buffer tank moles	[mols]	$Pow_{MS,gen}$	Power generated as heat	[Watts]
Pow_{MS}	Power in	[Watts]	$Pow_{MS,recommend}$	Recommended power	[Watts]
$Pow_{MS,gen}$	Power generated as heat	[Watts]	$Pow_{MS,recommend,min}$	Minimum recommended power	[Watts]

Model Description

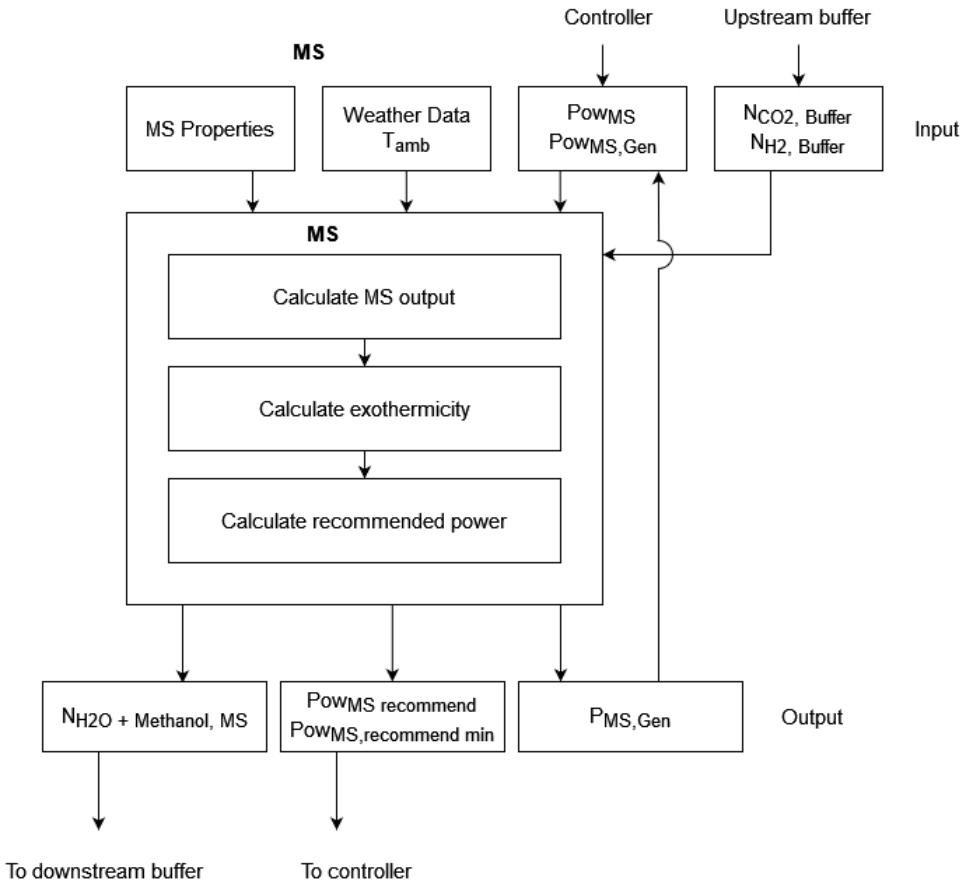

Figure 4.10: MS subsystem model schematic

The purpose of the model is to simulate the microplant's methanol synthesis process. The objective is to calculate the molecules of methanol and water produced based on the inputs and system conditions specified. This is mainly done by defining the subsystem's parameters such as volume, and mass required. The power is supplied to the heating elements whose thermal resistances have been utilised based on experimental data. Further, the production and input mass flows have been derived by considering the efficiency of the working system with the predicted outputs by simulations performed by A.C. de Jong. These factors implicitly simplify the complex nature of the subsystem while incorporating thermal losses.

T_{ms} is the temperature of the MS reactor at any given time step, while the temperature setpoint ($T_{mssetpoint}$)

is the set point temperature of the methanol synthesis plant which is constant for the entire duration of the simulation. Running the MS reactor at $T_{mssetpoint}$ would yield the maximum production of methanol and water. At T_{msmin}, the reactor produces the minimum Methanol and water and below it does not yield any outputs. It is hence implied that the minimum power that needs to be supplied to the reactor is $P_{ms,min}$. This is further used as a constraint in the control algorithm.

Verification
The methanol reaction is extremely dependent on the temperature of the reactor. Figure 4.11 show the relation between production and temperature.

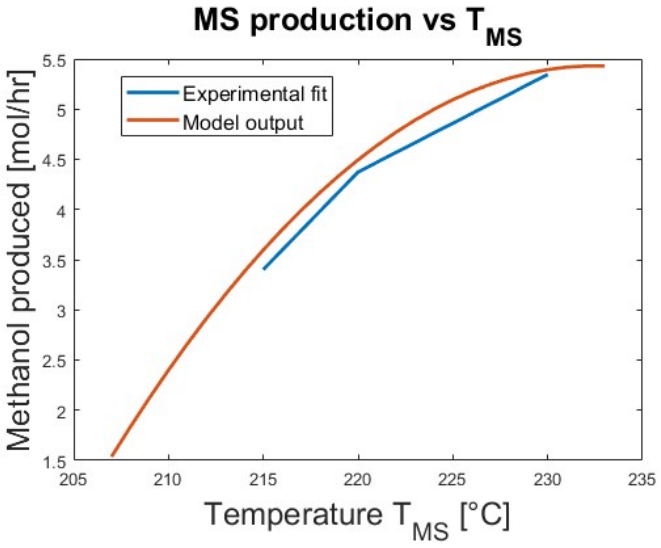

Figure 4.11: Methanol production to temperature in the MS reactor

The experiments conducted at ZEF by A.C. de Jong [38], have been used to develop the model. The model output curve has been benchmarked based on the efficiency of the experimental data with theoretical calculations to provide production values outside the temperature range of the experiments.

Further, the exothermicity has been verified in Section 6.3 which describes the overall power consumption during continuous operation.

Recommendation: A recommendation for the MS model would be to introduce heating modes that bring realistic approximations in the production of methanol while heating the reactor to the minimum operating temperature.

4.6. Distillation System (DS)

The Distillation system (DS) is modelled based on a model on COCO [51] and experimental data performed at ZEF [41] previously. The model's goal is to produce pure methanol.

Model Assumptions
The major assumptions of the model are

- The model runs under steady-state conditions for the entirety of the time step without any thermal inertia.
- There are no losses in the subsystem.
- The mixture of Methanol and water behaves as an ideal liquid.
- **mass flow min**: ensure min mass flow based on Cherise's results.

Model Inputs and Outputs
The main inputs for the DS subsystem are listed below:

- **Moles of methanol and water mixture added**: The total number of moles input into the system is used to calculate the final production of methanol.
- **Power input:** The power supplied to the DS subsystem to heat the system.

The outputs of this model are listed below:

- **Moles of methanol produced**: This is the final output of both the DS subsystem and the entire DAC microplant each time step.
- **Moles of Water produced:** Water is a by-product of the distillation system and is released from the system as waste.

Table 4.5: Input/output parameters for the distillation subsystem

Symbol	Input Parameters	Unit	Symbol	Output Parameter	Unit
n_{buffer}	Buffer tank moles	[mols]	$n_{Methanol}$	Methanol Produced	[mols]
Pow_{DS}	Power in	[Watts]	n_{Water}	Water Produced	[mols]

Model Description

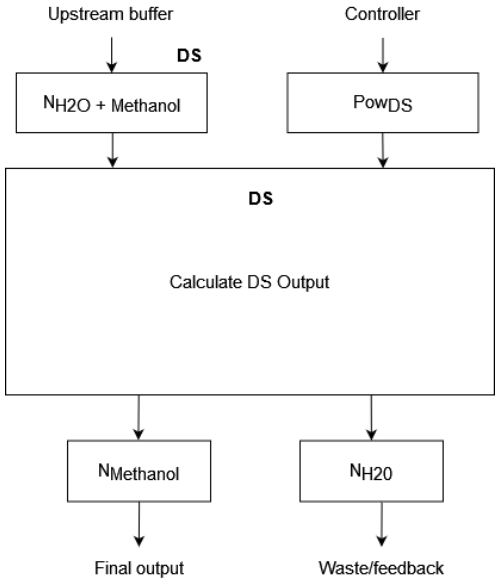

Figure 4.12: DS subsystem model schematic

The DS subsystem is modelled to always produce grade AA methanol whose mass fraction is 99.645%. The model utilises the following function to produce methanol with power as an input. This equation has been derived based on the experimental and outputs of the COCO model.

$$n_{methanol} = 0.01852 \times (Pow_{DS} - 1.526) \tag{4.3}$$

The model hence has a minimum power rating Pow_{DSmin} of 82 Watts below which there is no production of methanol.

Verification and behaviour
The DS model is based on the prediction of the COCO model by previous works at ZEF. Figure 4.13 shows the production of grade AA pure methanol comparing them between data from COCO and the fit developed in Equation 4.3.

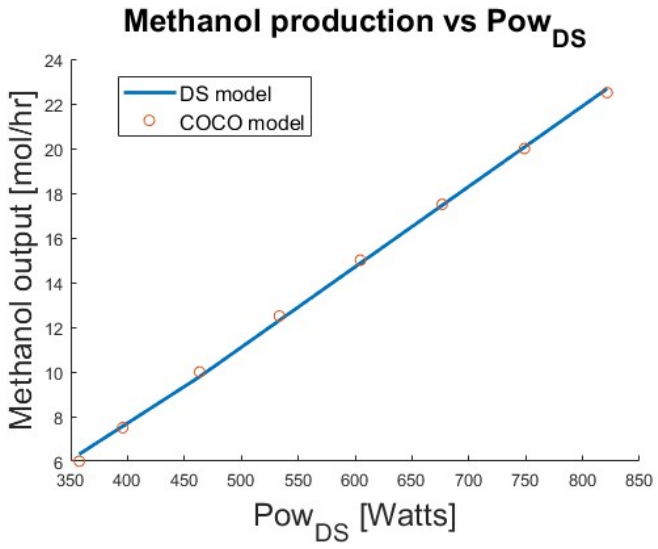

Figure 4.13: Production to power curve for the DS subsystem

4.7. Battery System

This battery system is an energy storage device, allowing the capture and release of energy to manage fluctuations in production and consumption overnight. By simulating this battery system's operation, the model aims to predict key outputs such as state of charge (SOC), power charged and discharged and remaining energy capacity.

Model Assumptions
The battery system is designed by assuming the following:

- There is no degradation in the battery. ie, there is no reduction of charging and discharging capacity through multiple charging cycles.
- A constant coulombic efficiency has been assumed.
- The battery operates at a constant voltage irrespective of the state of charge.

Model Inputs and Outputs
The following are the inputs to the battery system:

- **Power input:** The power input is the power supplied directly from Solar PV into the battery and is used to charge the battery.
- **Power required:** This is the power estimated to be drawn by the microplant during the discharge cycle.
- **Charging state:** It is the state variable that defines the mode the battery runs on at any given time step. The modes are charge, float and discharge.

The main outputs of the battery system are:

- **Power discharge:** The power supplied by the battery to the microplant during the discharge mode.
- **State of Charge:** The state of charge (SOC) of the battery at the end of every time step. This is used by the controller to decide the charging state mentioned above.

Table 4.6: Input/output parameters for the battery subsystem

Symbol	Input Parameters	Unit	Symbol	Output Parameter	Unit
Pow_{in}	Power input	[Watts]	$Pow_{discharge}$	Power Discharge	[Watts]
Pow_{req}	Power required	[Watts]	SOC	State of charge	%
State	Charging state	-			

Model Description
The model simulates the behaviour of a battery system used for energy storage in various aspects which are further explained in detail.

The battery parameters are defined based on the battery specification sheets. Essentially the parameters utilised are the battery voltage ($V_{battery}$) in Volts and the charging capacity ($Q_{maxcharge}$) and discharging capacity ($Q_{maxdischarge}$) in Ampere-hours at their respective C-rating. Further, the maximum and minimum SOC (SOC_{max} and SOC_{min})and initial SOC ($SOC_{initial}$) have been defined.

The battery further calculates the remaining capacity ($Q_{remaining}$) in Ampere-hours during charging and discharge cycles. This further updates the SOC (SOC). The SOC and $Q_{remaining}$ allow the model to calculate the power output during discharge based on equations in the previous chapter.

4.8. Buffer Tanks

The Buffer tank model is intended to simulate the buffer tank and respond to production and consumption processes. The code provides insight into how these buffer tanks interact with the rest of the system by monitoring moles of substances, pressures, fill percentages, and ratios.

Model Assumptions
The main assumptions of the model are stated below:

- The model assumes steady-state conditions.
- The moles added and consumed are assumed based on pressure sensor information and opening and closing duration of valves.
- Gases are modelled assuming they behave as ideal gases between 1 Bar and 55 Bars.

Model Inputs and Outputs
The inputs used in the model are as follows:

- **Moles Added:** The moles added into the buffer tank are an input based on the moles produced by the upstream subsystem.
- **Moles Consumed:** The moles consumed are the total number of moles fed into the downstream subsystem.
- **Ambient Temperature:** The ambient temperature value is used as an input to calculate the maximum storage in buffer tanks storing gases.

The outputs of the model are:

- **Moles stored:** The total number of moles stored in the buffer tank.
- **Moles vented:** The total moles vented by the buffer tank are calculated using the tank's physical properties and maximum volume and pressure. This implies the use of the relief valve in the real system.
- **Pressure:** The pressure within the buffer tanks is determined based on the fill percentage of the buffer tank in the case of gases.
- **Addition-Consumption ratio:** It is the ratio of moles added into the subsystem to the moles consumed by the downstream subsystem. The implications of the A/C ratio are further elaborated in Section 5.3.

Table 4.7: Input/output parameters for the buffer tank model

Symbol	Input Parameters	Unit	Symbol	Output Parameter	Unit
n_{added}	Moles added	[mols]	n	Moles stored	[mol]
$n_{consumed}$	Moles Consumed	[mols	n_{vented}	Moles vented	[mol]
T_{amb}	Ambient temperature	[K]	P	Pressure	[Bar]
			ac_{ratio}	A/C ratio	-

Model Description
The code represents buffer containers as reservoirs that store substances and interact with two subsystems, one upstream and one downstream. There are four buffer tanks used. Two buffer tanks store Carbon dioxide and Hydrogen in the gaseous state and two buffer tanks are used to store liquids, one for water produced by AEC and another for the mixture of water and methanol produced by the methanol synthesiser. These buffer containers play a crucial role in the system's management of the availability and utilization of gases (CO2) and liquids (H2O). The model is also defined based on parameters such as tank volume, and maximum allowed pressure.

4.9. Summary

- The modelling concepts and model parameters for all subsystems have been elaborated. The model's performances have been checked, validated and verified where applicable.
- The Research sub-objective 2: Model each subsystem, has been achieved by studying the modelling criteria and approaches of all subsystem models.
- The subsystem models have been programmed using MATLAB and verified, further the integration of these subsystems is required and control methodologies must be identified.

5

Control and integrating the microplant model

This chapter sheds light on the sub-research question 3: ”Design the control algorithms and integrate the model”. The system is integrated in Section 5.1 and various microplant architectures are discussed in Section 5.2. Then, the control algorithm is designed in Section 5.3. In Section 5.4, the temporal granularity effects are discussed and finally, in Section 5.5, the key performance indicators have been discussed.

5.1. Integrating the model

In Section 3.2, we have meticulously developed models for each subsystem of the microplant. This section delves into the seamless integration of these subsystem models over which the controllers shall be designed to provide a comprehensive overview of the microplant's functionality in Section 5.3. The schematic of the completely integrated microplant is shown in Figure 5.1.

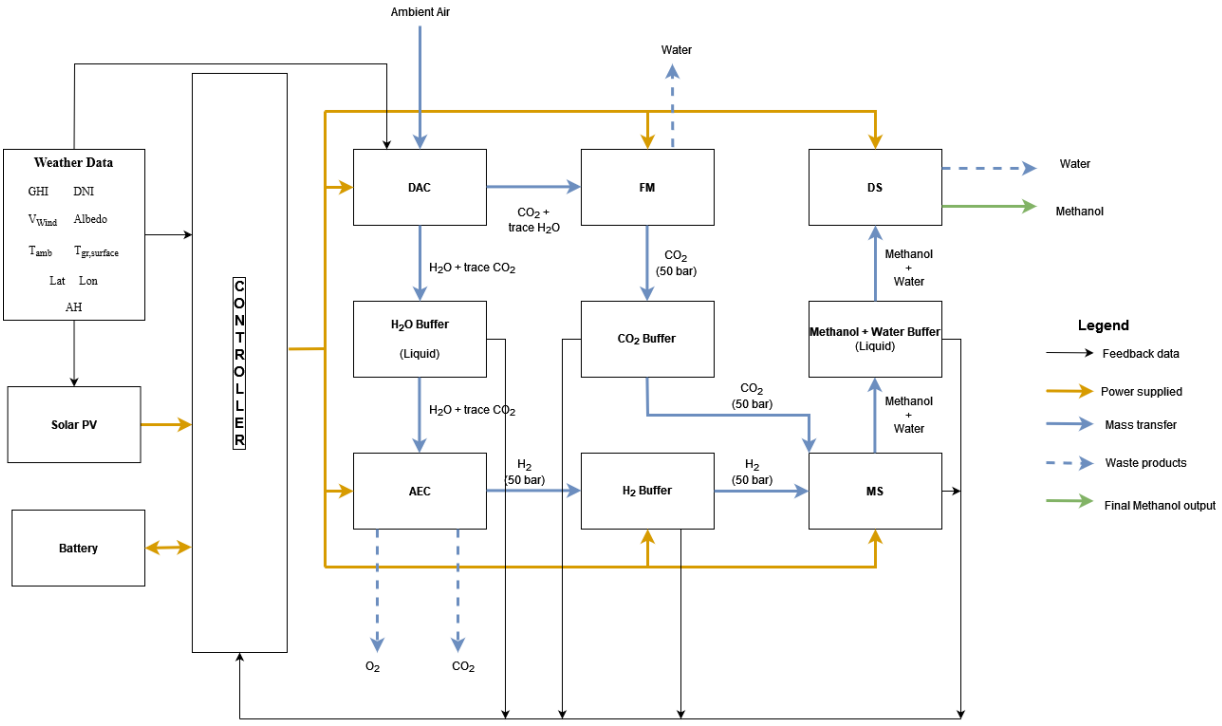

Figure 5.1: Schematic on the entire integrated microplant model

The integrated system operates in a synchronized manner, utilizing data importation and processing, power distribution, mass transfer, and controller input information as described in Chapter 3. This section

elucidates how these components interconnect and operate together cohesively.

5.1.1. Data Processing and Solar PV Model

The model initiates by importing and processing data, as explained in Section 3.1. This data, encompassing various environmental parameters, is crucial for accurately modelling the solar PV output for the entire operational period. Notably, the solar PV subsystem model is distinct in that it operates independently and does not require feedback from the system. The microplant's operation, on the other hand, hinges on the PV power generation, making the solar PV subsystem model exclusive to the time series model.

Further, the data on the physical parameters and properties of components are imported and saved which is utilized by the subsystem models in each iteration subsequently.

5.1.2. Time Series

After initialising all properties, weather data and solar PV output, a time series is started which simulates the microplant for the duration selected and at varying temporal granularity time steps (5 min, 10 min, 15 min, 20 min, 30 min and 1 hour). The model then is divided into three portions, power management, mass balance and information transfer.

Power management

Once the time series commences, the controller takes charge. Its primary function is to manage and distribute incoming power from the solar PV to the relevant subsystems. It begins by managing battery states (charging, floating, or discharging) and then distributes power accordingly to all subsystems. To ensure efficient power distribution, the controller assumes the use of DC-DC converters. Direct hookups have been avoided due to varying power requirements among subsystems. The solar PV output initially converted to 12V, is subsequently distributed to all subsystems. Battery sizing and parameters dictate the utilization of buck-boost DC-DC converters depending on the operating voltage of the battery. With the exception of the Alkaline Electrolysis Cell (AEC), which operates based on maximum power point where energy is drawn by the stack, all subsystems are run on 12V. The power distribution directions are illustrated by orange arrows in Figure 5.1.

Mass balance

The energy supplied to each subsystem, managed by the controller, facilitates the production of various materials in multiple steps. These produced substances are channelled into their respective buffer tanks. Waste products are considered to exit the system which is depicted with dashed arrows in Figure 5.1. If there's an excess of material in buffer tanks, it implies that material is vented from these tanks. Mass transfer processes are depicted by blue arrows in Figure 5.1.

Once the controller decides the subsystem status, the model runs according to the ZEF microplant process where the DAC subsystem model is run, followed by AEC, MS and then DS. The buffer tank models are run after all subsystems have been implemented as data on addition and consumptions are finally calculated. Finally, the FM subsystem model runs which recommends energy to be distributed to the subsystem in the next iteration. This is done to ensure the CO_2 produced in the previous substep can be pressurised and stored in the CO_2 buffer tank.

Information Transfer

The controller relies on input data from the system to make informed decisions. Specifically, it requires information about the total number of moles in each buffer tank, which is calculated based on the pressure within these tanks. This data is calculated through pressure and temperature sensors embedded in the system in the buffer tank subsystem model.

Additionally, the controller is required to calculate the Addition/Consumption (AC) ratio which it does through two methods: utilizing mass flow rate sensors positioned upstream and downstream of each buffer tank to get real-time flow rates. This would negate the requirement of further processing sensor data but requires investment from ZEF into flow sensors. Another method is to estimate the ratio based on pressure changes within buffer tanks during valve openings and closings. The latter method is feasible due to the automated valve motion within the system.

5.1.3. Postprocessing

After completing the simulation for the entire duration chosen, the model provides a short report on the microplant performance, creates a log of the system behaviour and brings out additional plots for analysis.

5.2. Microplant Architectures

The microplant architectures play an important role in the integration of the model. These architectures use the subsystem models built in Chapter 4.

The design of the microplant depends on understanding various system architectures, each catering to specific operational scenarios and optimization goals. This is essentially important since the microplant performance can vary depending on location and local weather conditions. This can seriously affect the capital and operational costs of running the microplant and impact the payback periods. This variability prompts an analysis to identify relevant system architectures for various weather situations and locations. The model has been built to work with the following system architecture variables.

Solar PV Tracking: The model can simulate the microplant's performance under two conditions: ground-mounted PV modules or a single-axis PV tracker. This allows for an assessment of how solar tracking affects yield.

Battery Integration: The system can be tested both with and without batteries to gauge the impact of energy storage on microplant performance and continuity during low or no irradiance periods.

Parallel Methanol synthesis reactors: Preliminary simulations have indicated that the MS subsystem is undersized. Therefore, exploring the use of two MS reactors in parallel during peak PV production is a potential avenue for enhancing performance.

Water feedback: Currently, water produced after distillation is considered waste. Investigating the possibility of recycling this water back into the system could potentially improve yields o Hydrogen produced and subsequently, final Methanol production.

The integration of subsystem models and controllers into the microplant model is crucial for understanding its performance. By simulating various system architectures and considering factors like solar tracking, battery integration, and water reuse, we can systematically assess and optimize the microplant's operation and find feasible solutions for the company to set up the microplants.

5.3. Control Algorithms

Designing a robust and efficient control algorithm for the Zero-Emission Fuel (ZEF) microplant is critical to achieving optimal operation and performance. The primary objective of this endeavour is to distribute the available power among the various subsystems in order to achieve the highest possible yield from each subsystem and ultimately maximize methanol production.

To accomplish this, the control algorithm operates on two distinct levels, each of which contributes to the overall operational efficacy of the microplant as shown in Figure 5.2.

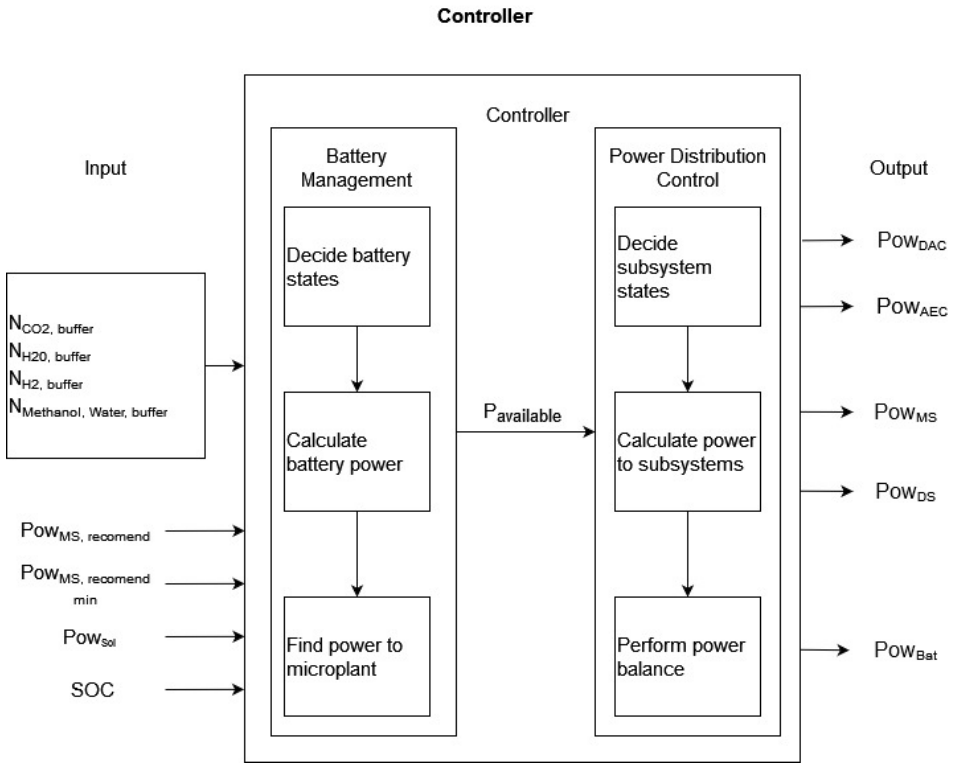

Figure 5.2: Schematic of the control algorithm

The first level of control pertains to battery management, a critical component of the energy management system of the microplant. The battery control algorithm regulates the charging, discharging, and preservation of the state of charge (SOC) of the battery.

The second level of control entails power distribution among all microplant subsystems at every timestep. This control mechanism is intended to distribute available power so as to maximize the aggregate output of each subsystem.

5.3.1. Battery Management

Battery management is accomplished by analytically determining the optimal mode of operation for the battery, i.e., charging, discharging, or operating in a floating state. In the pursuit of efficient battery management, a distinct controller has been designed, and tailored to address specific operational scenarios and priorities.

Input and Output

The input variables for the Battery control are as follows:

- **SOC:** State of charge of the battery decides the charging rate.
- **Minimum SOC:** Minimum SOC value to control battery charging mode and ensure battery health.
- **Maximum SOC:** Maximum SOC value to control battery charging mode and ensure battery health.
- **Solar PV input:** The solar PV input charges the battery and plays a crucial role in deciding the charging mode.
- **MS recommended power:** It is important in deciding the battery power output in the Battery Control 2.
- **Minimum MS recommended power:** The minimum value needed to be supplied by the battery.
- **DS power required:** An important contributor to the power supplied in the discharge mode.

The inputs above are required to provide the outputs below:

- **Battery Charge mode:** The controller decision about the battery mode between charge, float and discharge.
- **Battery power change:** The power supplied to charge the battery or the power drawn from the battery.

Table 5.1: Input/output parameters for the battery control

Symbol	Input Parameters	Unit	Symbol	Output Parameters	Unit
SOC	State of Charge of Battery	[%]	$State_{Battery}$	Battery Charging mode	[-]
SOC_{min}	Minimum State of charge	[%]	Pow_{Change}	Power supplied to/by the battery	[Watts]
SOC_{max}	Maximum state of charge	[%]			
Pow_{Sol}	Solar PV input power	[Watts]			
$Pow_{MS,recommend}$	Recommended power for MS	[Watts]			
$Pow_{MS,recommendmin}$	Minimum recommended power for MS	[Watts]			
Pow_{DS}	Power required by DS	[Watts]			

The main aspect of the controller is deciding the battery states. The decision tree for the same is shown in Figure 5.3.

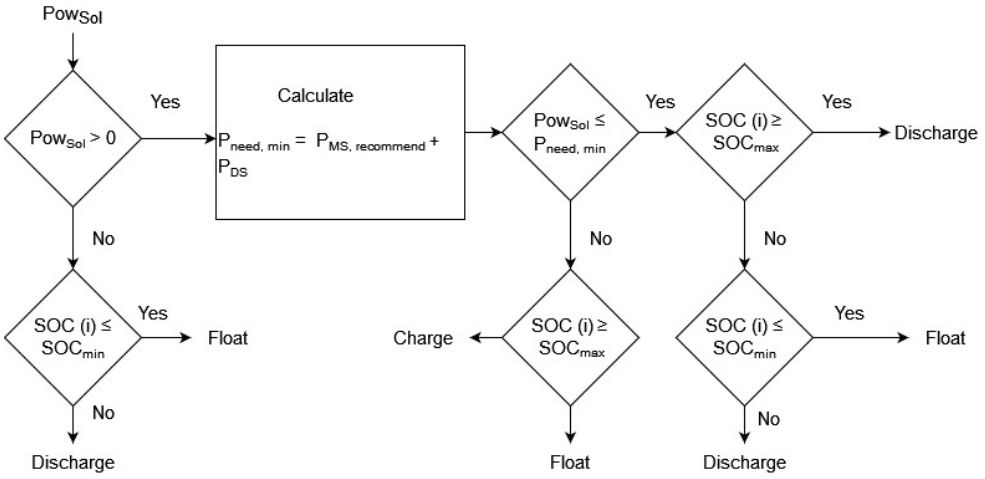

Figure 5.3: Schematic of the battery state decision tree.

The battery control prioritizes downstream subsystems such as methanol synthesis (MS) and distillation (DS) during nighttime or periods of low solar power generation as shown in Figure 5.3. The prioritization of MS and DS is strategic, as these subsystems have low power requirements when compared to AEC and DAC. Hence, these low-load systems are particularly suited for nighttime operation during the absence of solar irradiation. This controller's operation can be summarized as follows:

- **Charging Mode:** The controller determines the appropriate charging rate based not only on surplus solar power but also on the recommended power requirements of the MS and DS subsystems ($Pow_{DS} + Pow_{recommend}$). The battery is charged when the Solar PV (P_{sol}) input exceeds the combined power needs of these subsystems. The charging process continues until the SOC reaches the upper threshold (SOC_{max}).
- **Discharging Mode:** Conversely, when the solar PV (P_{sol}) input falls below the power recommended by MS and DS($Pow_{DS} + Pow_{recommend}$), indicating an energy deficit, the controller discharges the battery at a rate aligned with the power requirements of these subsystems. This ensures that the downstream subsystems run during periods of solar scarcity. The battery discharges at its maximum discharge rate until the SOC reaches the lower threshold (SOC_{min}).
- **Float State:** The controller maintains the battery in the float state when the SOC reaches either the maximum (SOC_{max}) or minimum (SOC_{min}) threshold. This means it neither charges nor discharges. This is done to preserve the battery lifetime.

After this, the battery subsystem takes over the Calculate battery power change. Once this is done, the power available ($P_{available}$) for the subsystems is given as output after battery charging or discharging has taken place.

5.3.2. Power Distribution control

The power distribution controller is a crucial component of the Zero-Emission Fuel (ZEF) microplant, with the responsibility of efficiently allocating available energy to the various subsystems in order to maximize methanol production.

There are two aspects to the controller. The initial mission of the power distribution controller is to determine whether the MS, DS, DAC, and AEC subsystems are powered on or off. This decision is determined by the number of moles in the upstream buffer tank. This method aligns the activation of subsystems with the availability of reactants, optimizing the overall system's performance. The latter mission is the effective allocation of available power to the remaining subsystems. This process is pivotal in ensuring that each subsystem receives sufficient energy for its operations while optimizing methanol production.

The power distribution control strategy prioritizes power distribution to the distillation subsystem (DS). This preference for DS is primarily motivated by two factors. First, the power requirements of DS can be precisely estimated and predicted, allowing for precise control. Second, DS operations are comparatively unaffected by weather conditions, ensuring the stability of the DAC subsystem's production of CO2 and H2O. The control system becomes more robust and manageable by mitigating the impact of environmental variability. The allocation of power between the DAC, AEC, and MS subsystems is where the control system is essential.

The "Constant System Flow Rate Control" strategy was particularly designed keeping in mind the specific challenges of the ZEF microplant. The power distribution controller is based on two fundamental concepts: the A/C ratio and the Change Factor. These ideas enable a sophisticated and dynamic control mechanism that seeks to optimize power distribution among the DAC, AEC, and MS subsystems.

The **A/C ratio**, also known as the Addition-Consumption ratio, is a metric used to calculate the deviation of mass flow in the buffer tanks. It is the ratio of the number of moles of a substance introduced to the buffer tank to the number of moles consumed by the subsequent subsystem as shown in Equation 5.1. The A/C ratio measures the equilibrium between the supply and demand of each substance within the system. Mathematically, the A/C ratio is defined as follows:

$$A/Cratio = \frac{n_{added}}{n_{consumed}} \tag{5.1}$$

The A/C ratio was chosen because it provides distinct information about the system. The A/C ratio can provide insight into the relative production/consumption rates of the upstream and downstream subsystems, as well as the current states of both subsystems. The A/C ratio also indicates the action that needs to be performed by the controller as shown in Table 5.2.

Table 5.2: Implications of AC ratio

A/C Ratio	Buffer Tank		Upstream subsystem	Downstream subsystem	Action needed	
	Addition	Consumption			Upstream	Downstream
Nan	No	No	Off	Off	None	None
0	No	Unquantifiable	Off	On	Calculate Cf	None
$0 < A/Cratio < 1$	Comparatively less	Comparatively high	On	On	Increase power	Reduce power
1	Equal	Equal	On	On	None	None
> 1	Comparatively more	Comparatively less	On	On	Reduce power	Increase power
Inf	Unquantifiable	No	On	Off	None	Calculate Cf

Based on the above table it is clear that the A/C ratio informs the decision-making of the controller to identify the highest deviation from the required A/C ratio which is 1. The A/C ratio = 1 indicates the ideal process and mass flow in the buffer tanks. The goal of the Constant System Flow Rate Controller is hence to bring the A/C ratio as close to 1 as possible.

In order to accomplish this, the **change factor** (Cf) is introduced. The change factor quantifies the amount of change in power allocation to a subsystem based on the A/C ratio's deviation from the target value of 1.

The change factor is equivalent to the error in a P-type controller. The formula for calculating the change factor (Cf) is shown in Equation 5.2.

$$\begin{aligned} Cf &= 1 \mp \tfrac{|\text{ A/C ratio } -1|}{2} && \forall \text{ A/C ratio } [0,2] \\ Cf &= 1 && \forall \text{ A/C ratio } = \text{ NaN \&\& A/C ratio } = \text{ inf} \end{aligned} \tag{5.2}$$

At the core of the Constant System Flow Rate Controller is a hierarchical control approach that optimizes power allocation between subsystems while sustaining equilibrium within the ZEF microplant. A high-level control strategy prioritizes subsystems in accordance with the buffer tank with the greatest deviation from the target A/C ratio of 1. This strategy ensures that the distribution of power is tailored to resolve the greatest imbalances in substance consumption and production. Afterwards, a low-level control mechanism that derives the change factor, functions on principles equivalent to a proportional-integral (PI) controller. It employs the subsystem-specific change factor (Cf), the $|$ A/C ratio -1 $|$ is the error of the system and dividing it by 2 brings in the integral element that dampens the control. This mechanism corrects the power distribution within individual subsystems based on their respective Cf values. The main way the Constant System Flow Rate Control differs is by allowing the freedom to control multiple subsystems at the same time, while a PI controller operates with only one input. By orchestrating these controls, the power distribution strategy systematically optimizes power allocation across subsystems while adhering to system constraints, enabling the ZEF microplant to operate in a harmonious and efficient manner. The controller decision tree can be seen in Figure 5.4.

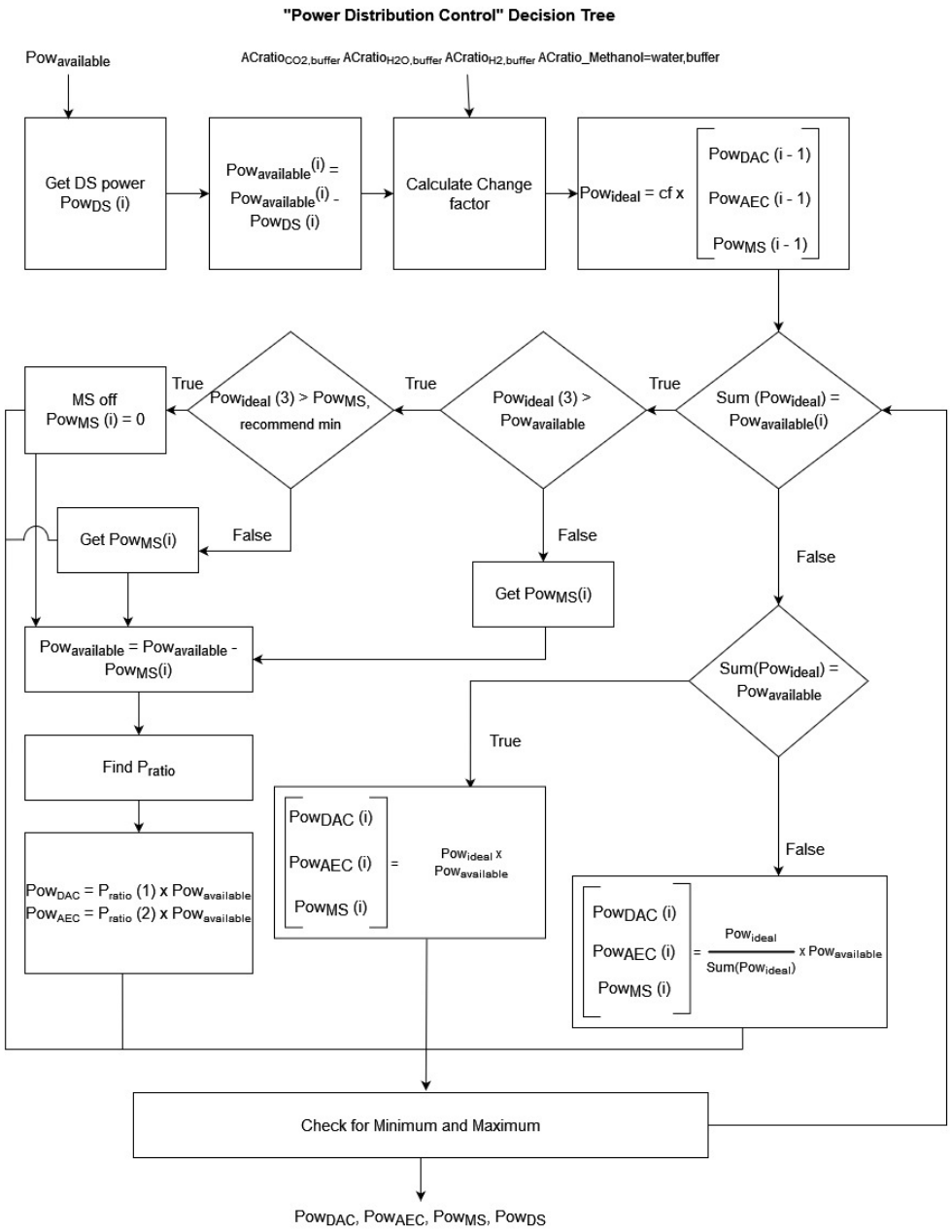

Figure 5.4: Schematic of the Constant system flow rate controller.

The controller was tested by supplying power for 40 hours in the simulation at constant absolute humidity (10 g/m^2) and constant ambient temperature (20°C). The weather conditions are kept constant as they do not play a role in the controller. These parameters only impact the production of the subsystems and the controller is designed to address these variations at any given time. The power supply is constant, then is linearly increased and decreased to a much lower level which is lower than $Pow_{MS} + Pow_{DS}$ which the controller prioritizes at lower irradiance levels as shown in Figure 5.5. In this test, the dynamics of the controller can be tested and understood.

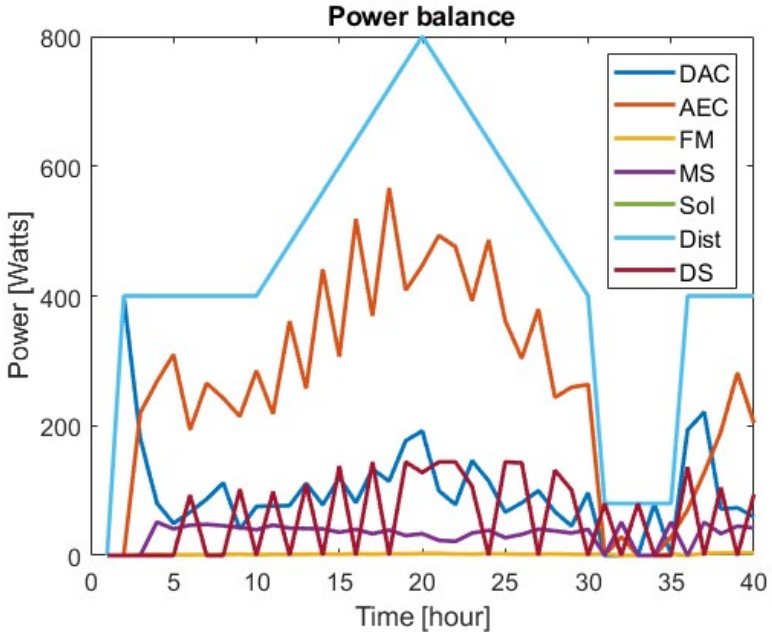

Figure 5.5: Testing the controller by supplying constant, increasing, and decreasing power supply.

In Figure 5.5, P_{Dist} is the total power that is distributed among all subsystems. There is a variation in the power supplied to individual subsystems even during constant power input. This is attributed to the controller attempting to normalise the addition consumption ratios to 1 as shown in Figure 5.6.

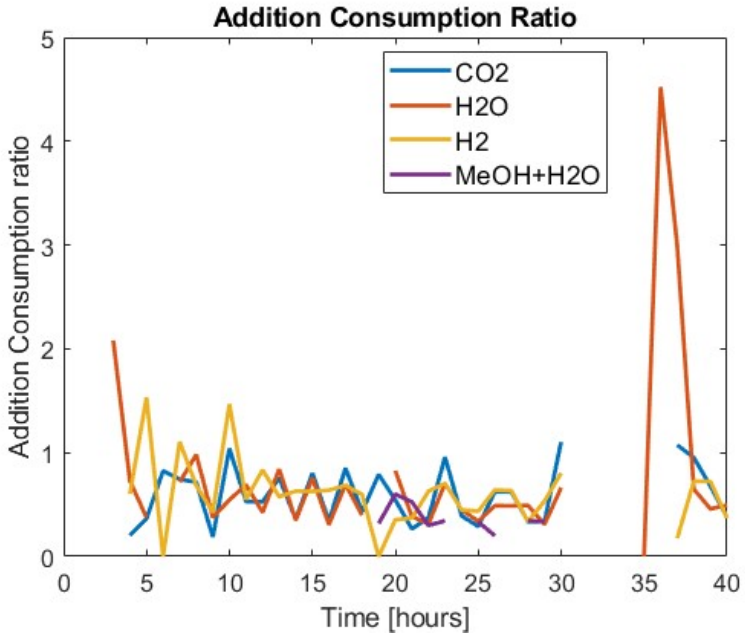

Figure 5.6: The addition consumption ratio of each buffer tank.

The addition consumption ratio is controlled to be as close to 1 as possible, both during constant power supply and during variable power supply. There are extreme peaks in the H_2O buffer tank's addition consumption ratio. This is observed every time the DAC is switched on from the off state. This is the nature of DAC which absorbs higher amounts of water and carbon dioxide during the lean loading phase and reduces slowly as the sorbent becomes rich. Between hours 30 and 35, there is a gap in the plot.

These gaps are the moments where the AC ratios are either 'NaN' or 'inf'. These implications can be seen in Table 5.2.

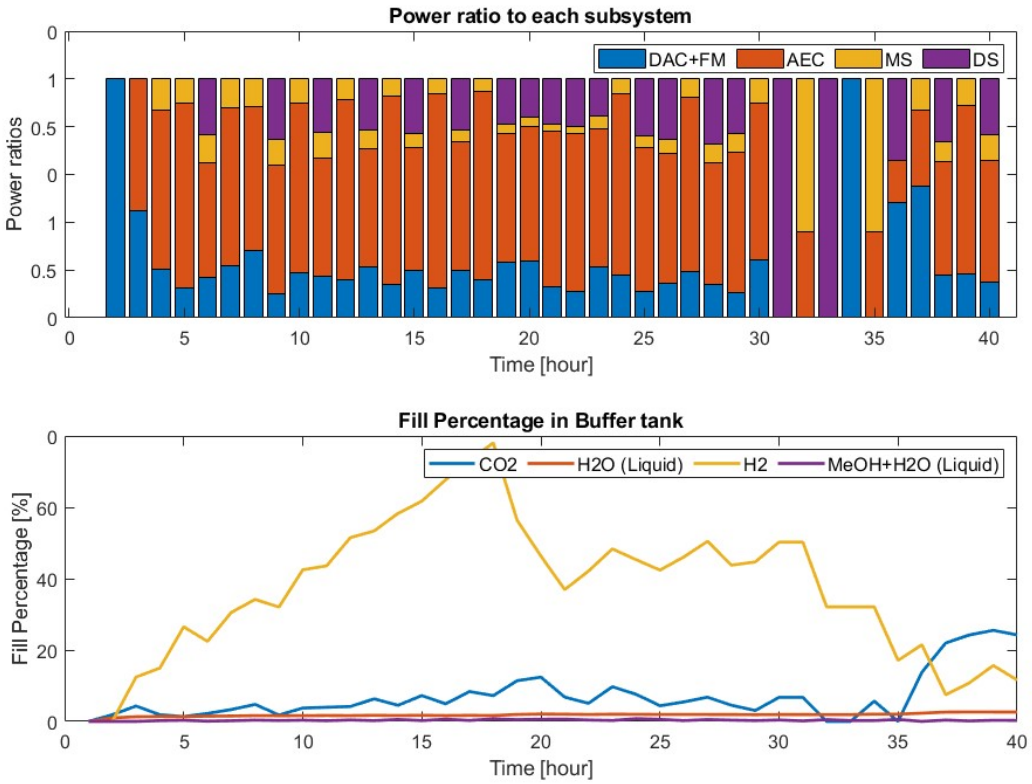

Figure 5.7: The power ratio of the power supplied to all subsystems.

The power ratio is defined as the ratio between the power supplied to a subsystem and the total distributed power in the microplant. The maximum power ratio is 1 (see Figure 5.7), which implies power balance has been achieved. Figure 5.7 can give a better understanding of how the microplant behaves. The first subsystem is to always be turned on in DAC as all buffer tanks are empty for any other subsystems to turn on. In the next timestep, the AEC is turned on and then MS is turned on. DS is turned on when there is at least 5 moles of Methanol water mixture in the upstream buffer. The total power distributed is managed to ensure power balance and ensure AC ratios are as close to 1 as possible. After hour 30, the priority is shifted towards DS. Once DS depleted its upstream tank, MS and AEC are turned on. The DAC is turned off until the CO_2 buffer is empty. It is hence, at the 34th hour that the DAC is turned on. In reality, these one-hour time steps are quite large to encompass real-time behaviour. The next section will discuss more on the temporal granularity in the model.

5.4. Temporal Granularity

The need for testing the model for temporal granularity is to verify real-time effects in the system and identify the most practical time step size for multi-scenario analysis. The setup involves simulating the microplant system for three days at Delft as the location at varying time steps as shown in Figure 5.8.

Compared to constant proportional control, it can be observed that the AC controller produces greater amounts of methanol at all time increments. When time step size is decreased from 60-minute bins to 30-minute bins, it is observed that methanol production increases in every instance. This effect is primarily attributable to a decrease in the production and consumption of substances in buffer tanks (as less amount is produced in a lesser time at constant power), despite the fact that the size of the tanks remains unchanged, thereby reducing the quantity of substance vented. This effect is most apparent in

the proportional control with constant proportions. The underlying rationale for this distinction lies in the fact that the constant proportional control allocates power to the AEC, MS, and DAC subsystems based on consistent ratios, irrespective of the availability of feed in the upstream buffer tanks. The A/C controller on the other hand is much more efficient in controlling the feed throughout the system and vents minimally.

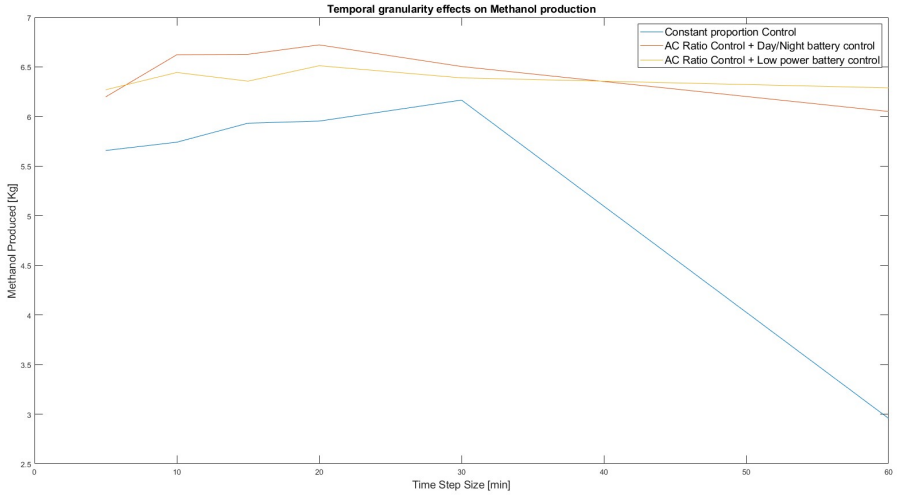

Figure 5.8: Temporal granularity assessment of the model

At lower granularity levels (5 minutes), a decline in production values is observed. This stems from sub-optimal power distribution, wherein power allocation is directed towards the AEC subsystem, despite insufficient availability of input feed water in the buffer tank to facilitate hydrogen production. This phenomenon results in the electrolyzer running dry, thus necessitating rectification in control strategies to optimize system performance. Addressing this issue is pivotal to ensuring efficient resource allocation and maintaining the system's operational robustness.

The model is more dynamic at smaller time steps, as expected. When running at smaller time steps, the model does not consider the process inertia. Since each time step is assumed to run at a steady state, smaller time steps ignore actual processes occurring in the system. For example, the time taken by the distillation system to achieve steady-state methanol production is 20 minutes as observed by experiments performed at ZEF which cannot be accounted for with time steps below 20 minutes. Most of the subsystems utilize heating elements that are unable to heat up or cool down within smaller time-step bins. On the other hand, higher time steps ignore short-term weather effects like short showers, cloudiness etc.

The model does however perform at a constant margin of being within 10% between each time step. Also, the computational load of simulating at smaller time steps increases linearly in this model. Keeping in mind the tradeoff between the accuracy of measurements and the time taken to run the simulations, the multi-scenario analysis going ahead would be performed at 30-minute bin sizes. This ensures real-time effects are not ignored by the model.

5.5. Key Performance Indicators

The microplant's performance at any given location and architecture can be understood by comparing key performance indicators (KPIs). There are 4 KPIs that can be used to evaluate the performance of the microplant total annual methanol production, process efficiency, primary efficiency or sun-to-fuel efficiency and finally, the annual capital cost to produce 1 kg of Methanol.

The total annual methanol production, of course, is the direct final output of the model and can be inferred directly after running the model.

The process efficiency is calculated as the ratio between the product of the total methanol produced and the High heating value (HHV) divided by the energy supplied to the controller. It can be formulated as

shown in Equation 5.3. This effectively shows the efficiency of the process from direct air capture until the final production of Methanol.

$$\eta_{process} = \frac{m_{methanol,total} \times HHV_{Methanol}}{Energy_{sol}} \tag{5.3}$$

Another efficiency, is the primary efficiency or the sun to fuel efficiency. This tells us the efficiency of the entire microplant including solar PV i.e. from solar irradiance to the energy contained by methanol. It can be calculated by Equation 5.4:

$$\begin{aligned} \eta_{sol} &= \frac{Pow_{MPP}}{G_{aoi} \times Area_{module}} \\ \eta_{stf} &= \eta_{process} \times \eta_{sol} \end{aligned} \tag{5.4}$$

It is important to note that the project being undertaken at ZEF is novel and unique and has not been done previously at the micro-scale. The DAC-based methanol synthesis processes are performed in large-scale industrial plants where solar arrays provide over 80,000 kW. These industrial-scale plants are orders of magnitude larger than the ZEF microplants which operate between 3.5 kW and 5kW based on the architecture [52]. The processes towards synthesizing Methanol also differ among these projects and so does the energy source. Many projects consume energy via solar PV + thermal industrial waste energy, solar PV + solar heating or other renewable sources and heat storage methods. Some research obtained sun to methanol efficiencies ($\eta - stf$) between 8.8% to 10.2% on Aspen plus which uses solar dish as energy input and undergoes low-temperature DAC in HVAC [53]. Other research has been able to generate primary efficiencies ($\eta - stf$) between 6.9% and 11.7% and process efficiencies ($\eta - process$) between 22.6% and 47.1 % [52]. In another research by Marchese et al., methanol synthesis has been performed by integrating direct air capture technology with Fischer tropsch synthesis and has been able to achieve a maximum process efficiency ($\eta - process$) of 36.3% [54].

Finally, the annual cost to produce 1 kg of Methanol is defined as the total capital cost associated with setting up one microplant divided by the total production in one year.

5.6. Summary

- This chapter discussed the model integration methodology by delving into various microplant architectures, and the control algorithm. The temporal granularity is tested for the performance of the model. Key performance indicators have also been devised to quantify the performance of the microplant
- The chapter hence, achieved the research sub-objective 3: ”Design the control algorithms and integrate the model”.
- With the model functioning, it is necessary to run simulations with various system architectures at different climate locations to find the feasibility of the ZEF microplant.

6

Simulations

The aim of this chapter is to achieve the research objective ”Analyse the microplant behaviour and predict the Methanol yield by implementing a cost-effective microplant system architecture at various geographic locations. ” To do this, the impacts of sizing of components is analysed in Section 6.2. Furthermore, in Section 6.3, the general behaviour of the microplant is discussed and the effects of various system architectures is discussed. Finally, the most feasible system architecture and geographical location is identified in Section 6.4.

6.1. Location Selection

The solar-powered ZEF microplant is very susceptible to weather conditions, mainly solar irradiance, absolute humidity and ambient temperature. Hence, multiple simulations would have to be performed at various locations. This section speaks about the selection of locations for simulations in Section 6.4.

The major area of interest at ZEF is southern Europe and northern Africa since these areas are gifted with high solar radiation which would increase the energy supplied to the microplant. Further, a higher absolute humidity is generally preferred, implying there would be a difference in the performance between areas near water bodies and those that aren't and the rainfall parameters. Ambient temperature also plays a critical role in the performance of the plant. Based on these parametrical requirements, the locations selected are shown in the map in Figure 6.1.

Figure 6.1: Locations selected in this thesis to analyse the microplant performance.

From Figure 6.1, the irradiance, absolute humidity and temperature values of the cities of interest were procured and tabulated in Table 6.1

Table 6.1: Weather Properties for 5 cities in Europe and Africa with their annual irradiation, ambient temperature and absolute humidity values.

Property/Location		Pias	Ioannina	Tripoli	Essaouira	Aoulef
Location Coordiates	**Lat**	38.02°	39.66°	32.89°	31.51°	26.9°
	Lon	-7.51°	20.85°	13.17°	-9.76°	1.1°
Irradiation [kWh/m^2]	**DNI**	2056	1629	1874	2090	2105
	DHI	574	632	728	700	814
Ambient Temperature [°C]	**Mean**	18.3	12.5	19.7	19.1	28.0
	Std	7.6	8.6	5.7	3.6	9.9
	Min	1.5	-9.2	8.8	10.4	1.9
	Max	43.6	33.8	30.1	32.3	48.54
Absolute Humidity [g/m^3]	**Mean**	9.5	7.9	13.2	11.7	4.2
	Std	2.5	3.1	4.6	2.6	1.5
	Min	3.0	1.1	4.2	5.6	0.8
	Max	16.9	15.7	25.1	17.9	13.42

From Table 6.1, the selection was done for the following reasons:

- **Pias, Portugal:** This location has moderate irradiance, ambient temperature and absolute humidity. This is also the location where the solar PV system has been validated. The location is not near a coastline.
- **Ioannina, Greece:** It receives the least irradiance and has the lowest annual temperature values, during winters and a large spread of temperature. It is also slightly on the drier side among the five locations.
- **Tripoli, Libya:** It is a coastal city with moderate irradiance and the highest absolute humidity amongst the rest while the temperatures are also moderate.
- **Essaouira, Morocco:** Essaouira is another coastal city with slightly high absolute humidity and solar irradiance with moderate temperatures.
- **Aoulef, Algeria:** Aoulef is a very dry city in the Sahara, which receives high irradiance and has the highest maximum ambient temperatures.

Figure 6.2 shows a comparison between weekly mean absolute humidity and ambient temperatures.

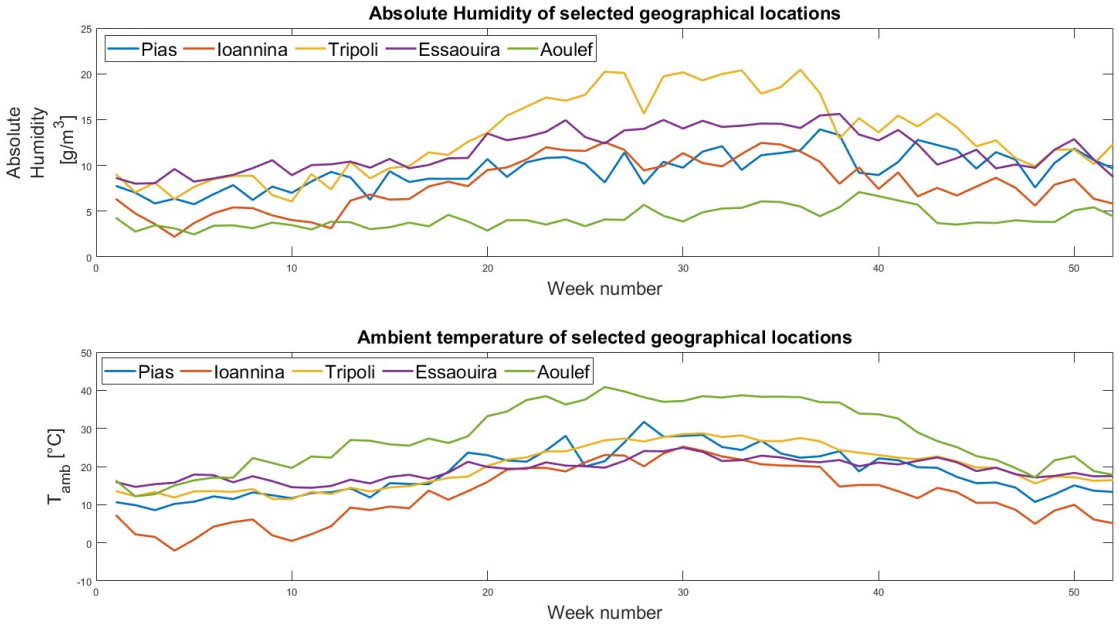

Figure 6.2: Weekly mean absolute humidity (top) and weekly mean ambient temperature at the selected locations.

6.2. System Sizing and Specifications

This section deals with the sizing impacts of various components/subsystems in the microplant which can be altered based on need. It is important to size the system for optimum performance and financial gain. In this section, the necessity and effects of sizing are looked into.

6.2.1. Solar PV sizing

Sizing the solar PV is crucial as the DC power supplied to the entire microplant (including charging batteries) is impacted. The solar PV subsystem sizing test has been performed in Delft while varying the number of PV modules and keeping all other parameters constant.

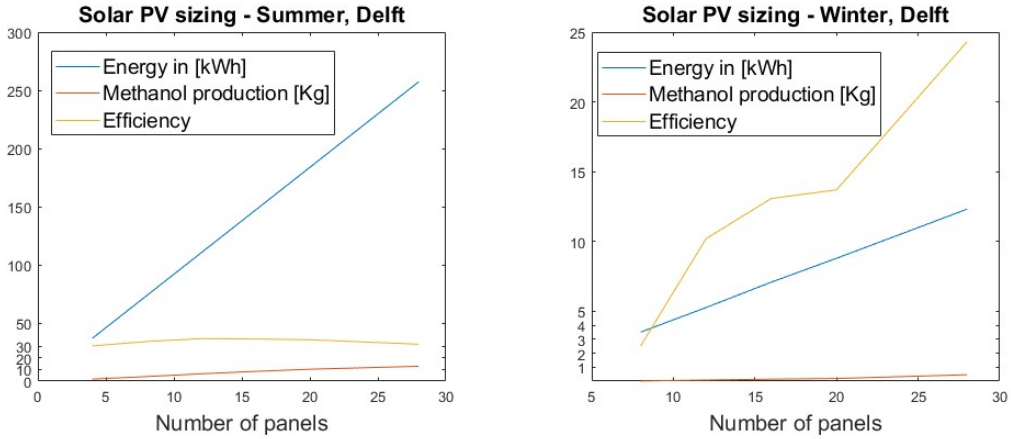

Figure 6.3: Solar PV sizing.

As seen from the Figure 6.3, in summer it is evident that increasing the number of PV modules increases the total Methanol production, while the process efficiency ($\eta_{process}$) of the system increases initially and then reduces. The initial increase is due to systems not running at their optimum production rates such

as the MS subsystem which hinders the overall Methanol production. The reduction in efficiency, later on, is due to an energy imbalance due to higher solar PV input than the consumption of the microplant during the day. This oversizing can be offset with a suitable-sized battery.

In the winter, on the other hand, the efficiencies are significantly lower for a very small number of panels. This is due to a lack of solar irradiance to power up any subsystem initially, as it can be seen in a period of 5 days, only 3.51 kWh was produced by the solar panels. The efficiency plateaus between 10 and 20 panels where the energy input is just enough to operate the distillation system minimally. Increasing the number of panels allows more energy in and a constant operation of MS and DS which increases the efficiency significantly.

The number of solar panels is directly proportional to the energy generated and the total Methanol produced, but the financial costs need to be kept in mind. An ideal sizing is done based on the load characteristics. The PV system is ideally sized based on the maximum load required as can be seen by Equation 6.1.

$$P_{load} = Pow_{DAC,max} + Pow_{AEC,max} + Pow_{MS,max} + Pow_{DS,max} \tag{6.1}$$

For the base case system, 12 415 Wp modules are selected. The specification sheet for the PV modules is provided in the **??**.

6.2.2. Battery

Batteries are generally based on the need. In the case of the microplant, if 24-hour operations are intended, then a battery must be chosen based on its charging and discharging capacity at a c-rating of C/10. C/10 is chosen as it provides an optimum discharge rate during winters where hours without sunlight are around 10 hours, and lesser in summer.

By adding batteries, the solar PV sizing is also altered as it needs to consider the battery's consumption during the day. This increase in PV panels also assists in increased production during winters and ensures 24-hour operation in summers as can be seen in Section 6.3.3. In this case, the load would be characterised by Equation 6.2.

$$P_{load} = Pow_{DAC,max} + Pow_{AEC,max} + Pow_{MS,max} + Pow_{DS,max} + Pow_{discharge,max} \tag{6.2}$$

For the simulations performed in this chapter a battery with 1140 Ah under C/10 at 18V has been chosen whose specifications are given in **??**. By, incorporating the battery, the PV system sizing increases to 16 panels instead of 12 panels.

6.2.3. Buffer Tanks

Buffer tanks are important to the ZEF microplant as they store feedstocks between subsystems to account for the variability of solar PV and the different production rates of all subsystems. Buffer tank sizes need to be optimized as oversized buffer tanks carry a financial penalty while undersized buffer tanks vent more material, which leads to performance losses. Figure 6.12 gives an understanding of how much the buffer tanks are used over the duration of the year,

It can be seen from the above Figure 6.12 that the CO_2 buffer tends towards a fill percentage of 100%. This shows that the CO_2 buffer tank is undersized. While the H_2 buffer tank is filled up in the summers. Even though it is oversized during the winter operation, undersizing the tank would cause higher losses during summer lowering the overall Methanol yield. On the other hand, the Methanol and water liquid buffer tank is highly oversized.

The sizing is location and weather-dependent due to the variable production of the DAC subsystem. A similar analysis can hence be performed. An optimal buffer tank sizing needs to be done for each location. It is also, important to note that the sizing depends on the temporal granularity since for larger timesteps, there is an increased production and hence a larger buffer tank is needed.

For this chapter, the following buffer sizes have been used. The volume of the H_2O and methanol-water buffer tanks are 0.1 m^3 since they are stored as liquids and the buffer tank do not have any other specifications. The CO_2 and H_2 buffer tanks are 0.2 m^3. This is due to cost and functionality limitations due to compressing gases at higher temperatures.

For the coming sections, the specifications used are shown in Table 6.2.

Table 6.2: Specifications of components in the simulation

Specifications		Base Case	Battery
Solar PV	**Wp @ STC**	415	415
	Series	2	2
	Parallel	6	8
Battery	**Capacity @ C/10**	N/A	1140
	V		18
Buffer	**CO_2 Volume (m^3)**	0.02	
	H_2O Volume (m^3)	0.1	
	H_2 Volume (m^3)	0.02	
	Methanol+Water Volume (m^3)	0.1	

6.3. Microplant behaviour: System Architecture

Understanding the behaviour of the microplant at the selected location in Pias, Portugal is crucial for evaluating its performance under various system architectures. Pias has been chosen for two reasons. The solar PV system has been validated at the location and Portugal is also a location of importance for locating the microplant. This analysis is shown for Pias to understand the model behaviour in detail. Section 6.4 shall delve into the feasibility of the plant at different locations.

In the base case scenario, the microplant operates with a single-axis tracker and a suitably sized PV system, omitting battery storage whose details are in the **Appendix**. This configuration serves as the reference point against which alternative system architectures are compared. By analyzing its performance, we can establish a baseline understanding of the microplant's behaviour in this specific environmental context. By contrasting these scenarios with the base case, we can discern the nuanced behavioural differences that arise under varying system architectures, providing valuable insights for optimizing the microplant's design and operation in the chosen location.

6.3.1. Base Case

The microplant, which is weather sensitive, also mirrors the behaviour of the weather. This means the microplant also has two distinct behaviours exhibited by solar irradiance, ambient temperature and absolute humidity. The behaviour can be categorised into diurnal and seasonal.

Base Case: diurnal behaviour

The microplant, in the base case operates only during the presence of sunlight, since it is not connected to batteries. The overall production of the microplant's subsystems and energy supplied are shown in Figure 6.4. To analyze the diurnal behaviour, two days have been analysed together so that it is possible to analyse complete day and night cycles and gain more insights.

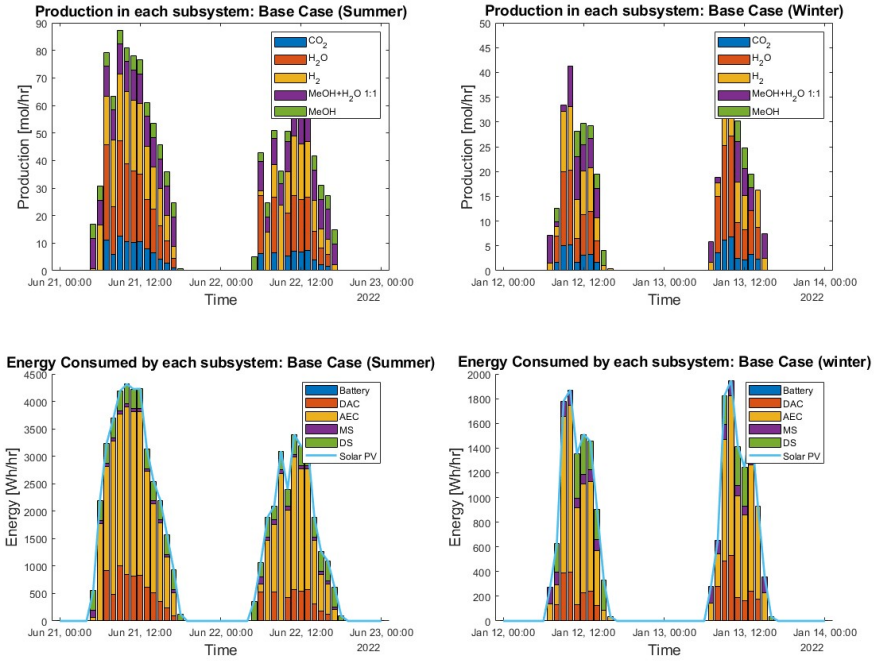

Figure 6.4: The production of each subsystem and the Energy consumed by subsystems. The plots on the left indicate two typical days during summer and the plots on the right show the behaviour on a typical day in winter. The time steps are 1 hour. The summer days are 21-22 June, 2022 and the winter day is 21 - 23 Feb, 2022

From Figure 6.4 a salient observation is the substantial energy demand by the Alkaline Electrolysis Cell (AEC). Also, the Methanol Synthesis (MS) subsystem exhibits reduced energy requirements during continuous operation as it tends towards the autothermal region. Notably, during the winter months, the Distillation System (DS) operates intermittently, primarily driven by the amount of methanol-water mixture in the upstream buffer tank since a minimum of 5 [mols] is required. This intermittent operation is influenced by factors such as reduced solar irradiance, limiting the production of CO_2 and water. Also, during winters, with limited energy available, the MS subsystem is limited by the availability of H_2 in the H_2 buffer tank. Lower Hydrogen availability implies a lesser yield by MS. This implies the heat generated by the reaction is not enough to reduce the energy requirements as most of the energy input is used to maintain the setpoint temperature.

It is also, important to understand how each of the subsystems behaves on a day-to-day basis. Figure 6.5 shows the power supplied to the subsystem, production of CO_2 and H_2O and the weather components which are absolute humidity and ambient temperature.

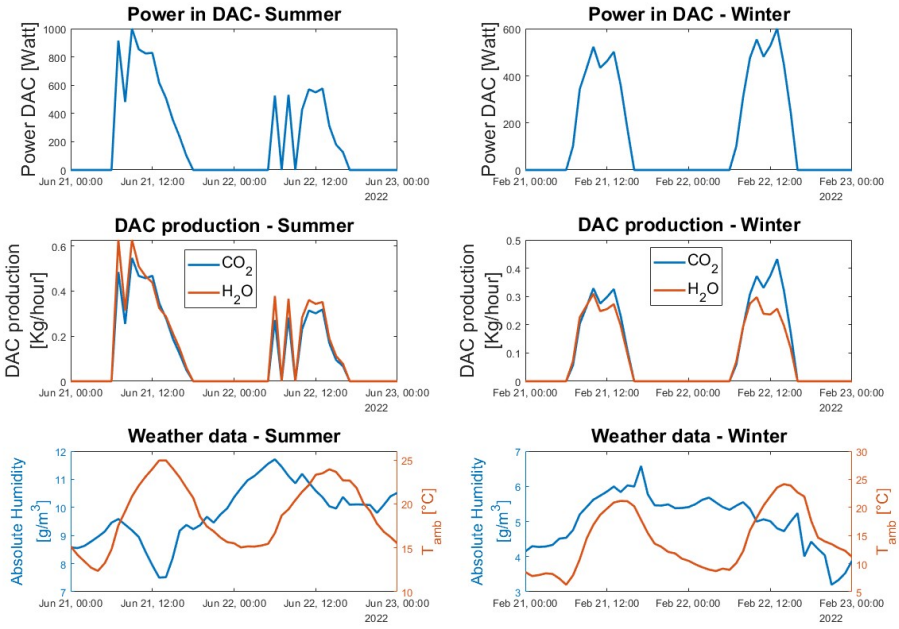

Figure 6.5: Performance of the DAC subsystem on two typical days each in winter and summer. The summer days are 21-22 June, 2022 and the winter day is 21 - 23 Feb, 2022

As expected, the power supplied to DAC increases and then decreases based on the power supplied by the solar PV. The DAC is operational longer during the summer than in winter and the maximum power supplied to the DAC is lesser in winter than in summers. The production of carbon dioxide and water is proportional to the power. But, it can also be observed that there are moments where the production of water differs as it is directly affected by the absolute humidity. The DAC is also turned off burning this period (on June 22), which occurs when both the CO_2 and H_2O buffer tanks are more than 70% full while the H_2 buffer tank is less than 30% full. This is done to redirect energy into the AEC to boost the production of Hydrogen. The production of water and carbon dioxide further impacts the behaviour of AEC and MS. AEC's diurnal behaviour can be seen in Figure 6.6.

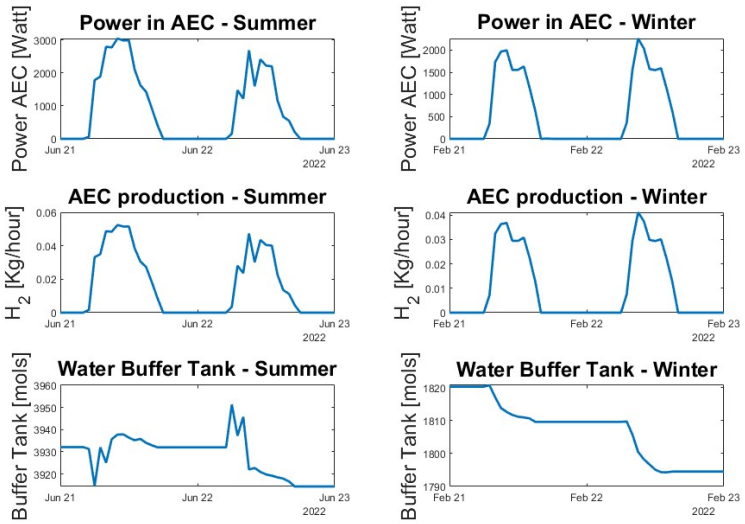

Figure 6.6: Performance of the AEC subsystem on two typical days each in winter and summer. The summer days are 21-22 June, 2022 and the winter day is 21 - 23 Feb, 2022

The AEC draws the most energy from the controller. This, in general, makes AEC behaviour quite stable due to the good performance of the DAC system which fills up the water buffer tank during the day. The consumption on these specific days is much less than that being produced, while consumption by AEC peaks during the afternoon when the most energy is provided to the stack. The increased power supply comes in the form of high current densities and also, high voltage to the stack. Higher voltages reduce the efficiency of the stack over the year can be seen in Figure 6.7.

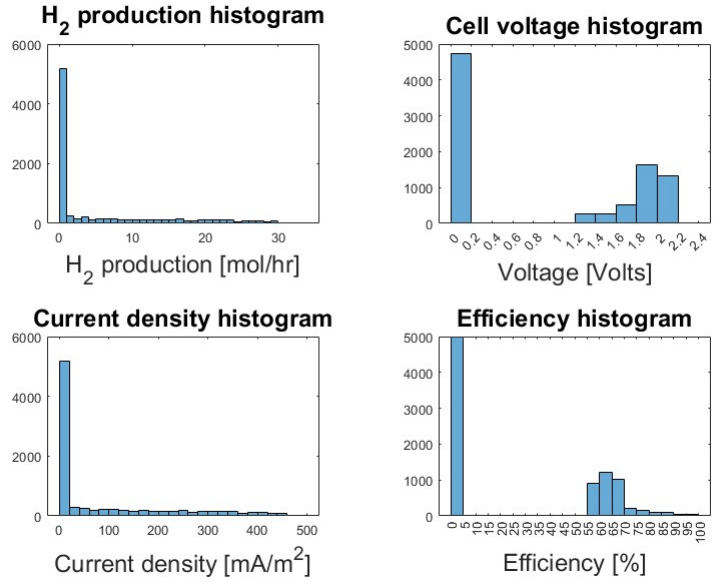

Figure 6.7: Performance histograms of AEC

These histograms in Figure 6.7 show the trends in the AEC clearly. There is a direct correlation between Hydrogen production and the current density. Focusing on the cell voltage and efficiency histograms, it is clear that there is an inverse effect. The stack performs between 60% and 70% per cent most of the time. This can be reduced by running the parallel AEC architecture which is analysed in Section 6.3.5. Next, the MS subsystem is assessed in Figure 6.8.

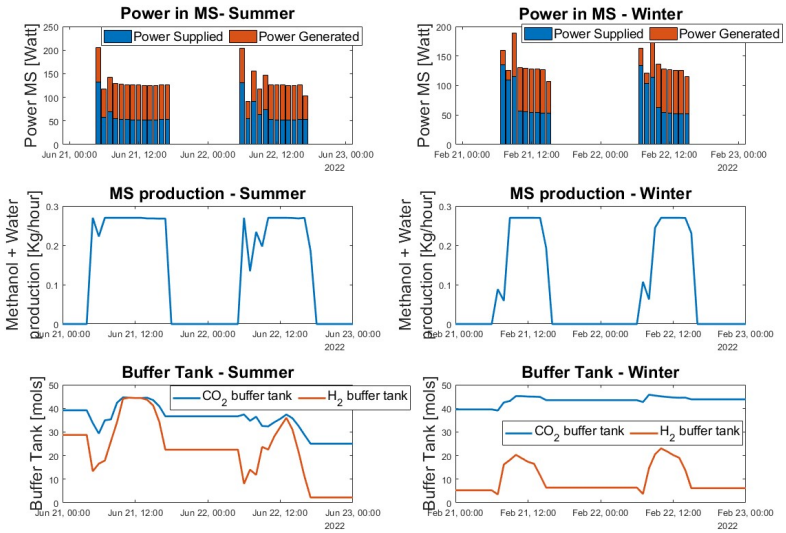

Figure 6.8: Performance of the MS subsystem on two typical days each in winter and summer. The summer days are 21-22 June, 2022 and the winter day is 21 - 23 Feb, 2022

From the Figure 6.8, it can be seen that the power supplied to MS reduces over the day unless the MS is shut down. Upon restarting, the power drawn from the controller is high. The heat generated depends on the production of methanol and water and can be compared to the amount produced. When low amounts of Methanol are produced, there is higher power drawn from the controller in the next iteration. In winter, it can be seen that sometimes, due to lower content in the upstream buffer tanks, especially Hydrogen, the production is largely reduced which drives up the power supplied to continuously heat up the reactor. After this, DS is analysed.

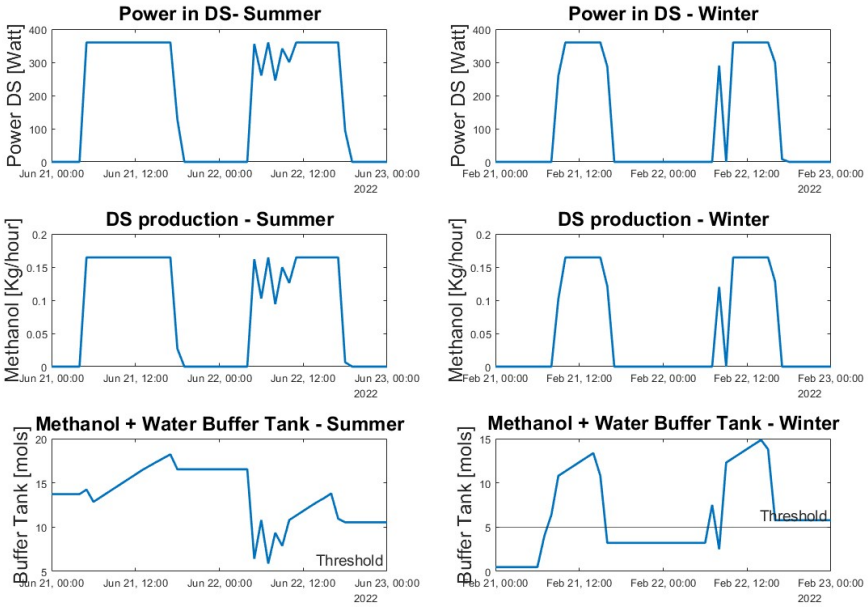

Figure 6.9: Performance of the DS subsystem on two typical days each in winter and summer. The summer days are 21-22 June 2022 and the winter day is 21 - 23 Feb 2022

In Figure 6.9, a direct correlation between power supplied and Methanol production is visible. Being, the most downstream subsystem, and especially with MS being a bottleneck to the operation of the microplant, there is high intermittency in running the DS which is turned on only if there are at least 5 moles in the upstream buffer tank. This is to ensure minimum flow in the distillation column. This intermittency can perhaps be reduced if central distillation columns for multiple microplants can be installed.

Base Case: seasonal behaviour
Examining the annual behaviour, it becomes evident that the microplant experiences seasonal variations in energy input, absolute humidity, and temperature.

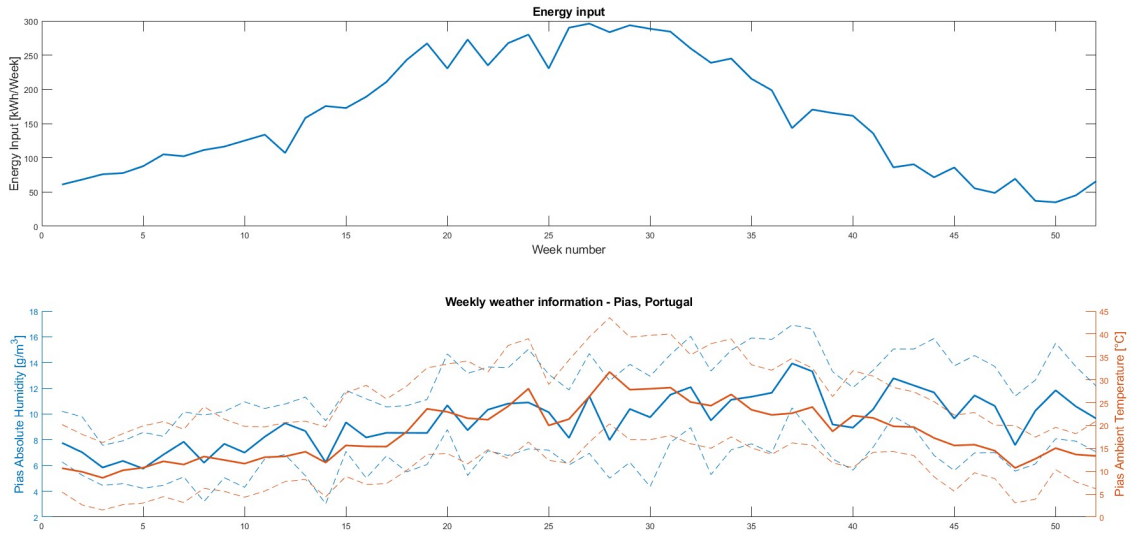

Figure 6.10: The total weekly energy input to the system (above). The weekly mean, maximum and minimum absolute humidity and ambient temperature during the year with week numbers in the x-axis

During the summer months as seen in Figure 6.10, characterized by higher solar irradiance and longer hours of daylight, the energy input increases. A similar increase in absolute humidity and ambient temperature is also observed. This is where in dynamics of production by DAC would be impacted. Higher energy input and higher absolute humidity increase DAC yield while a higher temperature inhibits the yield. These variations also impact the production of the microplant as shown in Figure 6.11.

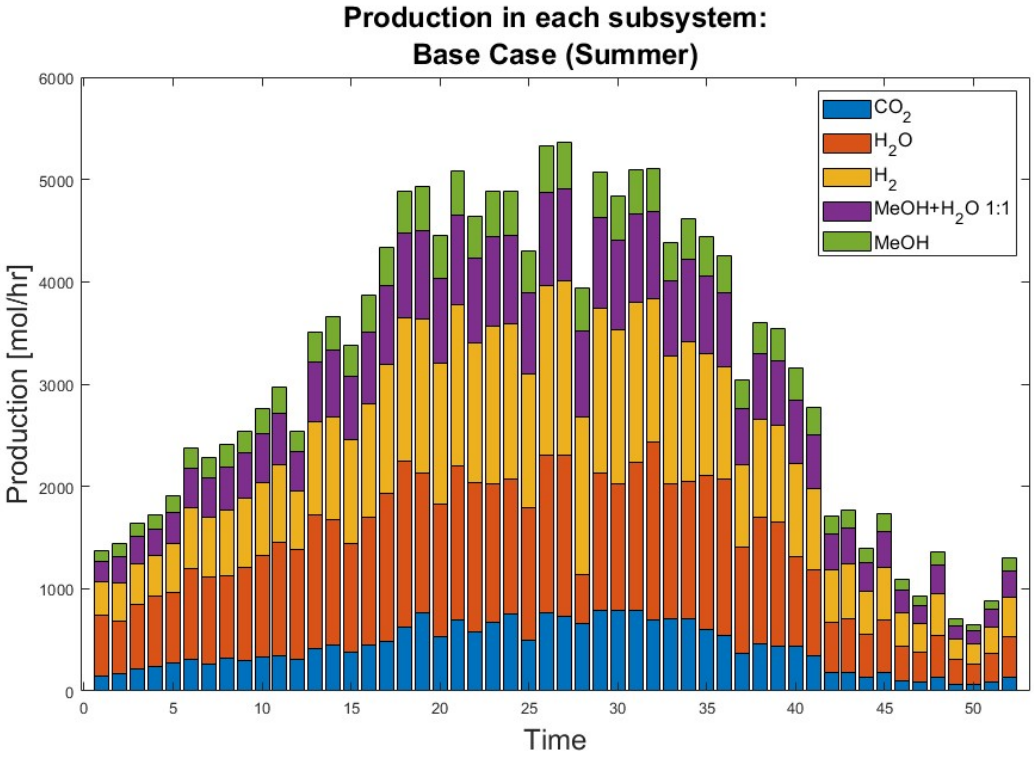

Figure 6.11: The total weekly production of all subsystems over 52 weeks.

The seasonal variation is correlated with the input energy, absolute humidity and ambient temperature. It can be seen that summer months have higher production when compared to winter. Absolute humidity plays a huge role in the production of water in the system. This can be corroborated in the dip in production in week 28. This can be attributed to 2 factors, lesser production of water due to a reduction in absolute humidity (Figure 6.10) and also using up of most of the CO_2 and H_2O buffers (Figure 6.12). The interplay of buffer feed, weather and PV energy play a major role in final production.

The microplant's controller exhibits dynamic prioritization of subsystems based on various factors. When the system faces hydrogen limitations, it prioritizes the AEC subsystem, while during water or CO_2 limitations, the Direct Air Capture (DAC) takes precedence. This prioritization is particularly noticeable in the summer and during morning hours. Since the DAC requires a minimum activation of 100W the MS or DS subsystems are operated. During this period, both subsystems deplete their upstream buffer tanks. Consequently, the electrolyser is generally prioritized in the morning to enhance hydrogen production for subsequent methanol synthesis as the microplant is, in general not CO_2 limited as shown in Figure 6.12.

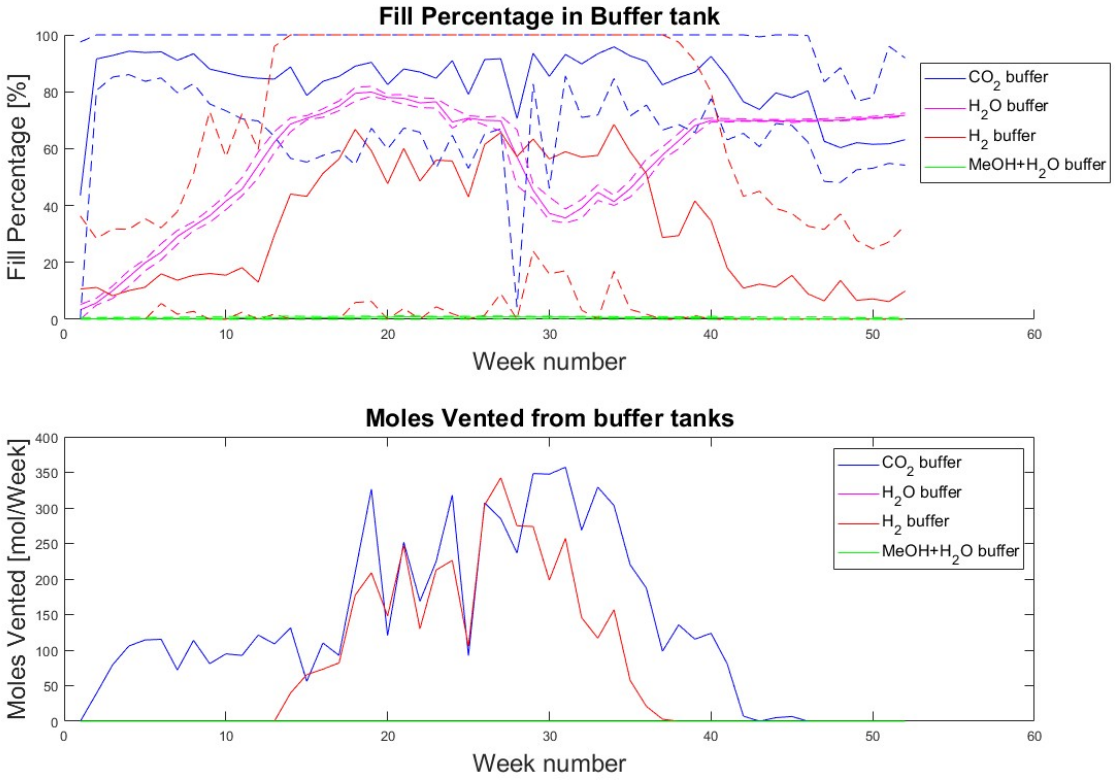

Figure 6.12: Mean, maximum and minimum weekly buffer tank fill percentage (above) and total weekly moles vented from each buffer tank (below)

Further insights into the microplant's behaviour are gained by analyzing the seasonal variation in buffer tank utilization based on insights from Figure 6.12. These variations are a function of production by upstream subsystems, consumption by downstream subsystems, and the physical properties of the tanks themselves. Carbon dioxide and water are consistently abundant throughout the year, with the CO2 buffer tank typically venting excess gas and consistently running above 50% during most of the year. However, the water content absorbed by the system experiences fluctuations, increasing in the first part of the year and decreasing during the summer due to reduced absolute humidity and higher consumption by the MS subsystem. The high venting of H_2 during the summers due to limited consumption by MS signifies a bottleneck in the system's flow and also due to the continuous operation of the AEC subsystem which produces more Hydrogen than required. Meanwhile, the methanol-water buffer tank, acting as more of an intermediary than a storage device, remains stable in its mass flow dynamics between MS and DS, with

its behaviour not distinctly resolved in weekly averages due to these dynamics. Furthermore, in this case, a total of 315 kg of substances (Carbon dioxide and water) were vented and 73 kg were still retained in the buffer tanks by the end of the simulation.

In assessing the microplant's behaviour, the total energy input over the year was 8.78 [MWh]. The Direct Air Capture (DAC) system, generated 952 kg of CO_2 and 930 kg of H_2O, while the Alkaline Electrolysis Cell (AEC) produced 95 kg of H_2. On the other hand, the Methanol Synthesis (MS) subsystem yielded 1461 kg of Methanol and water mixture, and the distillation system contributed to the final 467 kg of grade A methanol output. The process efficiency stands at 34% with 67% of the absorbed CO_2 converted into grade A methanol.

6.3.2. Solar PV fixed mounting architecture

In the fixed mount architecture, a fixed mount is employed instead of a single-axis solar tracker. This architecture is investigated to assess the cost-production trade-offs associated with the integration of single-axis trackers. Figure 6.13 illustrates the methanol output and energy input for both architectural configurations.

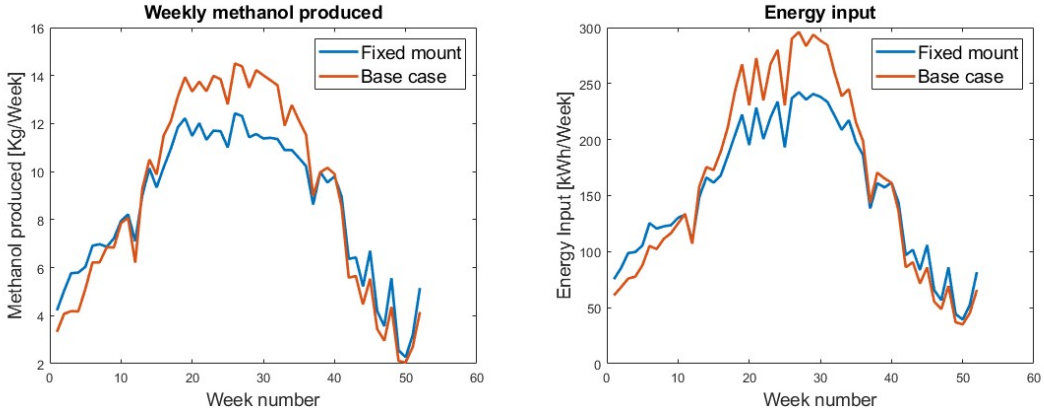

((a)) Weekly Methanol production.

((b)) Weekly Energy Input.

Figure 6.13: Comparison between Methanol production and weekly energy input between fixed mounting architecture and the base case architecture against the week number.

Analysis of the energy input reveals notable distinctions between the two architectures while maintaining the same number of solar PV panels. Particularly, when employing a single-axis tracker, there is a substantial surge in the total weekly energy input to the microplant compared to fixed mounting, especially during the summer months. In the base case, the system supplies 8.78 kWh over the entire year, while the fixed mounting architecture yields 8.19 kWh annually, representing a 5% reduction compared to the base case. It is crucial to emphasize that this value is specific to Pias, Portugal location in Portugal and may exhibit variations based on geographical locations.

Consequently, total methanol production exhibits a parallel pattern to energy input, peaking in summer and declining in winter. The base case generates more methanol during summer, while production becomes relatively comparable during winter, with a slight advantage for fixed mounting. The fixed mounting subsystem has a yield of 443 kg of Methanol which is 5.11% lesser than the base case that produces 467 kgs. Also, in this case, a total of 281 kg of substances (Carbon dioxide and water) were vented and 76 kg were still retained in the buffer tanks by the end of the simulation.

For a detailed daily breakdown of subsystem behaviour, please refer to Figure B.1. Remarkably, buffer trends remain akin to those observed in the base case since energy remains the primary variable in both scenarios can be seen in Figure B.2. Both plots can be found in Appendix B.

6.3.3. Base case + battery architecture

The base case + battery architecture introduces a battery into the existing system, necessitating adjustments in the sizing of the PV system to accommodate this addition.

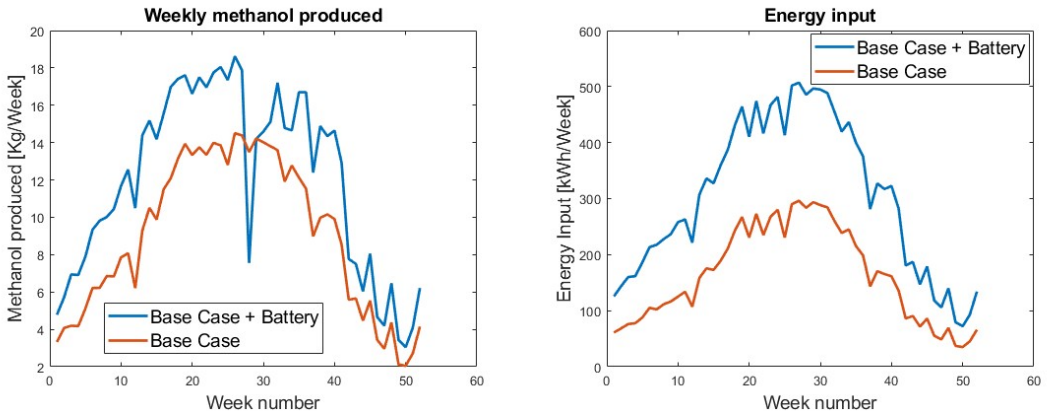

((a)) Weekly Methanol production.

((b)) Weekly Energy Input.

Figure 6.14: Comparison between Methanol production and weekly energy input between the base case + battery architecture and the base case architecture against the week number.

As depicted in the Figure 6.14(b), the base case + battery configuration notably benefits from increased energy input during both summer and winter. This additional PV capacity, attributed to the surplus panels, results in higher DC energy yields. Consequently, the base case + battery configuration produces 13.17 MWh annually, marking a 39% increase over the base case.

According to Figure 6.14(a) the methanol production scales similarly throughout the year in the base case + battery scenario, resulting in the production of 620 kgs of methanol, representing a 32% increase compared to the base case.

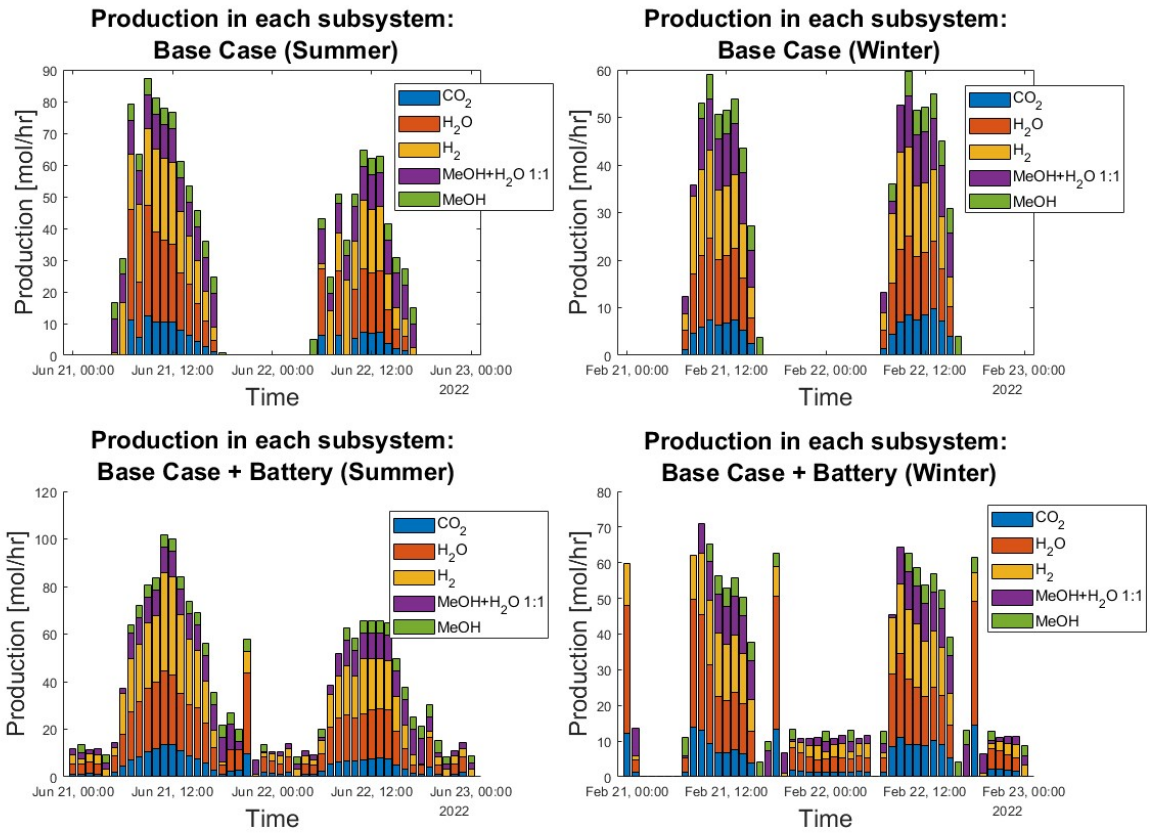

Figure 6.15: The production of all subsystems on two typical days in summer and winter. The plots in the top show the production in the base case while the ones below are for the base case + battery architecture. The summer and winter production plots are on the left and right respectively. The summer days are 21-22 June, 2022 and the winter day is 21 - 23 Feb, 2022

The behaviour of this configuration diverges notably from the base case as can be seen in Figure B.3. On average, subsystem yields in the base case + battery exhibit a consistent increase, with winter yields, for instance, surging by approximately 25%. Additionally, the inclusion of batteries extends the operational hours of the plant, enabling 24-hour functionality during summers and an overall increase in operational hours during winter.

Buffer tank dynamics (Figure B.4) remain relatively consistent for the water and methanol-water mixture tanks. However, there is a pronounced deviation in the behaviour in the hydrogen buffer tank, which experiences a decline to 0% fill during the summer weeks spanning from 26 to 37. This period coincides with optimal hydrogen and carbon dioxide production, facilitating increased methanol production. A comparable, albeit less pronounced, variation is observed in the carbon dioxide buffer tank. 519 kg was vented and 74 kg is stored in the buffer tank in the end.

6.3.4. Base case + parallel AEC architecture

The base case + parallel AEC architecture incorporates an additional AEC stack into the existing system, aiming to enhance hydrogen production efficiency by capitalizing on improved stack performance.

Based on Figure 6.16(b), there is no difference in energy input emerges between the two architectures, given the unchanged source of DC energy input.

However, a slight increase in methanol production is observed in the parallel AEC architecture scenario, yielding 472 kilograms of methanol in the year. Notably, this increase is more prominent during winter and certain summer weeks. The system operates with a process efficiency of 34.4%, with 65.6% of CO_2

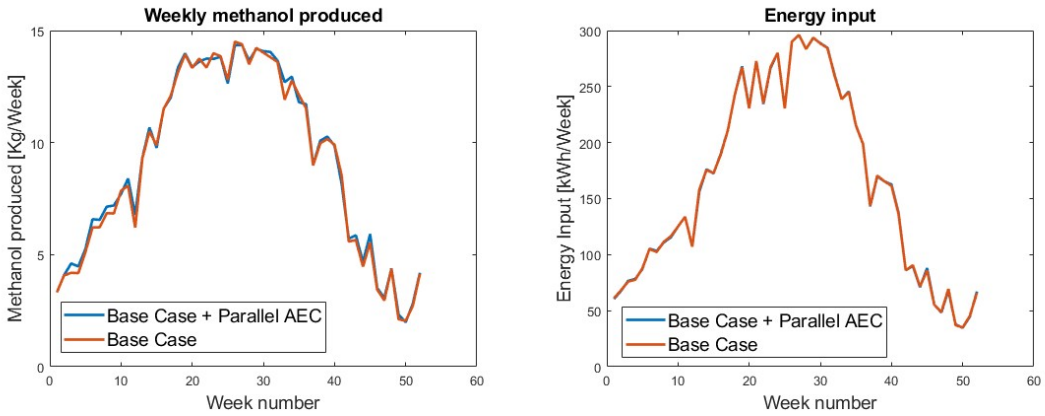

((a)) Weekly Methanol production. **((b))** Weekly Energy Input.

Figure 6.16: Comparison between Methanol production and weekly energy input between the base case + parallel AEC architecture and the base case architecture against the week number.

effectively converted into methanol while the sun to fuel efficiency is 6.4%. A more granular understanding of these dynamics is revealed by examining the microplant's daily production patterns.

The behaviour of the microplant under the base case + parallel AEC architecture presents two noteworthy distinctions shown in Figure B.5. Firstly, the cumulative production across all subsystems exhibits smoother trends, with dampened peaks. Secondly, there is an increased production of carbon dioxide and water, attributed to the increased energy supply to DAC which is derived due to the efficiency gains achieved by the AEC subsystem.

Buffer tank dynamics closely resemble those of the base case as can be seen in Figure B.6, with a total vented amount of 351 kilograms and 73 kilograms remaining at the end of the simulation.

6.3.5. Base case + parallel MS architecture

The base case + parallel MS architecture introduces an additional MS reactor operating in parallel with the existing system, which is primarily activated during peak energy demand periods. This is expected to result in higher methanol production.

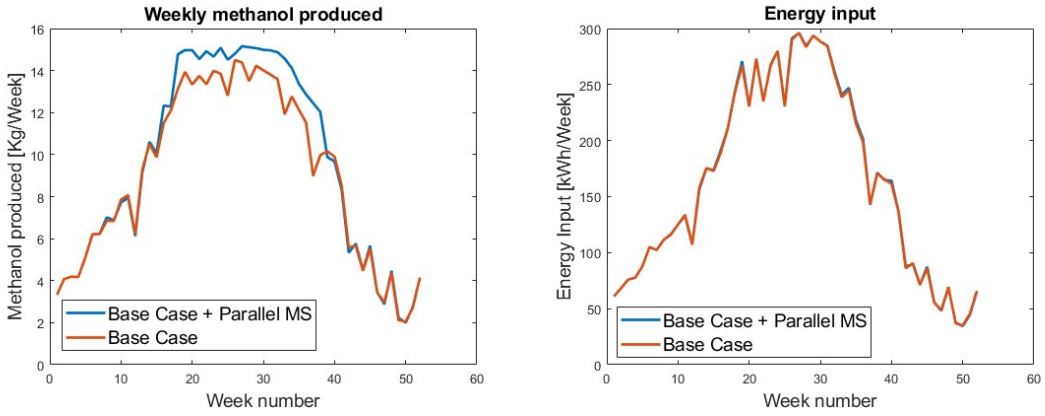

((a)) Weekly Methanol production. **((b))** Weekly Energy Input.

Figure 6.17: Comparison between Methanol production and weekly energy input between the base case + parallel MS architecture and the base case architecture against the week number.

As illustrated in Figure 6.17(b), no discernible variance in energy input exists between the two architectures, as there is no alteration in the DC energy input source.

However, a substantial increase in methanol production is evident in the parallel MS architecture scenario according to Figure 6.17(a), generating 497.32 kilograms of methanol, signifying a 6.37% improvement over the base case. Notably, this enhancement is primarily concentrated in the summer weeks. The system operates with an efficiency of 36.19%, converting 73.33% of CO_2 into methanol. A closer examination of daily production patterns provides insight into these dynamics.

Daily production behaviour reveals consistent operation during winters but an increased methanol-water mixture output during summers, which increases the production of methanol and tones back the production of Hydrogen in the system slightly which is visible in Figure B.7.

Significant differences emerge in the behaviour of buffer tanks can be seen in Figure B.8. While the Carbon dioxide and water buffer tanks exhibit minimal variation when compared to the base case. The methanol-water mixture buffer experiences substantial growth in the base case + parallel MS scenario. This growth diminishes overall hydrogen venting, which implies better management of H_2 in the microplant. 247.37 kilograms of substance is vented and 73 kgs is stored within the buffer tanks at the end of the simulation.

6.3.6. Base case + water feedback architecture

The base case + water feedback architecture incorporates a system where the water generated as a byproduct of the DS is redirected into the water buffer tank of the existing architecture, providing additional feedstock for the electrolyser.

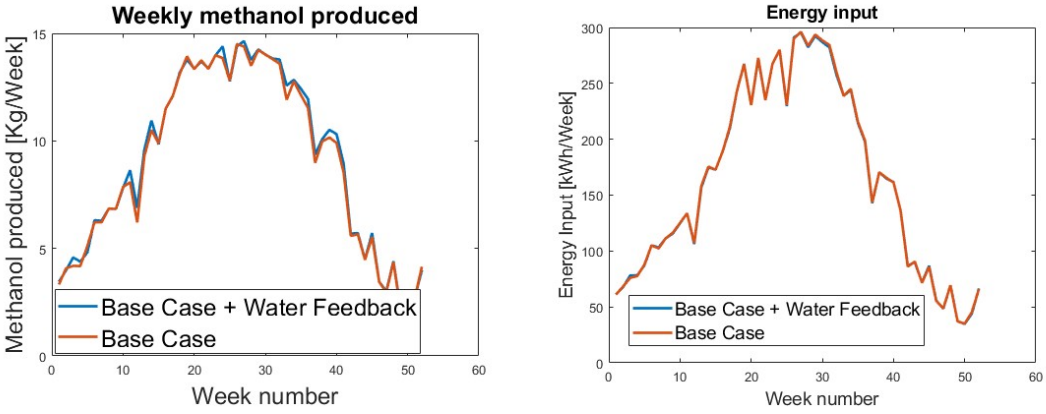

((a)) Weekly Methanol production.

((b)) Weekly Energy Input.

Figure 6.18: Comparison between Methanol production and weekly energy input between the base case + Water feedback architecture and the base case architecture against the week number.

As depicted in the Figure 6.18(b), no noticeable difference exists in the energy input between the two architectures, as the DC energy input source remains unchanged. While there is a very slight output increase over the year this architecture yielded 474 kilograms of methanol. There is only a 6.8 Kg increase when compared to the base case. The overall process efficiency of the architecture is 34.52% and 73.43% of CO_2 is converted into Methanol.

Daily production patterns exhibit limited variation, with minimal differences observed according to Figure B.9. However based on Figure B.10, distinctive behaviors emerge in the buffer tank dynamics. The base case + water feedback architecture accumulates excess water, with most of it subsequently vented. Notably, the reduction in stored water in the buffer tank during summer is less pronounced than in the base case. Additionally, the water buffer tank remains predominantly full throughout the year. Overall, 336 kilograms is vented and 101 kgs is stored in the buffer tanks at the end of the simulation. It is important to note that this is very location dependent and other locations may benefit from this architecture more than that in Pias.

6.4. Microplant behaviour: Location based analysis

This section highlights the performance of the microplant at different locations under different weather conditions with different system architectures to find the most feasible system architecture. The simulations

have been performed at 60 minute time steps for the locations stated above. The analysis is performed for 14 system architecture combinations. In total, 58 simulation runs have been performed. The setup, sizing and specifications of the parameters, and subsystems are given in **??**.

Table 6.3 analyses the total methanol production in each architecture combination at the given locations. The fixed mounting (F), single-axis tracker mounting (1°), battery (B), parallel AEC (AEC), parallel MS (MS) and water feedback (W) system architectures and their combinations have been analysed. The fixed mounting, single-axis tracker and battery architectures directly influence the energy supplied to the microplant while parallel AEC, parallel MS and water feedback influence the mass flow amongst subsystems and buffers and final methanol yield.

In total 14 such combinations have been analysed at each location, while only 2 combinations have been analysed for Aoulef as it was found to be impractical to set up microplants there(the reasons shall be discussed later in the section). 4 out of the 14 combinations are performed using the fixed mounting architecture. These 4 are further divided between battery architecture (F and F+B) and all the mass-flow architectures (AEC + MS + W). 10 combinations are simulated for single-axis tracking mounting with 5 with batteries (1° + B) and the remaining 5 without batteries (1°). In each bucket, architectures have been tested individually and with all of them combined.

After performing these simulations, Table 6.3 shows the final output of the systems.

Table 6.3: Annual Methanol Production for different system architectures at different locations [Kg Methanol]. The architecture abbreviations are as follows: F = Fixed mounting. B = Battery. AEC = Parallel AEC. MS = Parallel MS. W = Water feedback

Architecture/Location	Pias, Portugal	Ioannina, Greece	Tripoli, Libya	Essaouira, Morocco	Aoulef, Algeria
F	444	434	432	517	-
F+AEC+MS+W	507	763	455	568	-
F+B	624	624	626	735	-
F+B+AEC+MS+W	773	709	704	875	-
1°	467	451	459	545	248
1°+AEC	473	460	469	552	-
1°+MS	497	465	467	584	-
1°+W	474	451	461	546	310
1°+AEC+MS+W	529	493	491	567	-
1°+B	621	637	647	755	-
1°+B+AEC	632	650	661	773	-
1°+B+MS	754	712	720	865	-
1°+B+W	643	639	649	758	-
1°+B+AEC+MS+W	776	752	761	884	

From Table 6.3, certain trends can be observed. Firstly, the addition of batteries provides a significant increase in Methanol production when compared to their equivalent architectures without batteries in all locations. Secondly, a single-axis tracker also increases the methanol yield when compared to its counterparts in the fixed mounting architectures. Thirdly, The water feedback architecture and the parallel AEC architectures (both with and without batteries) have similar increments when compared to the simple ZEF microplant architecture. Fourthly, the largest and most significant yield increases are found in parallel MS architectures. Finally, the highest and lowest possible yields are highlighted in green and red respectively. The highest yields are produced by all architectures combined while the lowest yields across all locations are from the fixed mounting architecture. The highest yields are in average 1.7 times higher than the lowest yield architectures.

Table 6.4: The process efficiency and sun to fuel or primary efficiency for different architectures at different locations. The architecture abbreviations are as follows: F = Fixed mounting. B = Battery. AEC = Parallel AEC. MS = Parallel MS. W = Water feedback

Architecture/Location	Pias, Portugal	Ioannina, Greece	Tripoli, Libya	Essaouira, Morocco	Aoulef, Algeria
F	34.5 || 6.5	37.1 || 7	37 || 7	35.8 || 6.7	-
F+AEC+MS+W	39.5 || 7.4	39.6 || 7.4	39 || 7.3	39.3 || 7.3	-
F+B	32.4 || 6	35.6 || 6.7	35.7 || 6.7	34 || 6.3	-
F+B+AEC+MS+W	40.1 || 7.5	40.4 || 7.6	40 || 7.5	40.4 || 7.5	-
1°	34 || 6.3	36.4 || 6.8	36.4 || 6.9	34.6 || 6.5	12 || 2.2
1°+AEC	34.4 || 6.4	37 || 7	36.9 || 6.9	35.1 || 6.5	-
1°+MS	36.2 || 6.8	37.5 || 7	37.2 || 7	37.2 || 6.9	-
1°+W	34.4 || 6.4	36.4 || 6.8	36.5 || 6.9	34.7 || 6.5	15.1 || 2.8
1°+AEC+MS+W	38.6 || 7.2	39.8 || 7.5	38.9 || 7.3	39.3 || 7.3	-
1°+B	30 || 5.6	34.3 || 6.4	34.2 || 6.4	34.6 || 6.5	-
1°+B+AEC	30.6 || 5.7	35 || 6.6	35 || 6.6	32.8 || 6.1	-
1°+B+MS	36.6 || 6.8	38.3 || 7.2	38 || 7.1	36.7 || 6.8	-
1°+B+W	33.5 || 6.2	34.3 || 6.4	34.2 || 6.4	32 || 6	-
1°+B+AEC+MS+W	37.6 || 7	40.4 || 7.6	40.1 || 7.6	37.5 || 7	-

The process efficiency is the efficiency of the microplant disregarging the coversion efficiencies of the solar PV. It essentially is the efficiency of the process of capturing Carbon dioxide and water and converting it into Methanol. While, sun to fuel efficiency or the primary efficiency is the efficiency of the entire microplant. This considers the conversion of energy from solar irradiance until the methanol that is produced. Naturally, the efficiencies are higher when the yield of the microplant is higher which essentially happens when the parallel MS architecture is chosen. The parallel MS architecture has boosted the efficiencies when compared to the base case in most situations. Parallel AEC architectures do not make much of an impact toward the efficiencies, and so does the water feedback. But, it has to be noted that the combination of all the architectures drives upt the efficiency of the system. This is because of better flow between the systems and MS is no longer a bottle nexk in general. The added efficiecy of running a parallel AEC and extra water from water feedback makes the system more efficient when methanol synthesis is sped up. The maximum $\eta_{process}$ is 40.4% and the corresponding highest η_{stf} is 7.5%. This is because the average solar PV efficiency (η_{sol}) ranges between 18.6% to 18.8%. These efficiencies are comparable to those found in similar process systems across literature as can be seen in Section 5.5.

The feasibility of setting up a microplant is not only dependent on the total methanol yield and efficiencies, but also the financial capital required to set the microplant. The current costs for each subsystems are given in **??**. Based on research done by Akram and Ščasný, the cost of setting up a single axis PV tracker can be estimated to be 1.15 Euros/Wp and a fixed angle mounting system would cost 1.07 Euros/Wp when procured in bulk. The costs of batteries can be estimated to be within the range of 150 - 500 Euros/kWh [56], which for the selected battery in this thesis can be estimated to be 3,693.6 Euros and piping and pumping for the water feedback architecture is estimated to be 100 Euros.

With these costs, a better understanding into the feasibility of setting up a plant can be obtained by finding out the capital costs incurred to produce 1 Kg of methanol. The costs per Kg methanol have been tabulated in Table 6.5.

Table 6.5: Capital cost to produce 1 Kg Methanol for different system architectures at different locations [Euros/Kg Methanol]. The architecture abbreviations are as follows: F = Fixed mounting. B = Battery. AEC = Parallel AEC. MS = Parallel MS. W = Water feedback

Architecture/Location	Pias, Portugal	Ioannina, Greece	Tripoli, Libya	Essaouira, Morocco	Aoulef, Algeria
F	25.9	26.4	26.5	22.2	-
F+AEC+MS+W	27.8	30.4	31.0	24.8	-
F+B	28.6	28.	29.1	24.2	-
F+B+AEC+MS+W	26.5	28.8	28.4	23.4	-
1°	25.4	26.3	25.8	21.8	48.0
1°+AEC	28.4	29.2	27.3	24.3	-
1°+MS	25.8	27.6	28.8	22.0	-
1°+W	25.29	26.5	25.9	21.9	38.61
1°+AEC+MS+W	27.4	29.4	29.5	24.8	-
1°+B	29.7	28.9	28.5	24.4	-
1°+B+AEC	31.6	30.7	30.2	25.8	
1°+B+MS	25.7	27.2	26.9	22.4	-
1°+B+W	27.9	29.0	28.5	24.4	-
1°+B+AEC+MS+W	27.1	28.0	27.6	23.8	-

It can be inferred from Table 6.5, that the architectures with the highest production of methanol as deduced from Table 6.3 are not the most feasible opportunities. The most feasible architecture would be to find the lowest Capital cost to produce a kilogram of methanol which is displayed in green and the least feasible outcomes are displayed in red. From the table, it is evident that parallel AEC-based system architectures drive the capital costs up while parallel MS-based architectures have lower capital costs quite competitive to that of the most feasible options. At most of the locations the base case i.e. a single-axis tracker with no batteries and the default microplant is the most feasible option while for Pias, the base case + water feedback is the most feasible architecture. It can also be noted that Aoulef in Algeria is not a feasible location to set up the ZEF microplant since the architectures that yielded the most feasible outcomes for the other locations cost 1.93 times more than the average cost to produce 1 Kg of Methanol. Having performed two simulations at the most cost-effective architecture combinations and high costs, further analysis at Aoulef had been halted having been deemed to be too expensive to set up a plant for extremely small outputs.

Out of the locations analysed, Essaouira in Morocco is the most feasible location to set up the ZEF microplant and the most feasible architecture is the ZEF microplant powered by a solar PV array with single-axis solar trackers. This is because of high solar irradiation and high absolute humidity and lower temperatures.

6.5. Summary

- This chapter discussed the time step granularity of the model, the effects of sizing components, and analysed the behaviour of the integrated ZEF microplant. Simulations have been performed and feasible architectures and location has been identified.
- The chapter hence, achieved the research sub-objective 4: ”Analyse the microplant behaviour and predict the Methanol yield by implementing a cost-effective microplant system architecture at various geographic locations. ”.
- With the functioning model and simulations performed, Essaouira in Morocco is a strong candidate to set up the ZEF microplant with a single-axis solar tracker.
- The model can hence, be used as a tool to predict methanol production through the ZEF microplant for any geographic location.

7

Conclusions and recommendations

7.1. Conclusions

The primary objective of this thesis has been ”to build and use a model of an integrated microplant as a tool to predict methanol production and the performance of the microplant under multiple system architectures” at Zero-Emission Fuel (ZEF) The motivation behind this endeavour stems from the pressing need to harness renewable energy sources effectively and facilitate sustainable methanol production, thereby contributing to the mitigation of greenhouse gas emissions.

This research was characterized by a systematic process of building a modelling roadmap that entails preprocessing, building the model and performing simulations. In the preprocessing phase, data has been imported from the C3S database using the Copernicus ERA5 hourly data which has then been prepared for simulation steps.

Then subsystem models were individually developed, encompassing solar photovoltaic (PV) modules, direct air capture (DAC), fluid machinery (FM) alkaline electrolysis cell (AEC), methanol synthesis (MS), distillation (DS), buffer tanks and battery systems. These subsystem models have been designed based on previous experiments and parameters from the literature.

Integral to the microplant’s functionality is the deployment of a control algorithm which was explored within this thesis. The control mechanism operates on two distinct levels, namely battery management and power distribution. Battery management entails the optimization of charging, discharging, and the preservation of state of charge (SOC), facilitating efficient energy utilization. Power distribution control, on the other hand, orchestrates the allocation of available power among subsystems, leveraging the ”Constant System Flow Rate Control” strategy to ensure optimal methanol production while maintaining equilibrium within the system by using the addition-consumption ratio and incorporating the change factor.

For the integration of the microplant, various microplant architectures were designed to cater to diverse operational and weather scenarios. These architectural variations encompassed solar PV tracking, battery integration, parallel methanol synthesis reactors, parallel AEC and water feedback. Each configuration was tailored to address unique challenges and optimize performance based on location and local weather conditions, thereby providing valuable insights for practical implementation.

Furthermore, this thesis illuminated the behaviour of the microplant under varying temporal granularity. It was evident that the choice of time step size significantly influenced methanol production, underscoring the importance of optimizing control strategies to mitigate resource inefficiencies and ensure operational robustness. The temporal granularity also impacts the sizing requirements of the microplant and introduces more dynamics.

Ultimately, the feasibility of the ZEF microplant model has been examined, paving the way for potential real-world applications at 5 locations namely Pias, Ioannina, Tripoli, Essaouira and Aoulef. By scrutinizing its behaviour, control mechanisms, and 14 architectural combinations, this thesis has been able to predict the highest production of Methanol based on the location and system architecture which gave an insight that a single axis tracker, with battery, parallel AEC and MS with water feedback provides the highest yield at any location with the microplant set up in Essaouira producing 884 Kgs of methanol in one year. While the cost-effectiveness of setting up the microplant found that the architecture combination to provide the

highest methanol yield is not the most cost-effective solution. Further, the most cost-effective architecture varies based on the location as well. Setting up the microplant at Essaouira, Morocco with a single-axis tracker is by far the most cost-effective scenario among all simulations performed. The maximum process efficiency ($\eta_{process}$) found was 40.4% and sun to fuel efficiency (η_{stf}) was 7.5% with the fixed mounting, battery, parallel AEC, parallel MS and water feedback architecture combination at Essaouira.

In essence, this thesis offers a holistic perspective on the integration of solar fuels and innovative control strategies, underpinning the feasibility of the ZEF microplant as a promising solution in the transition towards sustainable energy alternatives.

7.2. Recommendations

Based on the learnings from the works of the thesis the scope has been considered and with newer insights, recommendations have been laid out

7.2.1. Building Subsystem models

- **Scope:** The model is designed to predict methanol production in a year with time steps larger than 5 minutes. Effects and dynamics below this temporal granularity have not been modelled. The model's accuracy can be improved by incorporating these effects, albeit, would increase the computation requirements.
- **Solar PV:** The solar PV system model does not account for cloudiness and other weather effects smaller than the time step selected. Incorporating these effects would make the model more true to real cases. More accurate temperature models and MPPT design can be implemented to improve the performance of the model.
- **DAC:** The current model is an ideal representation of absorption and desorption. Implementing viscosity effects would have more accurate production values. Also, the flow rate into the stripping column is constant. Allowing a dynamic flow rate based on the CO_2 STY would yield optimum production rates. Currently, the DAC system's operation is sub-optimal in these regards. The sorbent degradation effect is another factor that can be researched further.
- **Thermal inertia:** The time taken to heat up components can be considered. For example, the DS requires 20 minutes to achieve steady-state performance. Such effects in DAC and MS can also be incorporated.

7.2.2. Designing Controller and integration

- **Control Algorithm research:** Optimization of resources is important for the controller and it has been observed that the power distribution requires to be improved. Potential solutions can be to investigate multi-input multi-output controllers like Model Predictive Control, and machine learning algorithms.
- **Battery priority:** The controller has been designed to prioritise battery operation. That means the power distribution is first decided for the battery and then distributed to the system. The inverse can then be investigated where the microplant's energy requirements are prioritised, and then the battery is charged/discharged.

7.2.3. Simulation:

- **Control Algorithm research:** Optimization of resources is important for the controller and it has been observed that the power distribution requires to be improved. Potential solutions can be to investigate multi-input multi-output (MIMO) controllers like Model Predictive Control, and machine learning algorithms.
- **Level of Confidence analysis:** Copernicus data provides typical meteorological data through reanalysis. Using P70, and P90 data sets can shed insights into the behaviour of the system under extreme weather instances.
- **Weather disruptions:** All the simulations do not consider weather disturbances, such as cloudiness, rain, snowfall etc. Incorporating these in the input data set can give much more realistic microplant behaviours.

7.2.4. Future research

- **Central heat exchange:** It has been found that methanol synthesis plants from renewable energies generally have two sources of energy, electrical and waste heat from heat sources which brings down the capacity of required electrical power. The ZEF microplant does not have the possibility for external heat sources as it is location-independent and off-grid. To tackle this challenge, a central heat exchange needs to be investigated to improve the performance of the system. ZEF has been using heat exchangers within the scope of each subsystem, but utilising heat across subsystems would increase the efficiency of the microplant.
- **In-depth financial analysis:** The financial analysis performed is limited to estimating the capital cost of setting up a single micro plant. Further analysis is required that includes, labour, scaling up effects and analysing the net present value (NPV) of the system. Payback periods, break-even periods, revenues and subsidies can also be included to make the financial analysis robust.
- **Environmental impact assessment:** Performing an environmental impact assessment would be beneficial in understanding the potential of the microplant to absorb Carbon dioxide from the air and understand the impact the plant has in reducing greenhouse gas emissions.

References

[1] Robbert Biesbroek et al. *IPCC Sixth Assessment Report: Technical Summary*. Tech. rep. 2022. DOI: 10.1017/9781009325844.002. URL: https://www.ipcc.ch/report/ar6/wg2/.

[2] Unfccc. *ADOPTION OF THE PARIS AGREEMENT - Paris Agreement text English*. Tech. rep. 2015.

[3] "Summary for Policymakers". In: *IPCC* (2018), pp. 1–24. DOI: 10.1017/9781009157940.001. URL: https://doi.org/10.1017/9781009157940.001.

[4] Josep G Canadell et al. *SPM 673 5 Global Carbon and Other Biogeochemical Cycles and Feedbacks Coordinating Lead Authors: Lead Authors: Contributing Authors*. Tech. rep. 2021. DOI: 10.1017/9781009157896.007.

[5] International Energy Agency. *Net Zero by 2050 – Analysis*. May 2021. URL: https://www.iea.org/reports/net-zero-by-2050.

[6] Rahim Zahedi et al. "Modelling community-scale renewable energy and electric vehicle management for cold-climate regions using machine learning". In: *Energy Strategy Reviews* 43 (2022), p. 100930. DOI: https://doi.org/10.1016/j.esr.2022.100930. URL: https://www.sciencedirect.com/science/article/pii/S2211467X22001249.

[7] Sang-Bing Tsai et al. "Models for forecasting growth trends in renewable energy". In: *Renewable and Sustainable Energy Reviews* 77 (2017), pp. 1169–1178. DOI: https://doi.org/10.1016/j.rser.2016.06.001. URL: https://www.sciencedirect.com/science/article/pii/S1364032116302143.

[8] George A Olah. "Beyond oil and gas: the methanol economy". In: *Angewandte Chemie International Edition* 44.18 (2005), pp. 2636–2639.

[9] Occo Roelofsen et al. *How electrification can help industrial companies cut costs | McKinsey*. Sept. 2023. URL: https://www.mckinsey.com/industries/electric-power-and-natural-gas/our-insights/plugging-in-what-electrification-can-do-for-industry.

[10] Anthony Harriman. "Prospects for conversion of solar energy into chemical fuels: the concept of a solar fuels industry". In: *Philosophical Transactions of the Royal Society A: Mathematical, Physical and Engineering Sciences* 371.1996 (Aug. 2013), p. 20110415. DOI: https://doi.org/10.1098/rsta.2011.0415. URL: https://royalsocietypublishing-org.tudelft.idm.oclc.org/doi/full/10.1098/rsta.2011.0415.

[11] Parameswaram Ganji et al. "Photocatalytic Reduction of Carbondioxide to Methanol: Carbonaceous Materials, Kinetics, Industrial Feasibility, and Future Directions". In: *Energy & Fuels* (2023).

[12] Michele Aresta et al. "The changing paradigm in CO2 utilization". In: *Journal of CO2 Utilization* 3-4 (2013), pp. 65–73. DOI: https://doi.org/10.1016/j.jcou.2013.08.001. URL: https://www.sciencedirect.com/science/article/pii/S2212982013000322.

[13] Martin Bertau et al. *Methanol: the basic chemical and energy feedstock of the future*. Vol. 1. Springer, 2014.

[14] Daniel Sheldon. "Methanol production-a technical history". In: *Johnson Matthey Technology Review* 61.3 (2017), pp. 172–182.

[15] Carlos Arnaiz del Pozo et al. "Techno-economic assessment of long-term methanol production from natural gas and renewables". In: *Energy Conversion and Management* 266 (2022), p. 115785. DOI: https://doi.org/10.1016/j.enconman.2022.115785. URL: https://www.sciencedirect.com/science/article/pii/S0196890422005817.

[16] *Production of renewable methanol from captured emissions and renewable energy sources, for its utilisation for clean fuel production and green consumer goods*. Aug. 2022. URL: https://cordis.europa.eu/project/id/848757.

[17] *Orca is Climeworks' new large-scale carbon dioxide removal plant*. Sept. 2023. URL: https://climeworks.com/roadmap/orca.

[18] *Skytree Technology*. Sept. 2023. URL: https://www.skytree.eu/technology.

[19] *Products for Carbon Capture Soletair Power*. Sept. 2023. URL: https://www.soletairpower.fi/products/.

[20] Kunal Vidyarthi. *Dynamic Operation of an Integrated Direct Air Capture and CO 2 Compression System*. Tech. rep. 2022. URL: http://repository.tudelft.nl/.

[21] Arno H M Smets et al. *Solar energy : the physics and engineering of photovoltaic conversion, technologies and systems*, p. 462.

[22] *Optimum Tilt of Solar Panels*. Mar. 2017. URL: https://www.solarpaneltilt.com/.

[23] Matthew Lave et al. "Evaluation of Global Horizontal Irradiance to Plane-of-Array Irradiance Models at Locations Across the United States". In: *IEEE Journal of Photovoltaics* 5.2 (2015), pp. 597–606. DOI: 10.1109/JPHOTOV.2015.2392938.

[24] Ulrich Boke. "A simple model of photovoltaic module electric characteristics". In: *2007 European Conference on Power Electronics and Applications*. 2007, pp. 1–8. DOI: 10.1109/EPE.2007.4417572.

[25] International Energy Agency. "Direct Air Capture: A key technology for net zero". In: (). URL: www.iea.org/t&c/.

[26] Christopher W Jones. "CO 2 Capture from Dilute Gases as a Component of Modern Global Carbon Management". In: (2010). DOI: 10.1146/annurev-chembioeng-061010-114252. URL: www.annualreviews.org.

[27] Mahdi Fasihi et al. "Techno-economic assessment of CO 2 direct air capture plants". In: *Journal of Cleaner Production* 224 (July 2019), pp. 957–980. DOI: 10.1016/J.JCLEPRO.2019.03.086.

[28] Jennifer Wilcox. "Absorption". In: *Carbon Capture*. New York, NY: Springer New York, 2012, pp. 53–113. DOI: 10.1007/978-1-4614-2215-0_3. URL: https://doi.org/10.1007/978-1-4614-2215-0_3.

[29] Henrik Jilvero et al. "Heat requirement for regeneration of aqueous ammonia in post-combustion carbon dioxide capture". In: *International Journal of Greenhouse Gas Control* 11 (2012), pp. 181–187. DOI: https://doi.org/10.1016/j.ijggc.2012.08.005. URL: https://www.sciencedirect.com/science/article/pii/S1750583612001909.

[30] Øystein Jonassen et al. "Heat of Absorption of Carbon Dioxide (CO2) into Aqueous N-Methyldiethanolamine (MDEA) and N,N-Dimethylmonoethanolamine (DMMEA)". In: *Energy Procedia* 63 (2014). 12th International Conference on Greenhouse Gas Control Technologies, GHGT-12, pp. 1890–1902. DOI: https://doi.org/10.1016/j.egypro.2014.11.198. URL: https://www.sciencedirect.com/science/article/pii/S187661021402013X.

[31] Mrigank Sinha. *Direct Air Capture: Characterization and design of a novel absorption process*. 2019.

[32] Jie Yu et al. "Water Enhancement in CO2 Capture by Amines: An Insight into CO2–H2O Interactions on Amine Films and Sorbents". In: *Industrial & Engineering Chemistry Research* 57.11 (2018), pp. 4052–4062. DOI: 10.1021/acs.iecr.7b05114. URL: https://doi.org/10.1021/acs.iecr.7b05114.

[33] Fanhe Kong et al. "Research needs targeting direct air capture of carbon dioxide: Material amp; process performance characteristics under realistic environmental conditions". In: *Korean Journal of Chemical Engineering* 39.1 (2022), pp. 1–19. DOI: 10.1007/s11814-021-0976-0.

[34] Wenhua Li. “Simplified steady-state modeling for variable speed compressor”. In: *Applied Thermal Engineering* 50.1 (2013), pp. 318–326. DOI: https://doi.org/10.1016/j.applthermaleng.2012.08.041. URL: https://www.sciencedirect.com/science/article/pii/S1359431112005649.

[35] B A T M Boons. *SYSTEM INTEGRATION OF A HIGH PRESSURE ALKALINE ELECTROLYSER*. Tech. rep. 2022. URL: http://repository.tudelft.nl/..

[36] Claude Lamy et al. “A critical review on the definitions used to calculate the energy efficiency coefficients of water electrolysis cells working under near ambient temperature conditions”. In: (2019).

[37] Jörn Brauns et al. “Alkaline water electrolysis powered by renewable energy: A review”. In: *Processes* 8.2 (2020), p. 248.

[38] A.C. de Jong. *Power to Fuel: Optimisation and characterisation of a small scale methanol synthesis reactor*. Tech. rep. Delft: Tu Delft, Dec. 2022.

[39] Suresh Kanuri et al. *An insight of CO2 hydrogenation to methanol synthesis: Thermodynamics, catalysts, operating parameters, and reaction mechanism*. Apr. 2022. DOI: 10.1002/er.7562.

[40] A Keshavarz et al. “Simultaneous methanol production and separation in the methanol synthesis reactor to increase methanol production”. In: *Chemical Engineering and Processing-Process Intensification* 158 (2020), p. 108176.

[41] Cherise Tomsjansen. “Mini-Distillation System ”De Koolmees””. 2023.

[42] Michael Weij. *Optimization of a distillation system to measure in line dynamic purity of methanol*. Tech. rep. 2022.

[43] Shunli Wang et al. *Battery system modeling*. Elsevier, 2021.

[44] Håvard Breisnes Vika. *NTNU open: Modelling of photovoltaic modules with Battery Energy ...* 2014. URL: https://ntnuopen.ntnu.no/ntnu-xmlui/handle/11250/257839?locale-attribute=en.

[45] Epicpower. *Battery State of Charge calculation with EPC Converters*. Tech. rep. URL: www.epicpower.es.

[46] *ERA5 hourly data on single levels from 1940 to present*. 2023.

[47] James Barry et al. “Dynamic model of photovoltaic module temperature as a function of atmospheric conditions”. In: *Advances in Science and Research* 17 (July 2020), pp. 165–173. DOI: 10.5194/asr-17-165-2020. URL: https://doi.org/10.5194/asr-17-165-2020.

[48] *Solar park Ínsua - Chint*. Aug. 2023. URL: https://www.chintsolar.com/projects/solar-park-insua/.

[49] Jan. Kranendonk et al. *ZEF AEC Model*. 2022.

[50] Paul Vroegindeweij. *ZEF AEC Model*. 2022.

[51] Cherise Tomsjansen. *ZEF COCO Distillation column Model*. 2022.

[52] Jiyong Kim et al. “Fuel production from CO 2 using solar-thermal energy: system level analysis”. In: *Energy & Environmental Science* 5.9 (2012), pp. 8417–8429.

[53] Enric Prats-Salvado et al. “Synergies between direct air capture technologies and solar thermochemical cycles in the production of methanol”. In: *Energies* 14.16 (2021), p. 4818.

[54] Marco Marchese et al. “CO2 from direct air capture as carbon feedstock for Fischer-Tropsch chemicals and fuels: Energy and economic analysis”. In: *Journal of CO2 Utilization* 46 (2021), p. 101487. DOI: https://doi.org/10.1016/j.jcou.2021.101487. URL: https://www.sciencedirect.com/science/article/pii/S2212982021000548.

[55] Elahi G. Akram et al. “Techno-economic analysis of fixed versus sun-tracking solar panels”. English. In: *International Journal of Renewable Energy Development* 12.3 (May 2023), pp. 615–626. URL: https://www.proquest.com/scholarly-journals/techno-economic-analysis-fixed-versus-sun/docview/2830122128/se-2.

[56] Thomas Kaschub et al. “Solar energy storage in German households: profitability, load changes and flexibility”. In: *Energy Policy* 98 (2016), pp. 520–532. DOI: https://doi.org/10.1016/j.enpol.2016.09.017. URL: https://www.sciencedirect.com/science/article/pii/S0301421516304815.

[57] *Solar resource maps of World*. URL: https://solargis.com/maps-and-gis-data/download/world.

A

Weather Plots

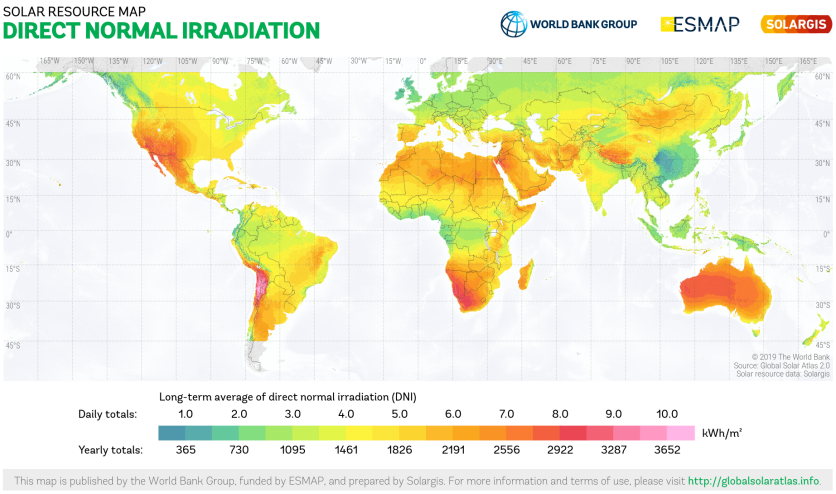

Figure A.1: World DNI map [57].

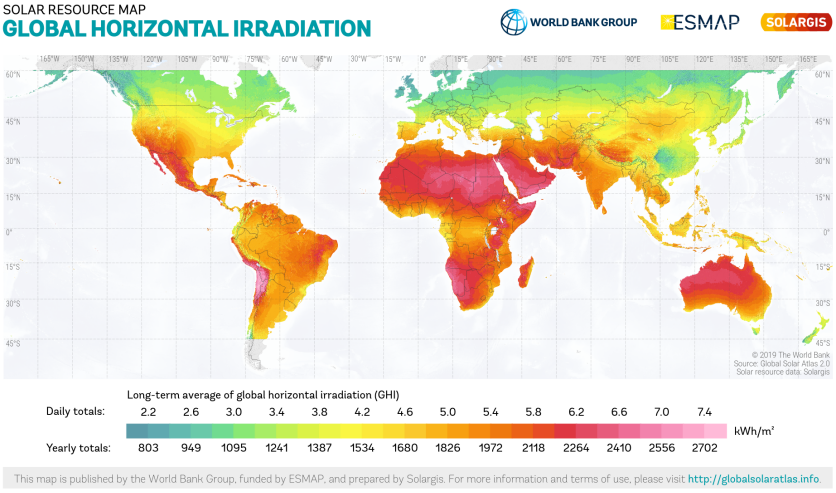

Figure A.2: World GHI map [57].

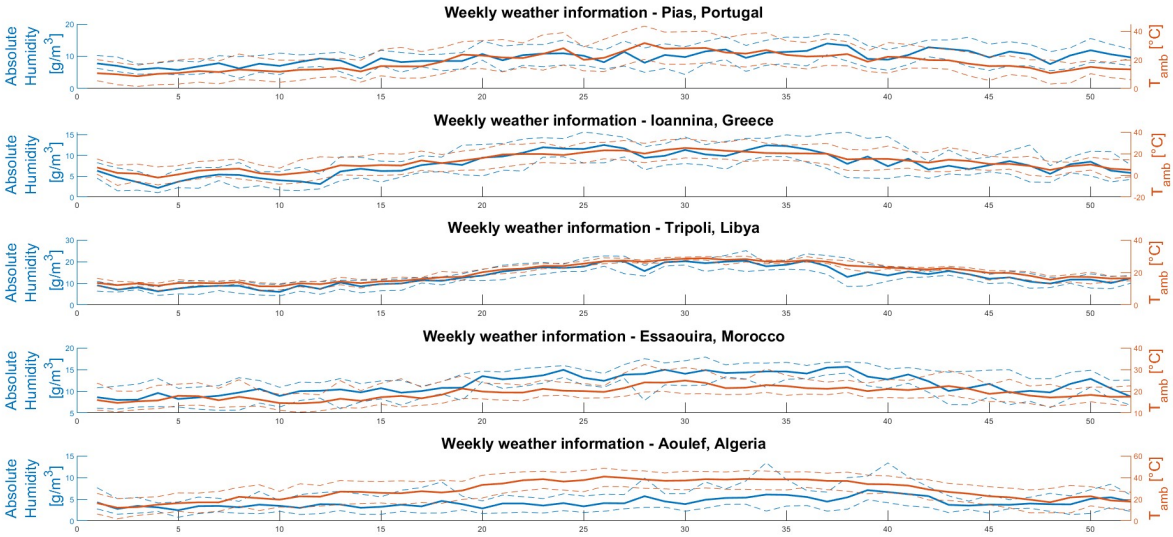

Figure A.3: Location-wise mean, minimum and maximum values of absolute humidity (left axis) and ambient temperature (right axis).

B

Microplant Simulation Parameters and Plots

B.1. Fixed Mounting Architecture plots

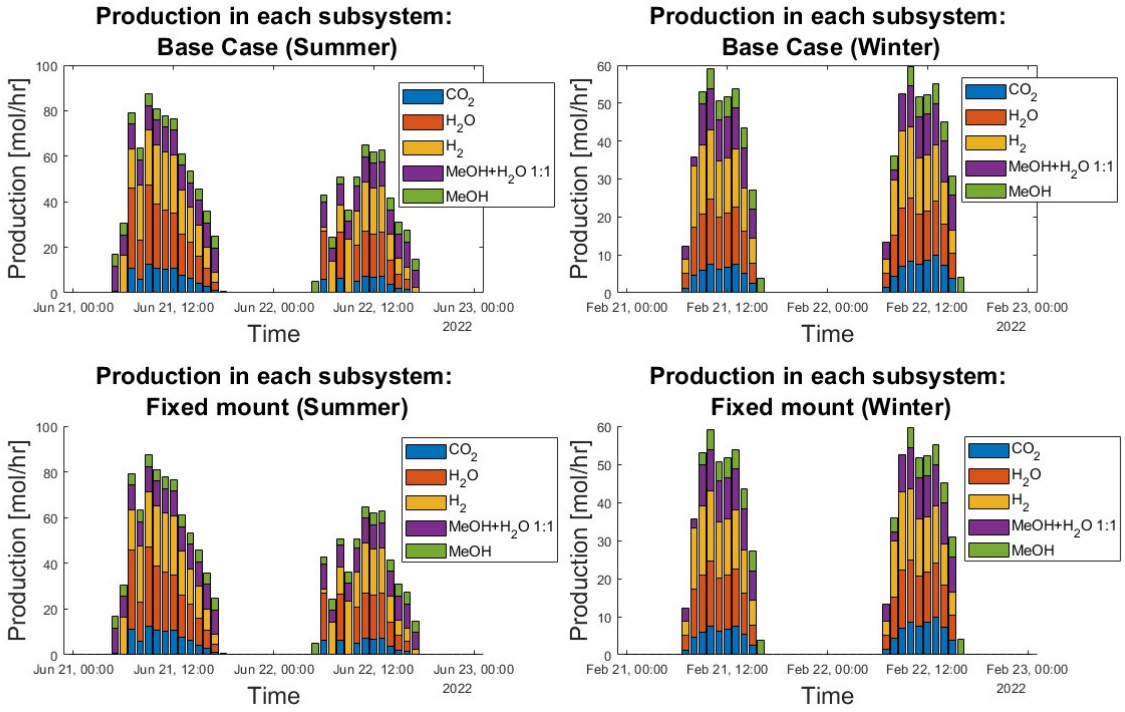

Figure B.1: The production of all subsystems on two random days in summer and winter. The plots in the top show the production in the base case while the ones below are for the fixed mounting case. The summer and winter production plots are on the left and right respectively. The summer days are 21-22 June, 2022 and the winter day is 21 - 23 Feb, 2022

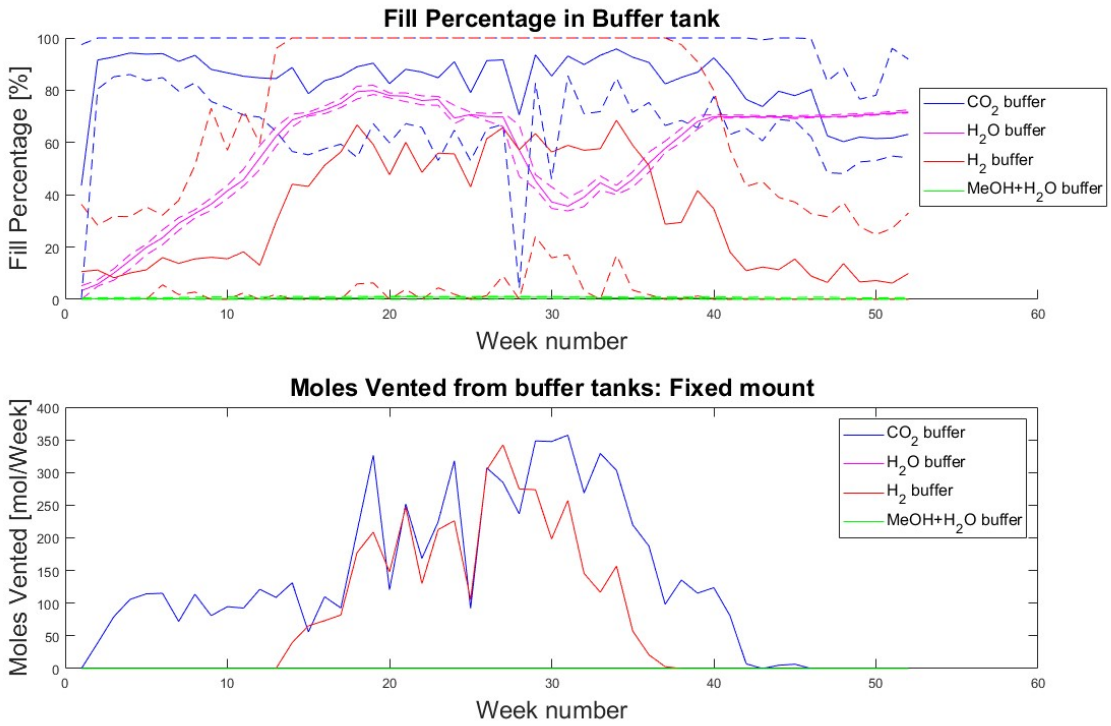

Figure B.2: Mean, maximum and minimum weekly buffer tank fill percentage (above) and total weekly moles vented from each buffer tank (below) in the fixed mounting architecture

B.2. Base Case + Battery Architecture plots

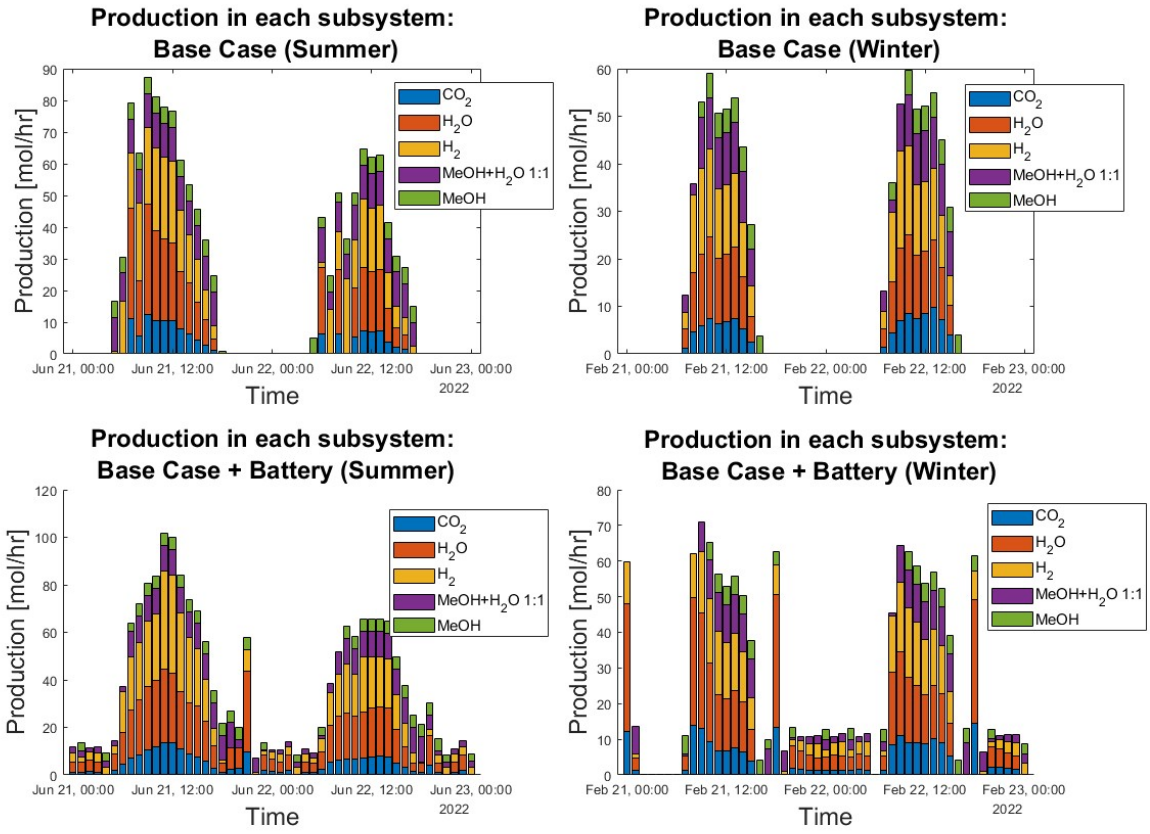

Figure B.3: The production of all subsystems on two random days in summer and winter. The plots in the top show the production in the base case while the ones below are for the base case + battery architecture. The summer and winter production plots are on the left and right respectively. The summer days are 21-22 June, 2022 and the winter day is 21 - 23 Feb, 2022

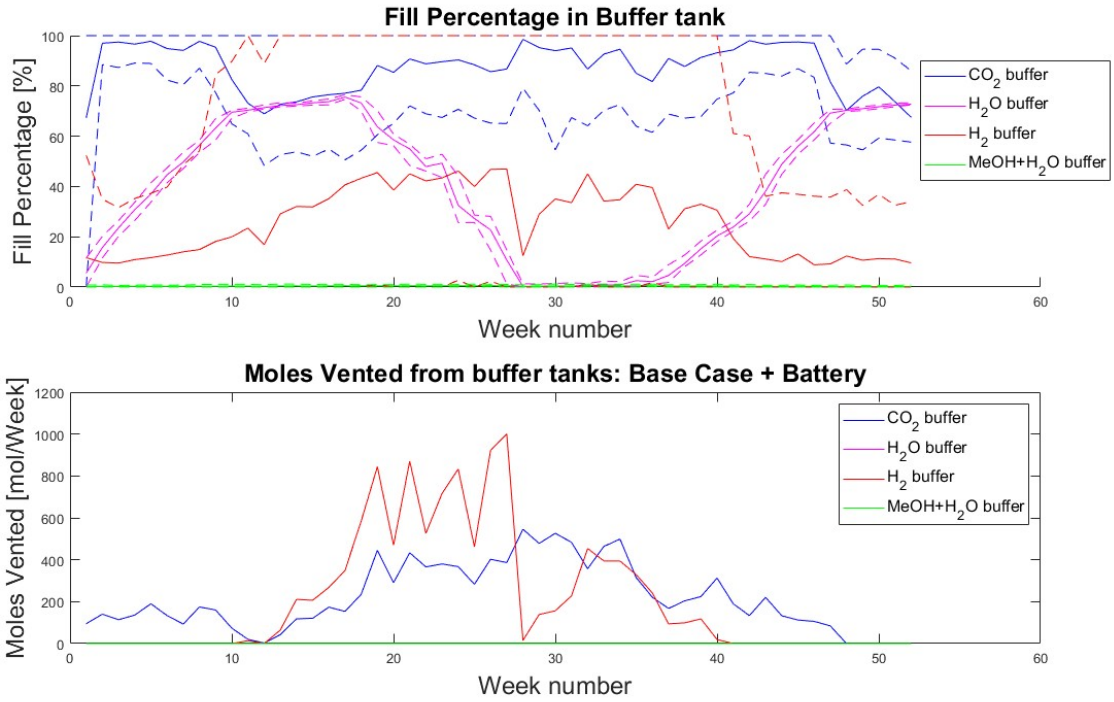

Figure B.4: Mean, maximum and minimum weekly buffer tank fill percentage (above) and total weekly moles vented from each buffer tank (below) in the base case + battery architecture

B.3. Base Case + Parallel AEC Architecture plots

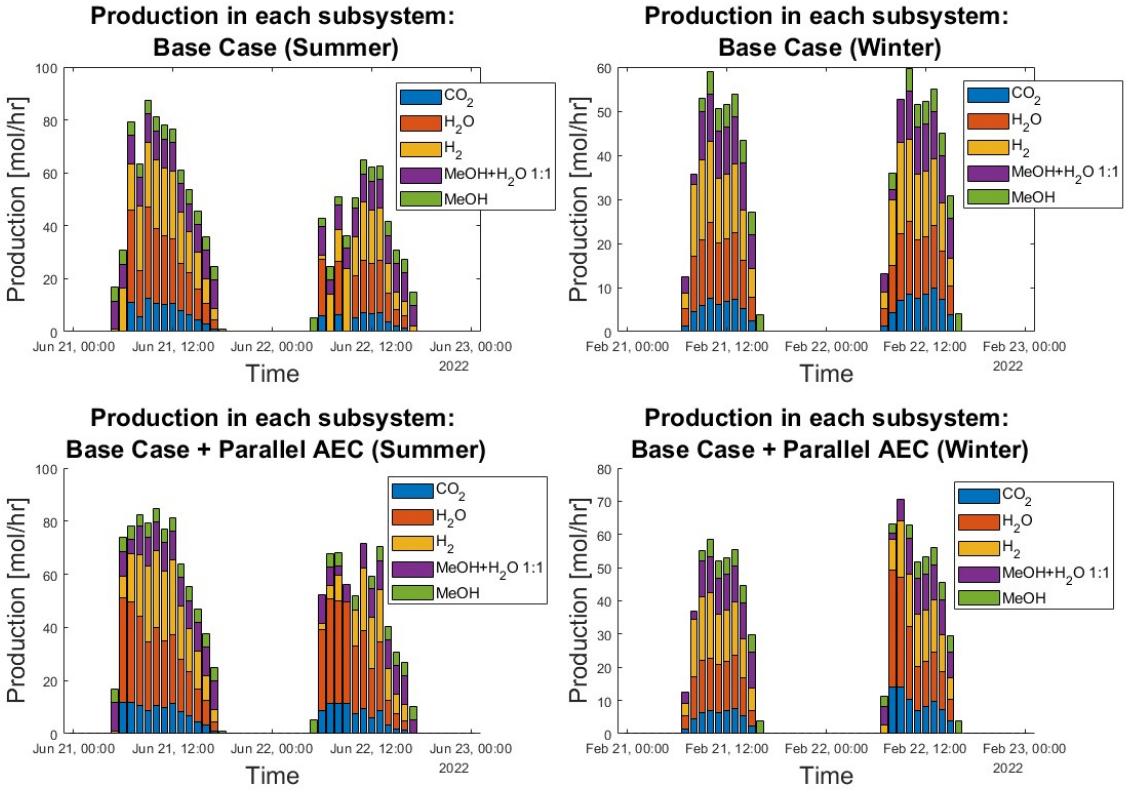

Figure B.5: The production of all subsystems on two random days in summer and winter. The plots in the top show the production in the base case while the ones below are for the base case + parallel AEC architecture. The summer and winter production plots are on the left and right respectively. The summer days are 21-22 June, 2022 and the winter day is 21 - 23 Feb, 2022

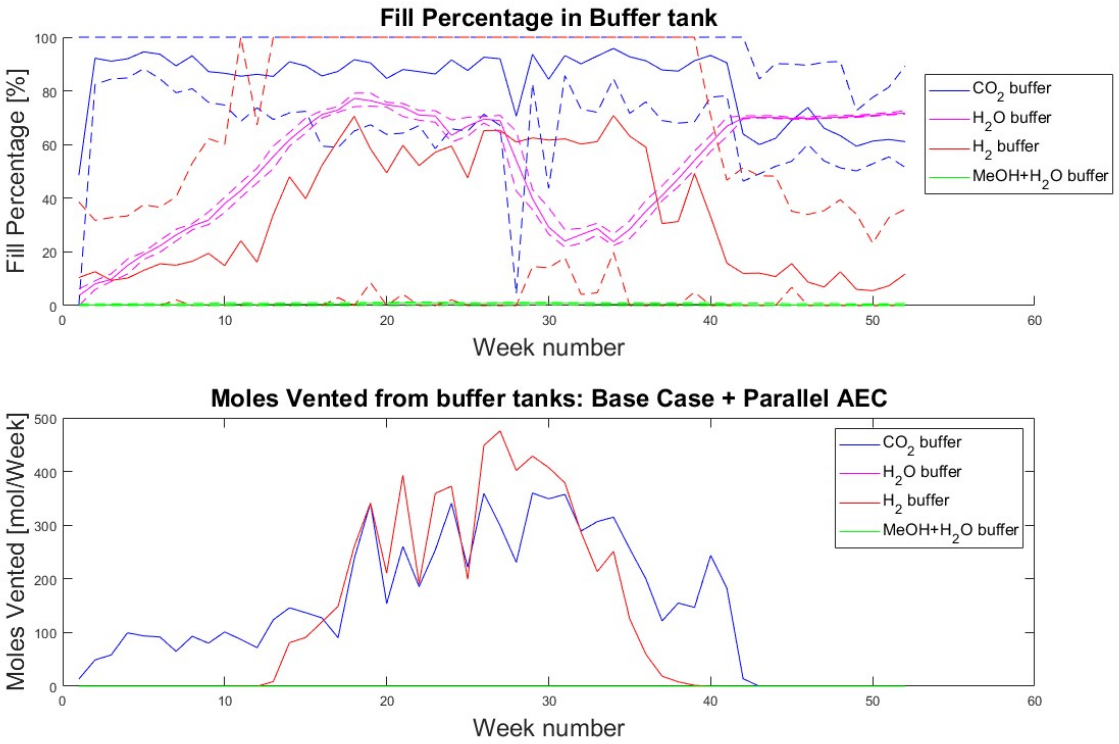

Figure B.6: Mean, maximum and minimum weekly buffer tank fill percentage (above) and total weekly moles vented from each buffer tank (below) in the base case + parallel AEC architecture

B.4. Base Case + Parallel MS Architecture plots

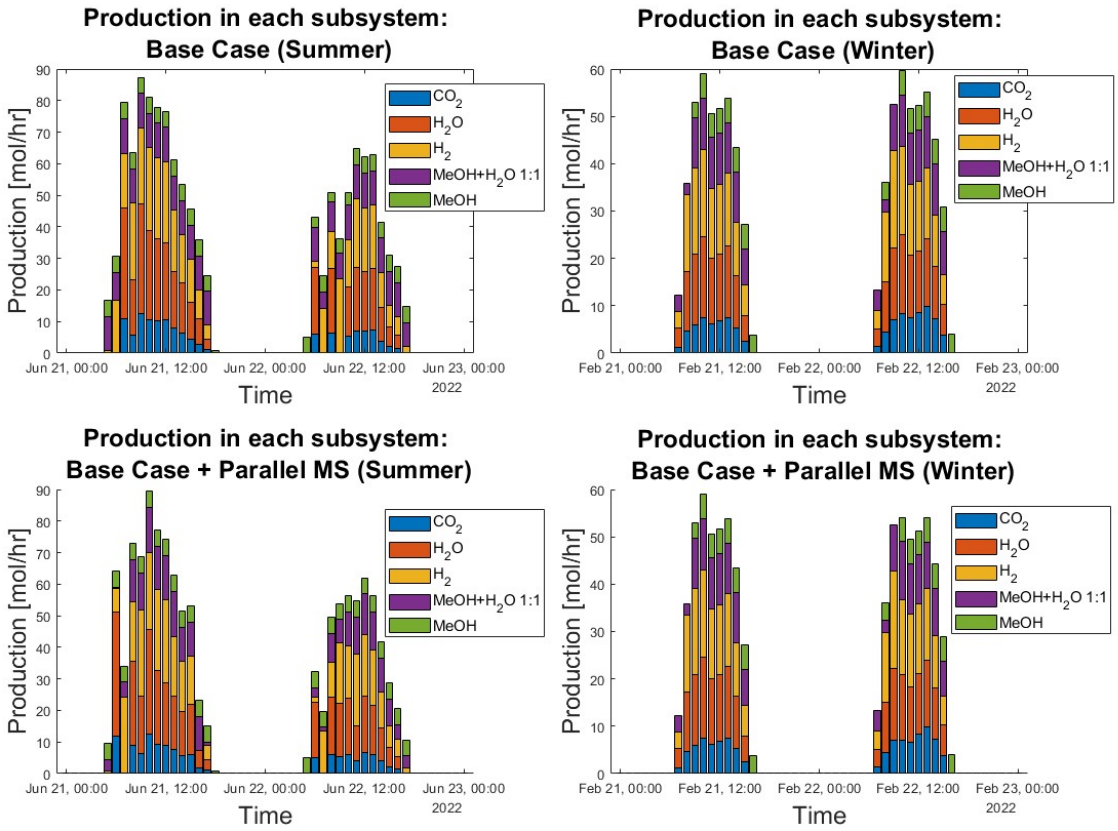

Figure B.7: The production of all subsystems on two random days in summer and winter. The plots in the top show the production in the base case while the ones below are for the base case + parallel MS architecture. The summer and winter production plots are on the left and right respectively. The summer days are 21-22 June, 2022 and the winter day is 21 - 23 Feb, 2022

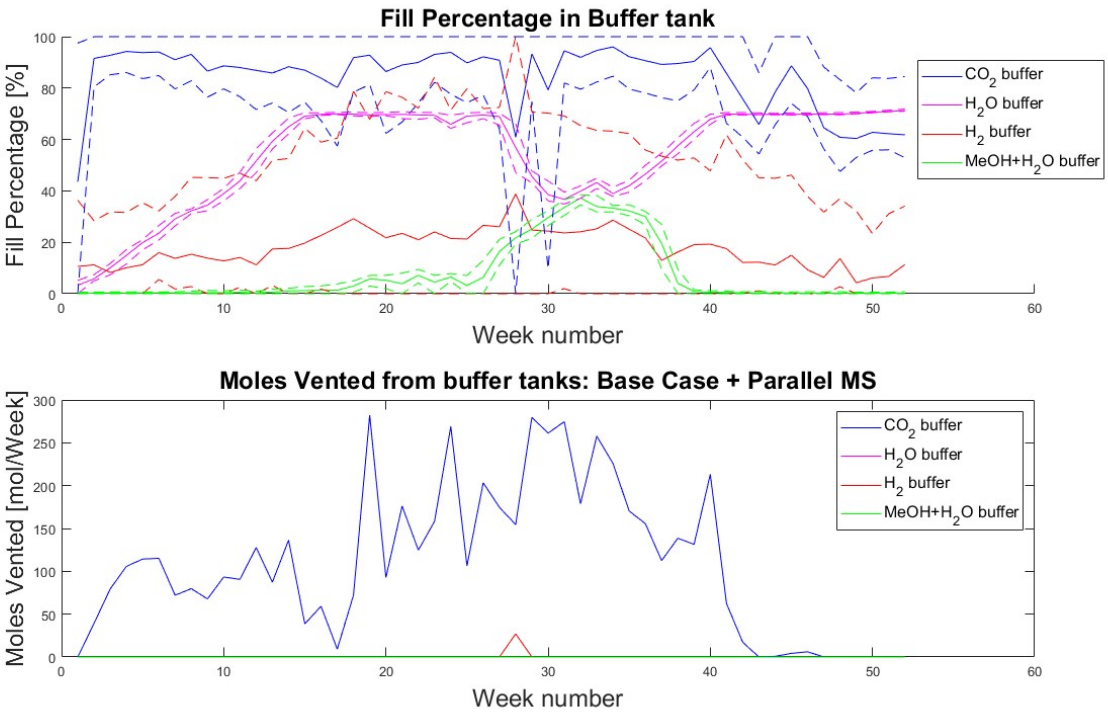

Figure B.8: Mean, maximum and minimum weekly buffer tank fill percentage (above) and total weekly moles vented from each buffer tank (below) in the base case + parallel MS architecture

B.5. Base Case + Water Feedback Architecture plots

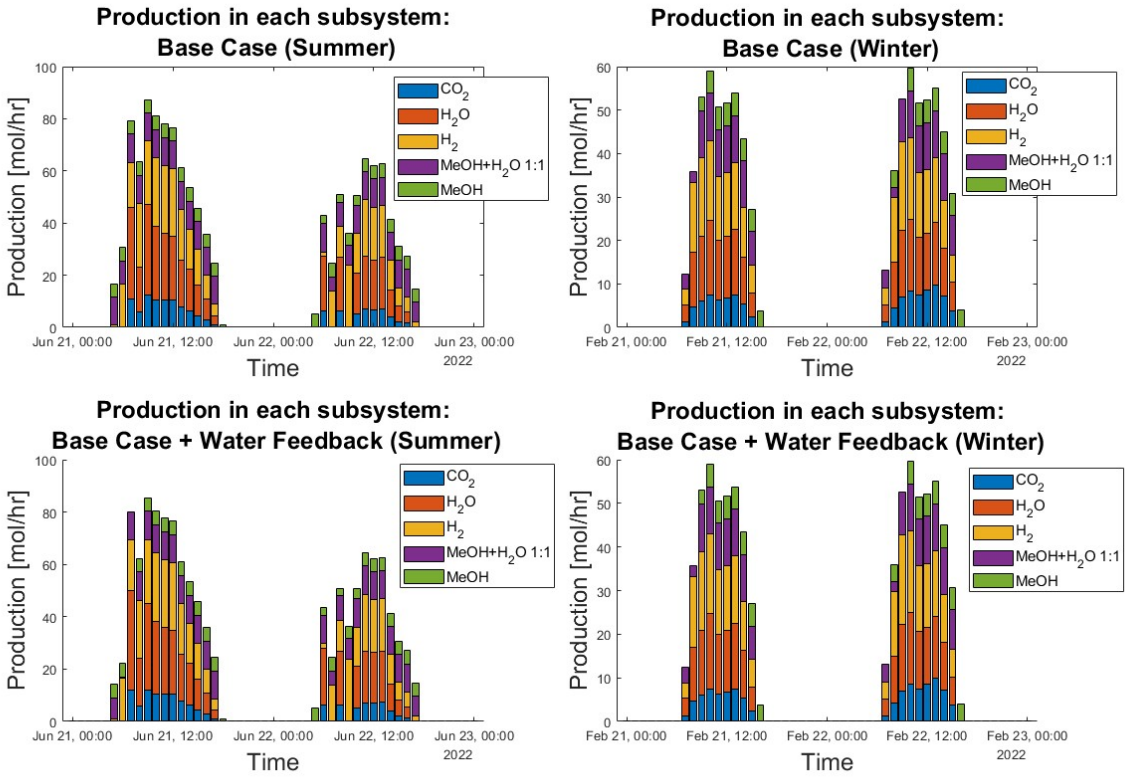

Figure B.9: The production of all subsystems on two random days in summer and winter. The plots in the top show the production in the base case while the ones below are for the base case + water feedback architecture. The summer and winter production plots are on the left and right respectively. The summer days are 21-22 June, 2022 and the winter day is 21 - 23 Feb, 2022

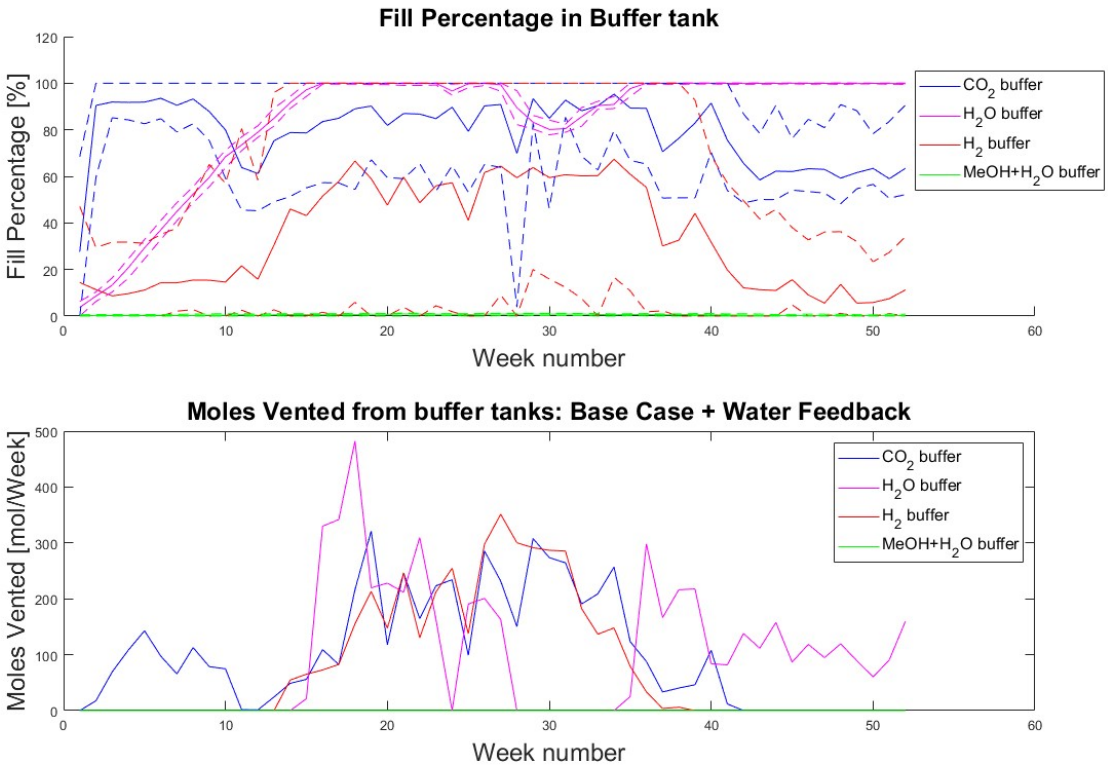

Figure B.10: Mean, maximum and minimum weekly buffer tank fill percentage (above) and total weekly moles vented from each buffer tank (below) in the base case + water feedback architecture